Winter 12-14-2018

Development of Glucocorticoid Prodrug for the Treatment of Lupus Nephritis

Xiaobei Wang
University of Nebraska Medical Center

DEVELOPMENT OF GLUCOCORTICOID PRODRUG FOR THE TREATMENT OF LUPUS NEPHRITIS

By

Xiaobei Wang

A DISSERTATION

Presented to the Faculty of
The University of Nebraska Graduate College
In Partial Fulfillment of Requirements
for the Degree of Doctor of Philosophy

Pharmaceutical Sciences

Under the Supervision of Professor Dong Wang

University of Nebraska Medical Center
Omaha, Nebraska

November, 2018

Supervisory Committee:

Tatiana K. Bronich, Ph.D. Joseph A. Vetro, Ph.D.

Geoffrey M. Thiele, Ph.D. Dong Wang, Ph.D.

Acknowledgments

First and foremost, I would like to give my sincere gratitude to my mentor Dr. Dong Wang, who not only provided constant support to my research work, but also inspired me with his own hard working and enthusiasm in science during all these years. I am so thankful that he has been always available for my questions and generously shared his life wisdom for my education. From him, I learned how to become a real scientist with creative and critical thinking, integrity, and persistency.

I would also like to sincerely thank my graduate supervisory committee members Drs. Geoffrey Thiele, Tatiana K. Bronich, and Joseph A. Vetro for their valuable guidance, suggestions, and encouragements throughout my Ph.D. training. I am grateful for Dr. Geoffrey Thiele for him always generously providing his guidance and wisdom as immunologists and Dr. Tatiana K. Bronich for her expert advises in the micellar field. I would like to thank Dr. Vetro for their scientific training and valuable inputs on my research project and scientific fostering.

I would like to acknowledge Dr. Kirk W. Foster, who is a clinical pathologist in UNMC. Despite of his busy schedule, he is always patient in providing guidance and answers I needed for the pathological evaluations;

I also want to express my gratitude to Dr. Yazen Alnouti and Dr. Nagsen Gautam for UPLC/MS-MS method development and pharmacokinetic data analysis; Dr. Fang Yu and Fang Qiu for statistical analyses.

I want to sincerely appreciate the help from Dr. Craig L. Semerad, the director of the Flow Cytometry Research Facility at the University of Nebraska Medical Center (UNMC) for his generous guidance and assistance with flow cytometry. I also want to acknowledge Lijun Sun in Tissue Sciences Facility at UNMC for assistance with IHC analysis.

I was fortunate to work with wonderful colleagues from Dr. Dong Wang's lab. I would like to especially than Dr. Fang Yuan for teaching me the animal models and biological assay techniques when I first joined the lab. I wish to thank Dr. Zhenshan Jia, Dr. Rongguo Ren and Dr. Junxiao Yang for their guidance on chemistry and professional advices throughout this project. I would like to thank Gang Zhao and Dr. Xin Wei and Yangyang Gao for offering help on the animal and IHC studies.

I would like to express my many thanks to all the faculty members in the department for tutoring and teaching me in the PSGP courses, which help me open the doors to a brand-new field. I also would like to thank the past and present staff members in COP, especially Mrs. Elaine Payne, Mrs. Jamie Cook, Mrs. Renee Kaszynski, Mrs. Michelle Parks, Mrs. Katina M. Winters for their dedicated and generous help to me in the past five years.

I would also like to express my sincere gratitude to the UNMC Graduate Fellowship, NIAID, NIAMS, NIH/COBRE grant for the financial support in the past years.

Last but not the least, I would like to acknowledge my family and friends. Words failed me to express my gratitude to my parents, who are always supportive without any condition. I owe a special thanks to my husband, Enquan Xu, for his consistent encouragement and support. Without his urge, I might not even start this fantastic journey. I would sincerely thank my friend and colleague Fang Yuan for leading me to this project, and Laura Weber, for her continuous accompany and encouragement during the past five years. I would also like to thank Tian Zhou, Zhen Ye, Fangfang Qiao, Xiaoyan Wang for their encouragements and lifelong friendship. If you have a dream, you need to protect it. I appreciate everyone who has strong faith in me and helps me to protect and chase my dreams.

Xiaobei Wang

University of Nebraska Medical Center

November 2018

DEVELOPMENT OF GLUCOCOTICOID PRODRRUG FOR THE TREATMENT OF LUPUS NEPHRITIS

Xiaobei Wang, Ph.D candidate

University of Nebraska Medical Center, 2018

Supervisor: Dong Wang, Ph.D.

Nephritis is one of the major complications of systemic lupus erythematosus (SLE). While glucocorticoids (GC) are frequently used as the first line treatment for lupus nephritis, long-term GC usage is often complicated by severe adverse effects. To address this challenge, we have developed a polyethylene glycol (PEG)-based macromolecular prodrug (ZSJ-0228) of dexamethasone, which self-assembles into micelles in aqueous media. When compared to the dose equivalent daily dexamethasone 21-phosphate disodium (Dex) treatment, monthly intravenous administration of ZSJ-0228 for two months significantly improved the survival of lupus-prone NZB/W F1 mice and was much more effective in normalizing proteinuria, with clear histological evidence of nephritis resolution. Different from the dose equivalent daily Dex treatment, monthly ZSJ-0228 administration has no impact on the serum anti-double-stranded DNA (anti-dsDNA) antibody level but can significantly reduce renal immune complex deposition. No significant systemic toxicities of GC (e.g. total IgG reduction, adrenal gland atrophy and osteopenia, *etc*.) were found to associate with ZSJ-0228 treatment. *In vivo* imaging, flow cytometry and pharmacokinetic studies reveal that the fluorescent or ^{125}I-labeled ZSJ-0228 primarily distributes to the

inflamed kidney after systemic administration, with renal myeloid cells and proximal tubular epithelial cells mainly responsible for its kidney retention. Collectively, these data suggest that the potent local anti-inflammatory/immunosuppressive effects and improved safety of ZSJ-0228 may be attributed to its tropism and cellular sequestration in the kidney. Pending further optimization, ZSJ-0228 may be developed into an effective and safe therapy for improved clinical management of lupus nephritis.

TABLE OF CONTENTS

LIST OF FIGURES

LIST OF ABBREVIATIONS

ACCESS ..... Abatacept and Cyclophosphamide Combination Therapy for Lupus Nephritis

ACN ..... acetonitrile

ACR ..... American College of Rheumatology

APC ..... antigen-presenting cell

AUC ..... area under curve

AuNCs ..... gold nanoclusters

BLys ..... B lymphocyte stimulator

BMD ..... bone mineral density

BV/TV ..... bone volume/tissue volume

CIA ..... collagen-induced arthritis

C_{max} ..... the maximum concentration

CMC ..... Critical Micelle Concentration

DCC ..... N, N'-Dicyclohexylcarbodiimide

DCM ..... dichloromethane

Dex ..... Dexamethasone 21-phosphate disodium

D_h ..... hydrodynamic diameter

DLS ..... dynamic light scattering

DMAP 4-dimethylaminopyridine

DMF ..... dimethylformamide

dsDNA ..... double stranded DNA

ELISA ..... enzyme-linked immunosorbent assay

ELVIS ..... Extravasation through Leaky Vasculature and subsequent Inflammatory cell-mediated Sequestration

ESRD ..... end-stage renal disease

EXPLORER ..... Exploratory Phase II/III SLE Evaluation of Rituximab

FcR ..... Fc receptor

GC ..... glucocorticoid

GR ..... glucocorticoid receptor

H&E ..... hematoxylin and eosin

HOBt ..... hydroxybenzotriazole

HPA ..... hypothalamic-pituitary-adrenal

HPMA ..... N-(2-hydroxypropyl) methacrylamide

IS ..... internal standard

LN ..... lupus nephritis

LPS ..... lipopolysaccharide

LUNAR ..... Lupus Nephritis Assessment with Rituximab

MCP-1 ..... monocyte protein-1

mPEG..... methoxy polyethylene glycol

MPS ..... mononuclear phagocyte system

MRT ..... mean residence time

MS..... multiple Sclerosis

MTT.....3-[4, 5-dimethylthiazol-2-yl]-2, 5 diphenyltetrazolium bromide

MW..... molecular weight

NF-κB..... nuclear factor-κB

NET..... neutrophil extracellular trap

NIRF..... *In vivo* near-infrared fluorescence

NTA..... Nanoparticle Tracking Analysis

PAS..... Periodic Acid-Schiff

PDCs.....plasmacytoid dendritic cells

P-Dex ..... (HPMA) copolymer-based dexamethasone conjugate

PDI ..... polydispersity index

PEG ..... polyethylene

PK/BD ..... Pharmacokinetics/biodistribution

RA .....rheumatoid arthritis

ROI.....region of interest

ROS ..... reactive oxygen species

RPTEC.....renal proximal tubule epithelial cell

SEGRM..... Selective glucocorticoid receptor modulator

SLE ..... Systemic Lupus Erythematosus

SLEDAI ..... Systemic Lupus Erythematosus Disease Activity Index

T2T..... treat to target

TBAF.....tetra-n-butylammonium fluoride

TBS ..... tert-butyldimethylsilyl

TBSC.....tert-butyldimethylsilyl chloride

TEM ..... transmission electron microscope

T_H cell.....T helper cell

WBC.....white blood cell

ZSJ-0228.....polyethylene glycol (PEG)-based macromolecular prodrug

CHAPTER I. CURRENT TREATMENT OF LUPUS NEPHRITIS

1.1 Introduction

Systemic lupus erythematosus (SLE) is a severe chronic autoimmune disease with no cure. The hallmark of SLE is the presence of anti-double-stranded (ds) DNA antibodies depositing on the basement membranes of organs and tissues, including; kidney, joint, skin, pericardium, brain, lung and blood vessels. The prevalence of SLE is increasing, probably due to the identification of milder cases and improved survival rate. In the United States, approximately 1.5 million people are SLE sufferers.[1] According to the American College of Rheumatology, 90% of SLE patients are women of childbearing age.[2] People of African, Hispanic, or Asian tend to have a raised prevalence of lupus.[3] Findings from the Euro-lupus project-a prospective cohort study of 1000 patients with lupus followed up from 1991-showed significantly higher risk of lupus nephritis and a greater mortality rate in children than in patients who develop the disease as adults.[4]

Lupus nephritis is one of the most serious complications of SLE. It can be defined by the clinical picture, together with the inflammatory damage to nephrons in the context of SLE. The disease is initiated by immune complex deposition on the basement membranes of glomeruli, which triggers immune events including; activation of complement[5], binding of Fc receptors on neutrophils and

macrophages,[6] recruitment of inflammatory cells, and finally fibrosis. Lupus nephritis contributes directly to morbidity and mortality of SLE patients due to difficulty in the early recognition of renal disease and its poor prognosis. Only 25 to 50% of lupus patients show proteinuria or other abnormalities of renal function in the early course, although up to 60% of adults and 80% of children may develop overt renal disease later.[7] In the United States, lupus nephritis affects 30% of adults and 70% of children with SLE. Lupus nephritis is a major cause of end-stage renal disease (ESRD),[8] and the incidence of ESRD in SLE is increasing in the USA.[9, 10]

1.2 Pathogenesis of Lupus Nephritis

The pathogenesis of lupus is multifaceted and encompasses deregulation in adaptive as well as innate immune responses.[11-14] Immune complex accumulation in the kidney is the hallmark of lupus nephritis and triggers a series of events that results in kidney inflammation and injury. Numerous hypotheses have been proposed to explain the mechanism of glomerular immune complex accumulation, including the deposition of immune complexes from the circulating blood,[6] and the circulating nephritogenic antichromatin antibodies recognizing the glomerular basement membrane-associated chromatin fragments derived from apoptotic intraglomerular cells.[15] The latter hypothesis has been validated by recent reports for both murine[15, 16] and human lupus nephritis.[17-21]

Lupus nephritis is a highly heterogeneous disease which can be driven by different pathogenic mechanisms. It is initiated by the immune complex deposition on the glomerular basement membrane which triggers a cascade of inflammatory mediators activation (including Fc receptors[6] and complement[22]), inflammatory cell recruitment and eventual renal fibrosis. As the disease progresses, both innate and acquired immune pathways will be activated and cross-react to create interacting networks which makes it increasingly difficult to regulate.[23]

Intrarenal immune complexes, especially those involving IgG1 and IgG3 autoantibodies, can activate complement and recruit leukocytes to nephritic kidneys via the complement C3a and C5a, resulting in complement-mediated kidney damage observed in both murine and human lupus nephritis.[24-31] The recruited leucocytes and residential kidney cells both produce proinflammatory cytokines and chemokines in response to immune complexes and complement fragments. A typical example is the Increased serum IFN-α levels observed in lupus patients.[32] In lupus nephritis, circulating plasmacytoid dendritic cells (pDCs) accumulate in the kidneys and increase the renal levels of IFN-α upon activation by renal immune complexes.[33, 34] The IFN-α serum levels correlate with lupus activity and signs of immune activation.[35] IFN-α induces the maturation of conventional dendritic cells into potent antigen-presenting cells

(APC),[36] facilitates B-cell activation,[37] and promotes the development of $CD4^+$ T helper cells (T_H cells)[38] and $CD8^+$ memory T cells.[39] Recent work has uncovered aberrant expansion and dysregulation of several T_H effector subsets, including T_H-17 and T_H-1 cells, in lupus.[40-43] One of the critical mechanisms by which these effector T_H subsets contribute to lupus is via the production of cytokines, including IL-12, IL-21, and IFN-γ.[44-46] Aberrant activation of innate immune cells such as dendritic cells, macrophages, and neutrophils has also been associated with lupus pathogenesis.[47-51] Neutrophils and macrophages are recruited to the inflamed kidney and cause the direct renal injury through secreting proteolytic enzymes and oxygen radicals. Neutrophil debris may further contribute to lupus nephritis via releasing neutrophil extracellular traps (NETs), which can bind to the antichromatin autoantibodies [52-54]. Moreover, NETs can promote pDCs secretion of IFN-α [52], thereby amplifying the autoimmune activity.

In addition to circulating autoantibodies, immune complexes can also be produced within the renal parenchyma, where T and B cells aggregate and form ectopic lymphoid tissue, in the tubulointerstitial compartment [55, 56]. Interstitial plasma cells within the ectopic lymphoid tissue can produce autoantibodies in a clonally restricted fashion [57, 58], which may be an explanation for kidney-specific autoimmunity, and has been confirmed in a recent report showing that interstitial nephritis occurs in the complete absence of circulating

immunoglobulins in a murine lupus model [59]. Similarly, human pauci-immune nephritis has been observed in the lupus patients [60].

Collectively, the pathogenesis of lupus nephritis can be summarized as an inflammatory response to immune complexes in the kidneys. A cascade of inflammatory events, including complement activation, leukocyte infiltration, cytokine release from leukocytes and intrinsic kidney cells, renal parenchymalinjury and renal fibrosis amplify the renal inflammation via a series of positive-feedback loops. Inflammatory injury in kidneys results in the apoptosis and necrosis of intrinsic kidney cells, which is the source of the autoantigens. These autoantigens may cause intrarenal production of kidney-specific autoantibodies in the presence of infiltrated APCs, T cells, IFN-α and other cytokines. Therefore, treatment regimen should focus on firstly diminishing inflammation in active lupus nephritis to preserve renal parenchyma, followed by suppressing kidney-specific autoimmunity to prevent the reactivation of lupus nephritis.

1.3 Anti-inflammatory Therapies

As lupus nephritis is a severe manifestation of SLE, usually accompanied by end-stage kidney disease or renal replacement challenges, glucocorticoids plus an immunosuppressive has been the standard therapy for severe lupus nephritis.

Since the 1980s, some novel biologics or small molecules were found useful in the inflammation control.

Glucocorticoids (GCs). Among these treatment options, GC is one of the most potent and widely used drugs for lupus. It is naturally produced by the adrenal gland and its therapeutic effect is activated through binding to GC receptor (GR). In American College of Rheumatology (ACR)'s new guidelines for clinical management of lupus nephritis [2], the recommended treatment regimen consists of a pulse GC treatment followed by low/high-dose daily GC plus an immunosuppressive medication. Compared to the previous guidelines [61], the major change is that new immunosuppressants (e.g. mycophenolate mofetil) have been added as alternatives to cyclophosphamide due to concerns regarding the adverse effects of this immunosuppressive agent including; leukopenia, alopecia, vulnerability to infections, gonadal toxicity, haemorrhagic cystitis, uroepithelial tumors and an increased incidence of other malignancies [62]. However, no alternatives have been recommended for GC. The ACR guidelines recommend treatment with three pulses of intravenous methylprednisolone for all lupus nephritis patients [2]. In current clinical practice, oral prednisone or prednisolone is generally commenced at a dose of 0.7–1.0 mg/kg body weight daily, and reduced by 2.5–5.0 mg every 2 weeks until the long-term maintenance dose of 5.0–7.5 mg daily is achieved [62].

Laquinimod. Laquinimod is a small molecular derivative of quinolone-3-carboxamide. It has been investigated as an oral therapy for multiple sclerosis (MS) in two Phase II trials, and has completed a Phase II trial in lupus nephritis (clinical trial NCT01085097 at www.clinicaltrials.gov). Laquinimod seems to be able to reduce MS activity as an anti-inflammatory agent through decreasing the infiltration of monocytes into the central nervous system (CNS), and reducing proinflammatory cytokine and transcription factor expression, such as monocyte protein 1 (MCP-1) and nuclear factor-κB (NF-κB) [63, 64]. Suppression of inflammatory cytokine and chemokine genes and lower expression of NF-κB has been observed in the leukocytes and dendritic cells of healthy or MS patients treated with laquinimod. Even though Phase III studies for MS (clinical trial NCT00509145 at www.clinicaltrials.gov) have been shown to not significantly reduce relapses in MS among patients beyond a placebo, it proved oral administered once daily with laquinimod slowed the progression of disability and decreased the relapse rate in patients with relapsing-remitting MS [65].

Tocilizumab and Sirukumab (Anti-IL-6). IL-6 is a multifunctional cytokine produced by leukocytes as well as residential kidney cells that contributes to autoimmunity by stimulating B-cell differentiation and maturation, $CD8^+$ T-cell differentiation, autoantibody secretion, and renal mesangial cell proliferation [66-68]. Accumulating evidence supports a pivotal role of IL-6 in murine and human lupus nephritis. NZB/W F1 mice administered recombinant human IL-6 demonstrated an accelerated and severe form of membranoproliferative

glomerulonephritis [66, 69]. While administration of anti-IL-6 receptor antibody significantly attenuated proteinuria and prolonged the lifespan of NZB/W lupus mice, with only one out of ten dying from severe proteinuria [70]. IL-6 levels were increased in serum, urine, and glomeruli of mice and humans with SLE, and correlated with autoimmune activity [71, 72]. Toculizumab is a humanized monoclonal anti-IL-6 antibody (clinical trial NCT00046774, www.clinicaltrials.gov). A Phase I clinical trial in lupus patients evaluated the safety and efficacy of toculizumab. Sirukumab, another humanized monoclonal antibody against IL-6, is presently undergoing a Phase II clinical trial to demonstrate its safety and tolerability in lupus nephritis (clinical trial NCT01273389, www.clinicaltrials.gov). However, due to the multi-functional attributes of IL-6in inflammation, cell proliferation, and autoimmunity, it is difficult to determine therapeutic targets in the proper treatment phase, which may arise the inflammatory disorder if improperly used.

Eculizumab (Anti-C5). Eculizumab is a fully humanized recombinant IgG2/IgG4 monoclonal antibody against human complement fragment C5. It blocks the conversion of C5 to C5a and C5b, thereby preventing formation of the membrane attack complex (C5b-9) and the chemotactic fragment C5a. Although eculizumab is only approved for the treatment of paroxysmal nocturnal hemoglobinuria and atypical hemolytic uremic syndrome [73], it is conceivable that eculizumab could prevent direct complement-mediated injury to residential glomerular cells and reduce renal inflammation via diminishing renal leukocyte infiltration in lupus

nephritis. So far, it has been shown to be safe and tolerated in a Phase I trial in SLE [74].

1.4 Anti-autoimmunity Therapies

Rontalizumab and Sifalimumab (Anti-IFN-α). Rontalizumab and sifalimumab are humanized antibodies against IFN-α. Given IFN-α's critical roles in dendritic cell maturation, B-cell activation and T-cell development, it is a good strategy to neutralize the activity of IFN-α to prevent further disease flares. In a recent study of endogenous anti-IFN-α autoantibodies decreasing the IFN-α levels and SLE activity, 22% of 49 SLE patients were found to have naturally produced anti-IFN-α autoantibodies and a lower IFN-α gene signature than patients without such antibodies [75]. Patients with higher levels of anti-IFN-α autoantibodies and lower IFN-α gene signature were inclined to have less positive lupus serologic test results, lower SLEDAI (Systemic Lupus Erythematosus Disease Activity Index) score, and higher complement levels. Additionally, ~35% of these SLE patients with low IFN-α gene signature did not have anti-IFN-α autoantibodies, indicating that exogenous anti-IFN-α therapy might not benefit all patients. The safety and efficacy of rontalizumab and sifalimumab has been tested in three small Phase I studies with SLE patients having only mild or moderate disease [76-78]. In general, rontalizumab and sifalimumab inhibited the gene signature in a dose-dependent manner. However, the inhibitory effect was short lived and did not completely

reverse the expression of IFN-α genes. In the clinical trial of rontalizumab, neither the protein levels of IFN-α genes nor the levels of anti-IFN-α autoantibodies was decreased after therapy [76].

Belimumab (Anti-BLyS/BAFF). The B lymphocyte stimulator (BLyS, also termed BAFF) family is essential for B-cell development, selection and homeostasis. Mice genetically knocked out of BLys show the deficiency of mature B cells and immunoglobulin levels [79]. In contrast, overexpression of BLyS observed in transgenic mice and human SLE results in B-cell expansion and autoimmunity [80-82]. Belimumab, a fully humanized monoclonal anti-BLyS/BAFF antibody, can cause depletion of circulating B cells. Preliminary results from a Phase III study in SLE patients without lupus nephritis have demonstrated depleted peripheral B cells within 3-6 months with limited effects on memory B cells and plasmablasts. Patients who received belimumab plus standard care have shown an improved clinical manifestation, including prevention of disease flares compared to the placebo group over 52 weeks [83]. However, whether chronic B-cell depletion caused by the belimumab treatment will induce homeostatic expansion of autoreactive memory B cells and whether belimumab has an effect on B-cell selection over time needs to be further determined.

Cyclophosphamide and Mycophenolate Mofetil. Both of cyclophosphamide and mycophenolate mofetil are used as immunosuppression reagents targeting

activated lymphocytes. Glucocorticoids plus cyclophosphamide as standard induction therapy for severe proliferative lupus nephritis was recommended by the ACR guidelines published in 1999 [61]. However, outcomes after broad-spectrum immunosuppressive therapy remain unsatisfactory. In a comparison trial, cyclophosphamide and mycophenolate mofetil were equivalent in the induction of remission of lupus nephritis, with complete remission rates of 50% [84]. Clinical trials indicated combined treatment with cyclophosphamide and glucocorticoids correlated with an increased incidence of adverse effects and significantly higher mortality (18.2%, versus 3.7% in patients treated with glucocorticoids alone) when compared to glucocorticoids alone [85-87], even though the combined therapy was more effective in maintaining disease quiescence and improving renal outcomes [85, 86, 88]. Given the accumulating concerns regarding the adverse effects of cyclophosphamide, novel therapies are being investigated to decrease cyclophosphamide exposure. Mycophenolate mofetil is a selective, reversible and noncompetitive inhibitor of lymphocyte proliferation and has been used in the prevention of renal allograft rejection, as well as in the therapy of glomerular disorders. The greater efficacy and reduced incidence of adverse effects including infections make mycophenolate mofetil an attractive candidate to in the treatment of lupus nephritis [89, 90]. However, mycophenolate mofetil cannot replace the combined administration of cyclophosphamide with glucocorticoids in the treatment of severe lupus nephritis [91].

Rituximab (B-cell directed therapies). Rituximab is a humanized/mouse chimeric monoclonal antibody against CD20, a cell surface molecule present on most B cells but not plasma cells. The rationale for Rituximab treatment on lupus nephritis is depletion of autoreactive B cells. While rituximab is B-cell selective, two large clinical trials, LUNAR (Lupus Nephritis Assessment with Rituximab) and EXPLORER (Exploratory Phase II/III SLE Evaluation of Rituximab), failed due to lack of efficacy on SLE and lupus nephritis when combined with standard-of-care treatment [92, 93]. The reasons for the failure is still debated, however, there are some caveats to rituximab treatment should be considered. Because plasma cells do not express CD20, rituximab does not cause an immediate elimination in autoantibody levels, which might be one of the reasons for failure. Yet, a decline of the existing autoreactive plasma cells will occur resulting from the B-cell depletion. Furthermore, rituximab may even promote autoreactive B cells. BLyS/BAFF levels increase as B cells are depleted in response to rituximab treatment [94, 95], which may elevate the production of new autoreactive B cells.

Abatacept (T-cell directed therapies). CD28:B7 costimulatory interaction, the most critical signal driving T-cell activation, can be blocked via CTLA4 binding to B7 on the surface of dendritic cells or B cells. Abatacept, a fusion protein between CTLA4 and IgG heavy chain components, can interfere CTLA4:B7 binding so as to inhibit T-cell activation. Abatacept has been tested in two randomized controlled trials in lupus nephritis as a combinational therapy to either low-dose cyclophosphamide (ACCESS [Abatacept and Cyclophosphamide Combination

Therapy for Lupus Nephritis] Trial, clinical trial NCT00774852, www.clinicaltrials.gov) or MMF (clinical trial NCT01714817, www.clinicaltrials.gov). Murine studies showed that abatacept plus low-dose cyclophosphamide induced complete lupus nephritis remission [96, 97]. However, abatacept did not improve complete renal response rates in either clinical trial [98].

1.5 Summary

In recent years, more novel bioagents were developed to treat lupus nephritis, one of the most severe complicates of SLE and can drive a high mortality rate if improper treated. However, none of them showed enhanced efficacy and meanwhile showing less toxicity. The optimal treatment approach of lupus nephritis is to suppress the acute inflammation to maintain the renal parenchyma followed by the anti-autoimmune therapy to prevent the subsequent renal injury caused by the infiltrated inflammatory cells. Amongst all the anti-inflammatory, GC is one of the most potent and widely used drugs for lupus. A pulse GC treatment followed by low/high-dose daily GC plus an immunosuppressive medication is still the standard-care recommended by American College of Rheumatology (ACR)'s new guidelines for clinical management of lupus nephritis. Recently, mycophenolate mofetil is suggested to be used as alternative to cyclophosphamide for its higher tolerance in the lupus

patient. No alternatives have been recommended for GC, especially for the serious lupus nephritis treatment.

As a hydrophobic small molecular drug, GC can disperse into multiple systems (including nervous, cardiovascular, musculoskeletal, endocrine systems), resulting in the notorious GC-associated side effects. These adverse side effects contribute significantly to morbidity in lupus patients. Therefore, it needs to be careful to use GC in the long-term management. The actions of GC are mediated through two distinct pathways: transactivation and transrepression, which are postulated to be related to GC-associated side effects and anti-inflammatory effects, respectively. Even though some GC receptor agonists can activate the transrepression pathway to treat inflammation, it is inevitable to trigger the transactivation responsible for the GC-related side effects due to the poor selectivity. Herein, instead of using GC receptor agonists, modifying GC's PK/BD profile in organs might be a wise strategy for the lupus nephritis treatment.

Nanomedicine is a growing area of research. Rather than looking for new molecular targets in autoimmune disease, nanomedicine-based drug delivery system is designed at enhancing the tissue selectivity by altering its pharmacokinetics and biodistribution. In the previous study, we conjugated dexamethasone to a water-soluble N-(2-hydroxypropyl)-methacrylamide (HPMA) copolymer via an acid-labile hydrazone linker to obtain a macromolecular prodrug

of Dex (P-Dex). The enhancing therapeutic efficacy of P-Dex was achieved compared to dexamethasone treatment. However, a relatively high accumulation of P-Dex in liver and other GC-related side effects such as adrenal gland atrophy and WBC reduction still existed. In this thesis, we have developed a novel PEG-based prodrug that can target dexamethasone to nephritic kidney, retain the potent efficacy and reduce the GC-associated side effects. The hypotheses to be tested are: (1) A novel PEG-based dexamethasone prodrug was synthesized and the micellar structure will be determined. (2) When tested in lupus nephritis animal models, the PEG-Dex demonstrates potent efficacy with significantly reduced/abolished side effects; and, (3) The mechanism of the superior efficacy and safety of PEG-Dex compared to Dex is elucidated via pharmacokinetics studies.

CHAPTER II

SYNTHESIS AND CHARACTERIZATION OF PEG-BASED DEXAMETHASONE PRODRUG

2.1 Introduction

Glucocorticoid is one of the oldest synthetic drugs in the modern medicine. It was purified from the adrenal gland by Edward C. Kendall in the 1930s. Since then, the synthesis of these chemical compounds in large quantities became possible, resulting in the first application of cortisone in the treatment of rheumatoid arthritis (RA) [99]. Furthermore, the administration routes of glucocorticoids have been developed, including oral; intravenous, topical and phosphate derivatives applied to enhance the solubility in aqueous solution [100].

A treat-to-target (T2T) strategy including a number of fundamental principles in the SLE management was recently recommended and published by a European panel [101]. Briefly, lupus treatment should achieve the goals of; long-term survival, prevention of organ damage, optimization of life quality by adequate disease activity control, reduction of comorbidities, and treatment-induced side effects. Although the prognosis can be dramatically improved by lupus nephritis management, the treatment is potentially toxic, complex, prolonged and difficult

to plan and carry out. A typical example is the use of glucocorticoids and cyclophosphamide as induction therapy for proliferative lupus nephritis recommended by the ACR guidelines published in 1999 [61]. It might be a superior therapeutic approach in particular populations, such as African-Americans, however, it is also potential to induce a high infection risk and organ-associated adverse effects. Due to the fact that the activated targets of these therapeutic agents *in vivo* are ubiquitously distributed throughout the body, the systemic administration may result in the activation of these drugs in undesired sites which brings up the toxicities. Hence, the question of how to develop a novel drug delivery system of glucocorticoids which can target the drugs to inflamed kidney(s) become the major challenges in modern medicine. To help address these hurdles, this section will offer a brief but broad overview in the current research of novel nanomedicine-based drug delivery system of glucocorticoids.

2.2 Materials & Methods

2.2.1 Materials & Instruments

Dexamethasone was obtained from Tianjin Pharmaceuticals Group Co., Ltd. (Tianjin, China). Dexamethasone 21-phosphate disodium (Dex) was purchased from Hawkins, Inc. (Minneapolis, MN, USA). Heterofunctional PEGs were purchased from Rapp Polymere GmbH (Tuebingen, Germany) and Creative

PEGWorks (Chapel Hill, NC, USA). Piperidine was purchased from Sigma-Aldrich (St. Louis, MO, USA). Sephadex LH-20 resins were purchased from GE HealthCare (Piscataway, NJ, USA). IRDye 800CW NHS ester was purchased from LI-COR Biosciences (Lincoln, NE, USA). Alexa Fluor 488 NHS ester was obtained from Life Technologies (Carlsbad, CA, USA).

^{1}H and ^{13}C NMR spectra were recorded on a 500 MHz NMR spectrometer (Varian, Palo Alto, CA, USA). The mass spectrum analyses were performed with an LC/MS/MS system composed of an ACQUITY Ultra Performance LC (UPLC) system (Waters, Milford, MA, USA) and a mass spectrometer of Sciex 4000 Q TRAP with an ESI source (Applied Biosystems, Toronto, Canada). HPLC analyses were performed on an Agilent 1100 HPLC system (Agilent Technologies, Inc., Santa Clara, CA, USA) with a reverse phase C_{18} column (Phenomenex, Bondclone H16-441537-C18, 300×3.9 mm, 10 μm). The average hydrodynamic diameter, polydispersity index (PDI) and zeta potential of micelles were determined by dynamic light scattering (DLS) experiments using a Zetasizer Nano ZS90 (Malvern Instruments, Worcestershire, UK). The particle size distribution was analyzed using NS300 NanoSight (Malvern Instrument). The micelles morphology was observed using a Tecnai G2 Spirit transmission electron microscope (TEM) (FEI, Hillsboro, OR, USA) at an acceleration voltage of 100 kV.

2.2.2 The synthesis of ZSJ-0228 (Scheme 2)

The synthesis of compound 1. Imidazole (2.72 g, 40 mmol) and dexamethasone (7.84 g, 20 mmol) were dissolved in anhydrous N,N-dimethylformamide (DMF, 40 mL). After the solution was cooled to 0°C, tert-butyldimethylsilyl chloride (TBSCl, 3.3 g, 22 mmol) was added. The solution was maintained at 0°C for 3 hours and room temperature for 2 hours, with constant stirring. Ethyl acetate (100 mL) was then added and washed with brine (80 mL×4). The organic phase was separated and dried over $MgSO_4$. After removal of the solvent, the residue was purified with flash chromatography (ethyl acetate:hexane = 1:2) to produce compound 1 (9.98 g). Yield: 98.5%.

^{1}H NMR (500 MHz, DMSO-d6): δ (ppm) = 7.28 (d, J = 10.2 Hz, 1H), 6.22 (d, J = 10.2 Hz, 1H), 6.00 (s, 1H), 5.29 (s, 1H), 4.97 (s, 1H), 4.78 (d, J 2.61 (td, J = 13.6 Hz, 5.8 Hz, 1H), 2.36 (m, 2H), 2.11 (m, 2H), 1.76 (m, 1H), 1.62 (q, J = 11.8 Hz, 1H), 1.48 (s, 3H), 1.41 (d, J = 13.5 Hz, 1H), 1.33 (m, 1H), 1.06 (m, 1H), 0.88 (s, 9H), 0.87 (s, 3H), 0.77 (d, J = 7.2 Hz, 3H), 0.04 (s, 3H), 0.03 (s, 3H).

^{13}C NMR (125 MHz, DMSO-d6): δ (ppm) = 209.19, 185.45, 167.20, 152.94, 129.17, 124.29, 101.38 (d, J_{C-F} = 174 Hz), 90.52, 70.84 (d, J_{C-F} = 36.9 Hz), 68.14, 48.13 (d, J_{C-F} = 22.5 Hz), 47.65, 36.03, 35.33, 33.82 (d, J_{C-F} = 19.3 Hz), 32.09, 30.46, 27.42, 25.97, 23.11, 23.08, 18.34, 16.86, 15.38, -4.89, -5.04.

MS (ESI): m/z = 507.2 ($M + H^+$), calculated 506.3.

Synthesis of compound 2. NH_2NH_2 monohydrate (750 mg, 15 mmol) and compound 1 (2.53 g, 5 mmol) from the first step were dissolved in methanol (25 mL). After addition of acetic acid (60 mg, 1 mmol), the solution was stirred at room temperature for 5 hours. Ethyl acetate (100 mL) was then added and the solution was washed with brine (80 mL×4). The organic phase was separated and dried over $MgSO_4$. After solvent removal with rotary evaporation, the residue was purified with flash chromatography (ethyl acetate:hexane = 1:1) to produce compound 2 (1.14 g). Considering the recovery of unreacted compound 1 (1.24 g), we calculate the final yield at 85.8%. Because of the hydrazone bond formation, a mixture of two syn/anti configure isomers exist in the product. But they are indistinguishable on flash chromatography. The two isomers' molar ratio was determined to be 1.63:1 according to ^{1}H-NMR.

^{1}H NMR (500 MHz, DMSO-d6): δ (ppm) = 6.67 (d, J = 10.4 Hz, 0.38H), 6.39 (s, 0.62H), 6.28 (d, J = 10.4Hz, 0.38H), 6.23 (s, 2H), 6.03 (d, J = 11.5Hz, 0.62H), 5.98 (d, J = 11.5Hz, 0.62H), 5.76 (s, 0.38H), 5.09 (dd, J = 10.5Hz, 3.0Hz, 1H), 4.96 (s, 1H), 4.74 (d, J = 19.1Hz, 1H), 4.26 (d, J = 19.1Hz, 1H), 4.09 (m, 1H), 2.87 (m, 1H), 2.50 (m, 1H), 2.22 (m, 1H), 2.16 (m, 3H), 1.58 (m, 2H), 1.36 (s, 3H), 1.33 (d, J = 13.5 Hz, 1H), 1.26 (m, 1H), 1.02 (m, 1H), 0.85 (s, 9H), 0.81 (s, 3H), 0.74 (d, J = 7.2 Hz, 3H), 0.02 (s, 3H), 0.01 (s, 3H).

^{13}C NMR (125 MHz, DMSO-d6): δ (ppm) = 209.71, 170.98, 151.16, 144.73, 140.74, 140.62, 139.03, 132.91, 127.70, 121.61, 116.17, 110.81, 100.71 (d, J_{C-F} = 171.9 Hz), 100.50 (d, J_{C-F} = 171.9 Hz), 90.92, 90.87, 70.00 (d, J_{C-F} = 37.4 Hz),

69.93 (d, J_{C-F} = 37.3 Hz), 68.43, 60.29, 47.21 (d, J_{C-F} = 22.8 Hz), 47.05 (d, J_{C-F} = 22.8 Hz), 44.02, 36.41, 36.35, 35.62, 34.40 (d, J_{C-F} = 19.5 Hz), 34.36 (d, J_{C-F} = 19.5 Hz), 25.28, 25.24, 24.85, 24.82, 21.17, 18.58, 17.15, 15.63, 14.49, -4.67, -4.80.

MS (ESI): m/z = 521.5 ($M + H^+$), calculated: 520.3.

LC/MS: two peaks in the chromatography with the retention time at 5.74 min and 6.32 min were found with the same molecular weight at 521.356 (condition: A: 7.5 mM ammonium acetate; B: 95% MeOH and 5% Acetonitrile; A:B = 30:70).

Synthesis of compound 3. 4-Dimethylaminopyridine (DMAP, 201 mg, 1.65 mmol) and compound 2 (2.86 g, 5.5 mmol) were dissolved in anhydrous DMF (15 mL). After cooling to 0°C, Fmoc-glycine (2.12 g, 7.15 mmol) and dicyclohexylcarbodiimide (DCC, 1.70 g, 8.25 mmol) were added. The resulting solution was stirred at 0°C for 3 hours. Ethyl acetate (100 mL) was then added, and the solution was washed with brine (80 mL×4). The organic phase was separated and dried over MgSO4. After removal of the solvent, the residue was purified by flash chromatography (ethyl acetate/hexanes=1:1) to produce crude compound 3 (3.72 g). The yield is 84.5%. TLC indicates the presence of small amount of side products, which were difficult to separate. The crude product was used directly in the next reaction.

Synthesis of compound 4. Compound 3 (3.0 g, 3.75 mmol) was dissolved in dichloromethane (DCM, 10 mL) and then cooled to 0°C. After addition of piperidine (1 mL), the solution was stirred at 0°C for 3 hours. Ethyl acetate (100 mL) was then added and washed with brine (80 mL×3). The organic phase was separated and dried over MgSO4. After removal of the solvent, toluene (50 mL) was added and then evaporated to help remove the residue piperidine. After purification with flash chromatography (ethyl acetate followed by ethyl acetate:methanol = 2:1), 1.96 g of compound 4 was produced. The yield is calculated as 90.6%.

^{1}H NMR (500 MHz, DMSO-d6): δ (ppm) = 7.01 (d, J = 10.3Hz, 0.23H), 6.86 (d, J = 10.3Hz, 0.16H), 6.77 (s, 0.26H), 6.66 (d, J = 10.3Hz, 0.17H), 6.60 (d, J = 10.3Hz, 0.23), 6.59 (s, 0.25H), 6.46 (d, J = 10.3Hz, 0.26H), 6.41 (d, J = 10.3Hz, 0.26H), 6.28 (d, J = 10.3Hz, 0.25H), 6.19 (d, J = 10.3Hz, 0.26H), 6.02 (s, 0.16H), 5.92 (s, 0.20H), 5.21 (br, 1H), 4.98 (br, s, 1H) 4.77 (d, J = 19.0 Hz, 1H), 4.28 (d, J = 19.0Hz, 1H), 4.12 (m, 1.0H), 3.25 (s, 2H), 2.90 (m, 1H), 2.60 (m, 1H), 2.25 (m, 2H), 2.14 (m, 1H), 1.71 (m, 1H), 1.58 (m, 1H), 1.41 (d, J = 8.6Hz, 3H), 1.38 (d, J = 13.5Hz, 1H), 1.32 (m, 1H), 1.05 (m, 1H), 0.88 (s, 9H), 0.77 (d, J = 7.1Hz, 3H), 0.04 (s, 3H), 0.02 (s, 3H).

^{13}C NMR (125 MHz, DMSO-d6): δ (ppm) = 209.44, 174.80, 169.60, 157.62, 156.88, 152.11, 151.27, 146.38, 146.05,144.35, 143.81, 142.95, 139.56, 138.87, 126.74, 120.70, 116.73, 116.67, 111.46, 111.32, 100.98 (d, J_{C-F} = 173.4 Hz), 100.91 (d, J_{C-F} = 172.3 Hz), 100.76 (d, J_{C-F} = 173.4 Hz), 100.73 (d, J_{C-F} = 172.6

Hz), 90.72, 90.66, 70.13 (d, J_{C-F} = 37.4 Hz), 70.12 (d, J_{C-F} = 37.3 Hz), 68.28, 47.74, 47.49 (d, J_{C-F} = 21.5 Hz), 47.45 (d, J_{C-F} = 21.5 Hz), 47.23, 44.15, 43.77, 42.72, 36.22, 36.17, 34.10 (d, J_{C-F} = 19.5 Hz), 32.16, 31.19, 31.06, 30.20, 30.05, 27.58, 26.08, 24.55, 24.51, 24.19, 24.16, 24.10, 24.06, 18.45, 16.99, 15.52, 15.50, -4.79, -4.93.

MS (ESI): m/z = 578.3 ($M + H^+$), calculated: 577.3.

LC/MS: shows two peaks in the chromatography with the retention time at 3.91 min and 4.47 min were found with the same molecular weight at 578.347 (condition: A: 7.5 mM ammonium acetate, B: 95% MeOH and 5% Acetonitrile; A:B = 30:70).

Synthesis of compound 5. Compound 4 (444 mg, 0.768 mmol) was dissolved in anhydrous DMF (3 mL), followed by the addition of Fmoc-glutamic acid (135 mg, 0.366 mmol), HOBt (148 mg, 1.098 mmol) and DCC (226 mg, 1.098 mmol). The resulting solution was stirred at room temperature for 4 hours. Ethyl acetate (100 mL) was then added to the solution and washed with brine (80 mL×3). The organic phase was separated and dried over MgSO4. After the solvent removal, the residue was purified by flash chromatography (ethyl acetate:methanol =10:1) to afford crude compound 5 (471 mg). The yield is 86.5%. TLC indicates the presence of small amount of side products which were difficult to separate. The crude product was used directly in the next reaction.

Synthesis of compound 6. Compound 5 (450 mg, 0.3 mmol) was dissolved in DCM (4.5 mL) and cooled to 0°C. After addition of piperidine (1.5 mL), the resulting solution was stirred at 0°C for 3 hours. Ethyl acetate (100 mL) was then added and washed with brine (80 mL×3). The organic phase was separated and dried over MgSO4. After solvent removal, the residue was purified by flash chromatography (ethyl acetate followed by ethyl acetate:methanol = 3:1) to produce compound 6 (330 mg). The yield is 86.4%.

^{1}H NMR (500 MHz, DMSO-d6): δ (ppm) = 10.83 (m, 1.12H), 10.64 (m, 0.80H), 8.38 (m, 0.30H), 8.28 (m, 0.62H), 8.18 28 (m, 0.42H), 7.99 (m, 0.60H), 7.01 (m, 0.29H), 6.93 (m, 0.16H), 6.77 (s, 0.91H), 6.68 (s, 0.73H), 6.62 (m, 0.34H), 6.45 (m, 1.52H), 6.25 (m, 1.53H), 6.01 (s, 0.15H), 5.96 (0.31H), 5.17 (s, 1.0H), 5.15 (s, 1.0H), 4.95 (s, 2H), 4.77 (d, J = 19.1Hz, 2.0H), 4.28 (d, J = 19.1Hz, 2.0H), 4.19 (m, 0.53H), 3.95-4.15 (m, 4.91H), 3.70-3.90 (m, 1.68H), 3.26 (m, 1.54H), 2.90 (m, 2.15H), 2.55-2.75 (m, 3.93H), 2.15-2.35 (m, 5.23H), 2.05-2.15 (m, 5.04H), 1.87 (m, 1.10H), 1.72 (m, 3.07H), 1.59 (m, 2.23H), 1.41 (m, s, 6.87H), 1.31 (m, 3.38H), 1.05 (m, 1.99H), 0.87 (s, 18H), 0.85 (s, 6H), 0.77 (d, J = 6.9Hz), 0.03 (s, 6H), 0.02 (s, 6H)

MS (ESI): m/z = 1266.4 ($M + H^{+}$), calculated: 1265.7.

LC/MS: three peaks in the chromatography with the retention time at 5.07 min, 5.80 min and 6.54 were found with the same molecular weight of 1266.782 (condition: A: 7.5mM ammonium acetate, B: 95% MeOH and 5% Acetonitrile; A:B = 18:82).

Synthesis of ZSJ-0228. DCC (107 mg, 0.52 mmol), hydroxybenzotriazole (HOBt, 70.2 mg, 0.52 mmol) and mPEG-COOH (100 mg, 0.052 mmol) were dissolved in anhydrous DMF (3 mL) at room temperature and stirred for 1 hour. After addition of compound 6 (428 mg, 0.338 mmol), the solution was stirred at room temperature for 24 hours. LH-20 column was used to obtain the polymer fraction. After removal of the solvent, the polymeric residue was dissolved in tetra-n-butylammonium fluoride (TBAF, 1 M, 2 mL) and stirred for 2 hours. The resulting solution was again applied to LH-20 column to separate the polymeric fraction. After dialysis against DI water overnight (MWCO = 2 kDa), the solution was lyophilized to produce ZSJ-0228 (118.7 mg). The yield is 77.8%.

^{1}H NMR (500 MHz, DMSO-d6): δ (ppm) = 10.95 (s, 0.28H), 10.91 (s, 0.27H), 10.86 (s, 0.80H), 10.82 (s, 0.37H), 10.58 (m, 0.67H), 8.39 (m, 0.35H), 8.21 (s, 0.59H), 8.14 (m, 0.35H), 7.99 (m, 0.61H), 7.78 m, 0.30H), 7.71 (m, 0.69H), 7.54 (m, 0.1H), 7.02 (d, J = 10.3Hz, 0.53H), 6.90 (m, 0.26H), 6.78 (s, 0.69H), 6.60-6.71 (m, 1.25H), 6.42-6.47 (m, 1.14H), 6.27 (m, 0.41H), 6.21 (m, 0.73H), 6.00 (m, 0.26H), 5.96 (s, 0.53H), 5.14 (m, 1.98H), 4.93 (s, 1.85H), 4.66(m, 1.86H), 4.48

(dd, J = 19.2Hz, 5.8Hz, 1.80H), 4.40 (m, 0.67H), 4.34 (m, 0.40H), 4.00-4.25 (m, 6.66H), 3.92 (s, 2.55H), 3.86 (m, 0.52H), 3.83 (m, 0.36H), 3.51 (m, 183H), 3.25 (s, 3.24H), 2.93 (m, 1.92H), 2.63 (m, 1.43H), 2.36 (m, 0.66H), 2.20-2.35 (m, 5.71H), 2.05-2.15 (m, 4.46H), 1.97 (m, 1.45H), 1.84 (m, 1.16H), 1.71 (m, 2.15H), 1.60 (m, 2.48H), 1.42 (s, 7.95H), 1.31 (m, 2.55H), 1.23 (s, 1.07H), 1.05 (m, 2.12H), 0.84 (s, 6.00H), 0.77 (d, J = 7.1Hz, 5.74H).

MS (ESI): Two clusters of peaks were observed. One cluster is at around 1550, which are diion peaks. For example: n=44, calculated: $(M_{n=44} + 2Na^+)/2$ =1546.4, found 1546.7; n = 40, calculated: $(M_{n=40} + 2Na^+)/2$ = 1458.38, found 1458.3. The other cluster is at around 1100, which are triion peaks, n = 46 calculated $(M_{n=46} + 3Na^+)/3$ = 1068.0 found 1068.5.

MS (MALDI-TOF): One symmetric cluster of peaks (at about 3000) were observed, which represent the molecular weights of ZSJ-0228 plus sodium ion. For example: $M_{n=41}+Na^+$ = 2937.83, found 2938.28; $M_{n=43} + Na^+$ = 3025.84, found 3026.342; $M_{n=47} + Na^+$ = 3201.96, found 3202.425.

2.2.3 The Synthesis of Fluorescent-labeled ZSJ-0228

The synthetic routes for IRDye 800CW-, Alexa Fluor 488- and Alexa Fluor 647-labeled ZSJ-0228 are similar to the unlabeled ZSJ-0228 (Scheme 2), except the mPEG-COOH was replaced by Fmoc-NH-PEG-COOH. After Fmoc deprotection, the resulting NH_2-containing polymeric prodrug (100 mg) was dissolved in anhydrous DMF (1 mL) together with the NHS esters of IRDye 800CW (1 mg), Alexa Fluor 488 (1 mg) or Alexa Fluor 647 (1 mg). The solution was stirred at room temperature for 15 hours. After LH-20 column purification, fluorescent-labeled prodrugs were obtained. Using a Spectramax M2 Spectrofluorometer, the IRDye 800CW, Alexa Fluor 488 and Alexa Fluor 647 contents were determined as 126.94±0.75 μmol/g, 145.88±3.1 μmol/g and 85.13±1.49 μmol/g, respectively.

2.2.4 Critical Micelle Concentration (CMC) Analysis

Pyrene-based fluorescence probe method was used to determine the critical micelle concentration (CMC) of ZSJ-0228. For sample preparation, the stock solution of pyrene (0.02 mg/mL, in acetone) was added to a 96-well plate. After adding the aqueous solution of ZSJ-0228 at different concentrations to the wells, the plate was left at room temperature for 2 hours to allow acetone evaporation. The final pyrene concentration was maintained at 0.6 μM, which is slightly below its water solubility at room temperature. After transferring to a quartz 96-well plate, the fluorescence intensity was measured using a fluorescence microplate

spectrofluorometer. The excitation wavelength was set at 334 nm and the emission wavelength at 373 nm (I1) and 384 nm (I3). The ratio of fluorescence intensity I1/I3 was plotted against prodrug concentration to obtain the CMC value.[102]

2.2.5 Dynamic Light Scattering (DLS) Analysis

The hydrodynamic diameter (D_h), ζ-potential and polydispersity indices (PDI) of micelles were determined with a Malvern Zetasizer Nano-ZS at 25°C at 90° in triplicate. ZSJ-0228 were dissolved in ddH_2O at designed concentration, filtered through 20 µm syringe filter and vacuumed in the desiccator for 10 min to eliminate air bubbles before measurement. Data were analyzed by the Zetasizer software 7.12.

2.2.6 Nanoparticle Tracking Analysis (NTA)

The concentration and the size distribution of micelles were determined using an NS300 NanoSight with a low-volume flow cell plate and a 405 nm laser. The micelle solutions were pumped into the chamber using installed syringe pump. The measurements were conducted at room temperature, replicated five times

and further analyzed using NTA analytical software, version 3.2. Each video sequence was captured over 60 seconds.

2.2.7 Transmission Electron Microscope (TEM) Analysis

To understand the micelles morphology, transmission electronic microscopy (TEM) was used to visualize micelles at 80 kV. For sample preparation, one drop of the ZSJ-0228 micelle solution (2 mg/mL) was deposited on the formvar/silicone monoxide coated 200 mesh copper grids surface, and then dried overnight at room temperature. The analysis was performed at 25°C.

2.2.8 Drug Loading Measurement by HPLC

To quantify the dexamethasone content in ZSJ-0228, the prodrug was dissolved in HCl (0.5 mL, 0.1 N) and stirred overnight at room temperature. The sample (50 µL) was withdrawn and neutralized by addition of NaOH (50 µL, 0.1 N), then diluted in acetonitrile (ACN, 0.9 mL). The sample (in triplet) was analyzed using an Agilent 1100 HPLC system equipped with a reverse phase C_{18} column (Phenomenex, Bondclone H16-441537-C_{18}, 300×3.9 mm, 10 µm). Mobile phase: acetonitrile/water = 30/70; detection wavelength, 240 nm; flow rate, 1 mL/min;

Injection volume, 10 µL. The dexamethasone content in ZSJ-0228 was then calculated based on the HPLC analysis result.

2.2.9 *In Vitro* Release Profile of Dexamethasone

To understand the impact of pH values on the release of dexamethasone from ZSJ-0228, the prodrug (3 mg/mL) was dissolved in acetate buffers (pH = 4.5, 5.0, 6.5, and 7.4). Pluronic F127 (1 w/v % of buffer) was added as a surfactant to create the “sink” condition.[103] The micelle solutions were incubated at 37 °C with gentle agitation (60 r/min). At selected time points, the sampled releasing solution (0.1 mL) was neutralized with NaOH (0.1 N) and analyzed with HPLC in triplicate. The experiment was repeated three times in each pH buffer. The accumulative release of dexamethasone from ZSJ-0228 micelles was calculated according to the following equation, where 2 mL refers to the total volume of release medium, 0.1 mL is the sampling volume, and C_n refers to the concentration of dexamethasone at sampling time point *n*.

$$Cumulative\ release\ (wt\%) = \frac{2\ mL \times C_n + 0.1\ mL \times \sum_{i=1}^{n-1} C_i}{weight\ of\ dexamethasone\ in\ micelles} \times 100\%$$

2.2.10 Statistical Analysis

IBM SPSS 17.0 (IBM Corp., Armonk, NY, USA) or SAS 9.4 (SAS Institute, Cary, NC, USA) were used for statistical analyses in this study. Continuous outcomes were compared among $\geqslant$3 groups using the Analysis of Variance (ANOVA) or Kruskal-Wallis tests. Tukes post hoc t-test or Mann-Whitney U test with Bonferroni method for multiple comparisons were used for the pairwise comparisons.

2.3 Results

The main objective of this project is to develop a GC prodrug nanomedicine with organ/tissue specificity to LN. We hypothesize that such an approach would potentiate the GC's efficacy and reduce systemic toxicities. As shown in Scheme 1, the prodrug (ZSJ-0228) was designed by conjugating two dexamethasone molecules to a short methoxy polyethylene glycol's (mPEG, 1.9 kDa) chain terminus via a hydrazone/glycine/glutamate linker system. The apparent amphiphilicity of the prodrug allows its spontaneous self-assembly into micelles in aqueous media, rendering the hydrophobic dexamethasone water-soluble. According to the ELVIS mechanism, the systemically administered ZSJ-0228 would extravasate/filter at LN pathology, be sequestered by inflammatory cells and activated kidney cells, and subsequently release dexamethasone within the endosomal/lysosomal compartments (via the acid-cleavable hydrazone bond) to

exert its localized anti-inflammatory and immune-modulating effects without triggering systemic toxicities.

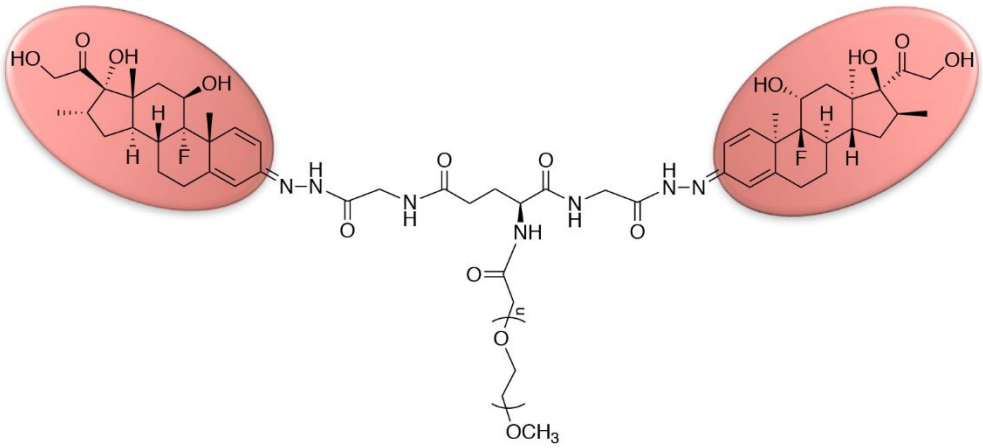

Scheme 1. The design of polyethylene glycol (PEG)-based amphiphilic dexamethasone prodrug ZSJ-0228, which can self-assemble into micelles in aqueous media. The oval shape highlights the dexamethasone structure.

2.3.1 The Synthesis of Amphiphilic Macromolecular Dexamethasone Prodrug (ZSJ-0228)

ZSJ-0228 was successfully synthesized according to the route illustrated in Scheme 2. The identity of the polymeric prodrug and the absence of free Dex were confirmed with NMR, MS, and LC-MS/MS. The multi-step synthesis is straightforward with high yield at each step. Tert-butyldimethylsilyl (TBS) was introduced in the first step to protect the 21-hydroxyl group and to improve solubility. The bulky presence of TBS sterically hinders access to the C-20

carbonyl group, resulting in the formation of hydrazone bond predominantly at the C-3, but not the C-20 carbonyl group. The presence of a local conjugation system also favors the C-3 hydrazone formation. Because of the use of hydrazone as the polymeric prodrug's activation trigger, multiple configure isomers of compound 6 were formed, which could not be separated chromatographically. Mass spectrum (negative ion ESI) of the isomer mixture showed the molecular ion $M+H^+$ at 1266.4 as a single peak (calculated molecular weight is 1265.7). After conjugation of compound 6 to mPEG-COOH, and the subsequent removal of the TBS protection, the prodrug ZSJ-0228 was prepared. The theoretical dexamethasone content in ZSJ-0228 is calculated as 26.7 wt%. After complete hydrolysis, HPLC analysis found 26.4 wt% of the prodrug we synthesized to be dexamethasone, suggesting a ~ 99% purity.

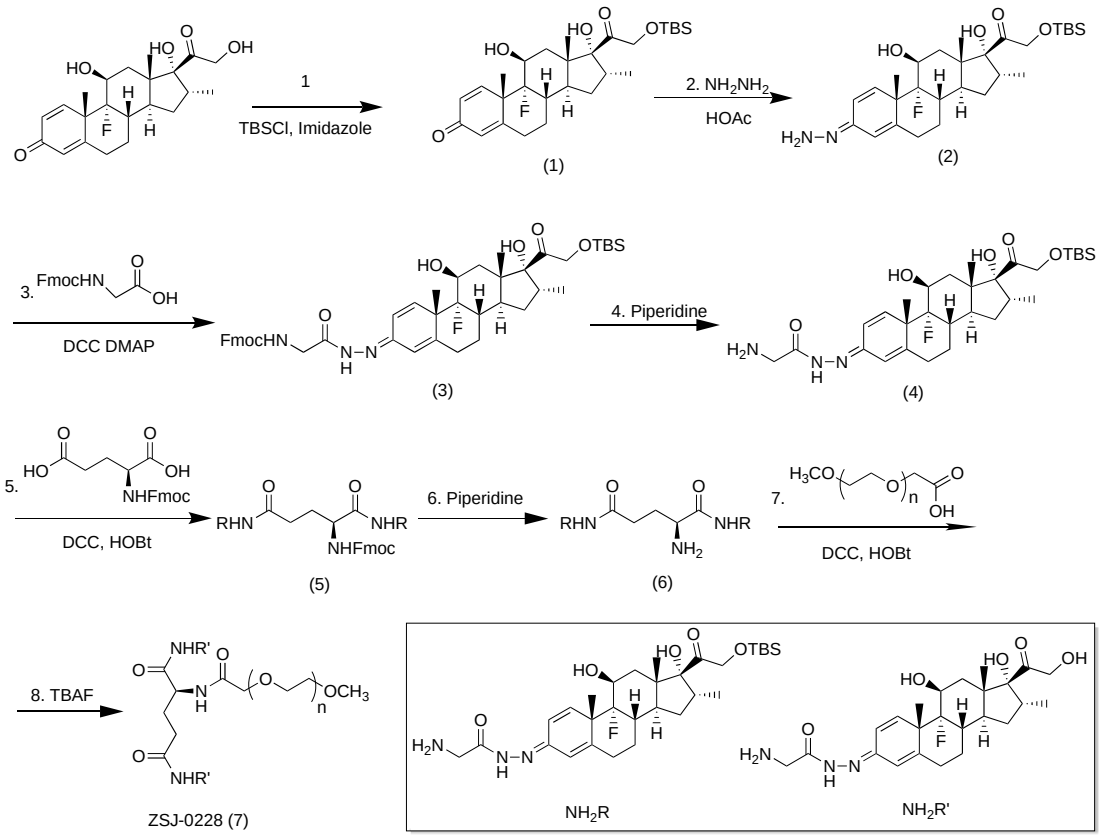

Scheme 2. The synthetic route for ZSJ-0228, a polyethylene glycol (PEG)-based amphiphilic dexamethasone prodrug. Reagents and conditions: 1. TBSCl (1.1 equiv), Imidazole (2.0 equiv), DMF, 0°C, 3h, r.t. 2h, 98.5%; 2. NH_2NH_2 (3.0 equiv), HOAc (0.2 equiv), MeOH, rt. 5h, 85.8% (brsm); 3. Fmoc-glycine (1.3 equiv), DCC (1.5 equiv), DMAP (0.3 equiv), DMF, 0°C, 3h, 84.5% (crude); 4. Piperidine (3 equiv), dichloromethane; 0°C, 3h, 90.6%; 5. Fmoc-glutamic acid (0.48 equiv), DCC (1.4 equiv), HOBt (1.4 equiv), DMF, rt., 4h, 86.5% (crude); 6. Piperidine (5 equiv), dichloromethane; 0°C, 3h, 86.4%; 7. M-PEG-COOH (0.15 equiv), DCC (1.5 equiv), HOBt (1.5 equiv), DMF, rt., 24h; 8. TBAF (20 equiv), THF, rt., 2h, 77.8% for two steps. TBSCl: tert-butylchlorodimethylsilane; DCC: N,N'-dicyclohexylcarbodiimide; HOAc: acetic acid; DMAP: 4-dimethylaminopyridine;

HOBt: 1-hydroxybenzotriazole; DMF: N,N-dimethylyformamide; TBAF: tetrabutylammonium fluoride; THF: tetrahedrofuran.

2.3.1 Characterization of ZSJ-0228 Micelles

As expected, the conjugation of hydrophobic dexamethasone dimer to the hydrophilic mPEG led to amphiphilic ZSJ-0228 prodrug's self-assembly into micelles upon direct dissolution in aqueous media. Using the pyrene-based fluorescence probe method, the critical micelle concentration (CMC) value of ZSJ-0228 was determined as 2.5×10^{-4} M. Dynamic light scattering (DLS) measurements (Figure 1A, Zetasizer Nano ZS90) revealed that the ZSJ-0228 can form micelles with an average micelle diameter of 33 nm and a net charge close to neutral. The DLS profile of the micelles was bimodal, suggesting the formation of heterogeneous particle populations. As shown in the transmission electron microscope (TEM) images, the micelles deposited on the substrate showed heterogeneity, with the majority of micelles showing the average diameter of ~30 nm (Figure 1C) and the minority having a larger average diameter of ~100 nm (Figure 1D). Nanoparticle Tracking Analysis (NTA, Nanosight NS300) was employed as an additional method to measure micelle size, distribution, and relative concentration. The NTA result (Figure 1B) seems to be in agreement with the DLS and TEM findings (as shown in Figure 1A, 1C, 1D), showing that the

diameter of micelles was mostly < 41 nm (90 %) with a small population around 100 nm (10 %, Figure 2B, insert).

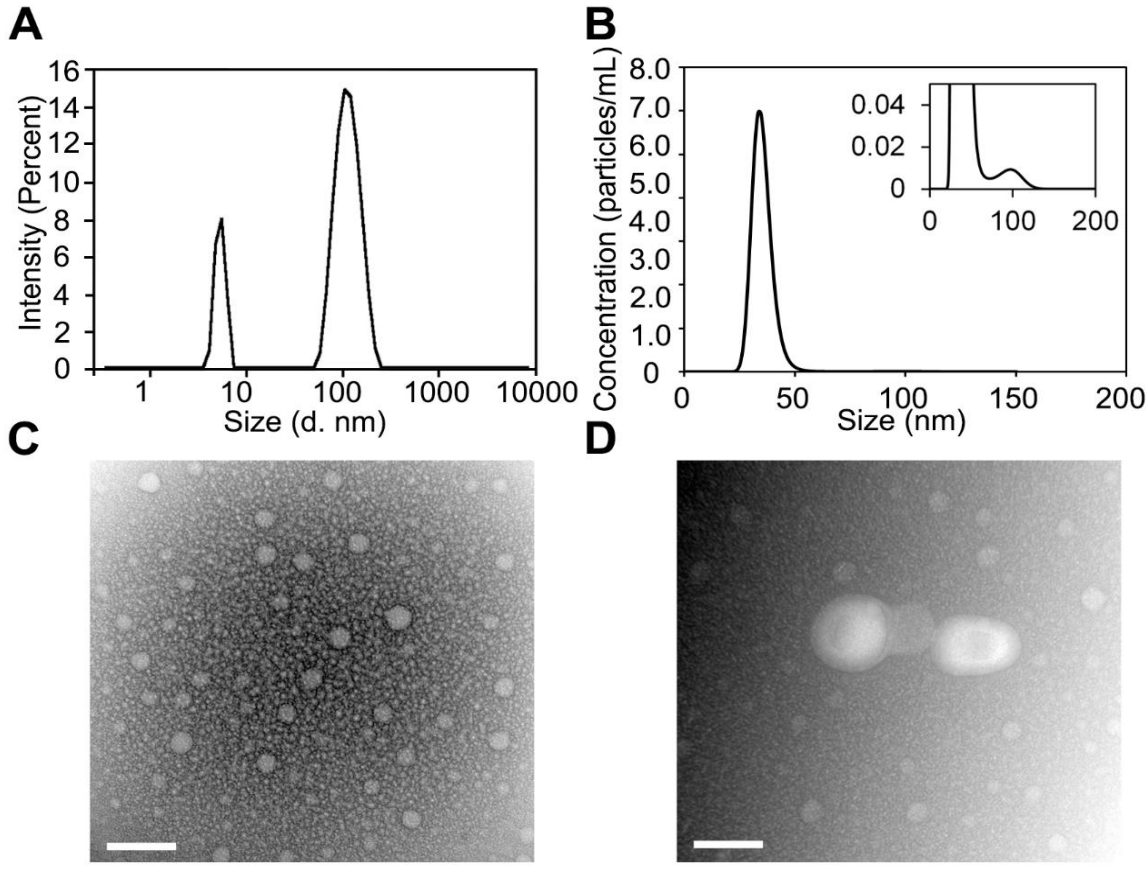

Figure 1. Characterization of ZSJ-0228 micelles. A. DLS profile of ZSJ-0228 micelles. The measurement was performed in triplicate. B. NTA measurement of ZSJ-0228 micelles. The measurements were repeated five times. C. Representative transmission electron microscope (TEM) image of ZSJ-0228 micelles. The average diameter of the micelles is estimated to be ~30 nm. D. Representative TEM image of larger ZSJ-0228 micelle population with the estimated average diameter of ~100 nm. Scale bar = 100 nm.

As the dexamethasone activation trigger, the hydrazone bond in the ZSJ-0228 design should only be cleaved under acidic environment. This was confirmed in an *in vitro* prodrug activation experiment (Figure 2) showing the near zero order release of the conjugated dexamethasone with an almost constant rate at ~1.32 %/day and 0.96 %/day for four weeks in the pH 4.5 and pH 5.0 acetate buffers, respectively. No dexamethasone release was detected in pH 6.5 and pH 7.4 buffers for the entire experiment duration.

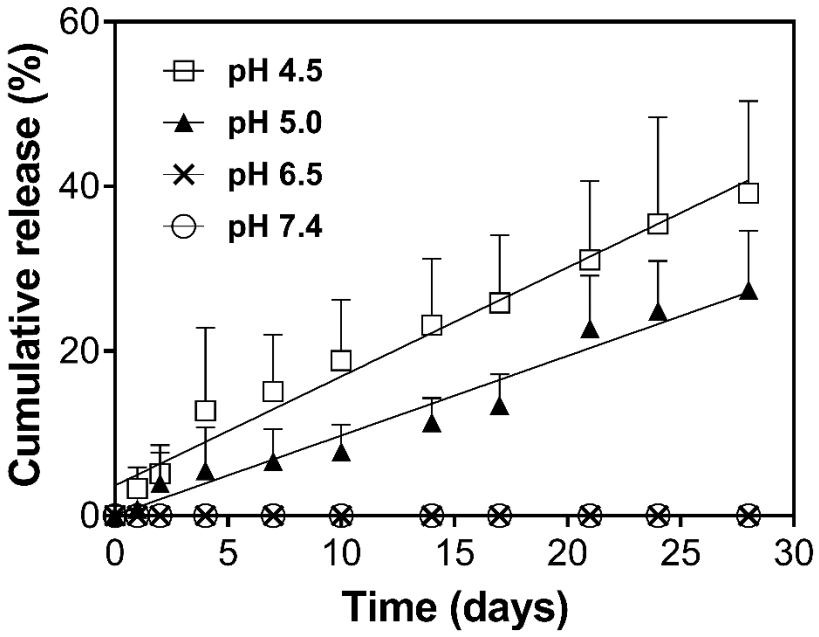

Figure 2. The *in vitro* release of dexamethasone from ZSJ-0228 at different pH values. The experiment was done in acetate buffer (pH 4.5 and 5.0) and phosphate buffer (pH 6.5 and 7.4) at 37°C. Pluronic F127 (1 wt% of

dexamethasone) was added to create the “sink” condition. Each experiment was performed in triplicate. Results are expressed as mean ± SD.

2.4 Discussions

Based upon ELVIS mechanism, we previously have developed a macromolecular prodrug of dexamethasone (P-Dex) using N-(2-hydroxypropyl) methacrylamide (HPMA) copolymer as the carrier. The prodrug was found to provide potent and long-lasting anti-inflammatory effect in multiple inflammatory disease models, including the NZB/W F1 LN mice.[104-108] Mechanistically, this pathophysiology-driven targeting of GC to nephritis is different from the active kidney-targeting drug delivery, [109, 110] in which different targeting ligands (e.g. peptides, sugar and folates, *etc*.) were employed to render the renal specificity.

While the therapeutic efficacy of P-Dex on the lupus model was strong and sustained, it could only circumvent osteopenia, but other GC toxicities (e.g. immunosuppression and adrenal gland atrophy, *etc*.) persist.[104] Optical imaging-based biodistribution studies and flow cytometry analyses of cells from all major tissues/organs suggest that the persisted side effects may be attributed to the prodrug’s internalization by circulating WBC and high-level deposition to the mononuclear phagocyte system (MPS, including phagocytic cells of liver and spleen). This hypothesis was partially supported by the amelioration of

splenomegaly in the P-Dex treated animals.[104] We posit that these off-target distributions and gradual activation of P-Dex may have led to the sustained presence of dexamethasone in the serum. While it may be at a low concentration and not enough to cause skeletal deterioration, the serum dexamethasone level can be sufficient to elicit systemic immunosuppression and adrenal gland atrophy.[111]

With these understandings, we proceeded to develop the next generation macromolecular GC prodrug, which is not only effective in resolving LN but also able to avoid typical GC adverse effects found with P-Dex. The focus of our effort was to further reduce dexamethasone levels in the serum by limiting the prodrug's sequestration by WBC and its deposition to the MPS.

Our previous findings suggest that the use of PEG as a prodrug carrier may significantly delay cellular internalization when compared to the use of HPMA copolymer carrier of the same size.[112] Therefore, we used PEG as the water-soluble drug carrier in the ZSJ-0228 design (Scheme 1). The selection of low molecular weight mPEG 1900 was based upon the prior findings that polymeric prodrugs with the lowest molecular weight demonstrate the highest kidney exposure and relatively lower liver deposition.[113, 114] PEG with a molecular weight of 0.4 or 1 kDa were not selected because they are mostly in wax or liquid form, which can be difficult to handle and purify during the synthesis. The

amphiphilic structure of ZSJ-0228 allows its self-assembly into micelles in aqueous media. Using DLS, TEM and NTA methods, we determined that the ZSJ-0228 micelle's average hydrodynamic diameter was around 30 nm, which may lead to a long serum half-life should the micelle remain stable.[115] The CMC value of the micelle, however, was determined to be relatively high (2.5×10^{-4} M). This type of micelle will disintegrate upon i.v. administration and dilution, significantly reducing its half-life in circulation. We anticipate that a shorter serum half-life of ZSJ-0228 would limit its distribution to the liver and spleen when compared to P-Dex,[113, 114] but still provide sufficient kidney exposure for therapeutic effects.

A hydrazone bond was used as the ZSJ-0228 prodrug's activation trigger. The linker's *in vitro* cleavage rate under acidic pH is relatively slow (Figure 2) when compared to other hydrazone linker-based prodrug designs.[116] Such slow activation kinetics may be explained by the presence of a large conjugation system, which involves four double bonds including two C=C bonds within the A ring of dexamethasone, one C=N bond, one C=O bond and the lone pair of SP2 electrons of the neighboring nitrogen. The large delocalization of electrons stabilizes the C-3 hydrazone and reduces the rate of C=N double bond cleavage which is responsible for the release of dexamethasone. When doxorubicin is conjugated to HPMA copolymer via hydrazone bond,[116] such structural stabilization does not exist. The slow *in vitro* hydrazone bond cleavage, however, does not necessarily predict a slow *in vivo* prodrug activation. Also contributing

to ZSJ-0228's *in vivo* activation is the pH value within lysosomal compartments, which can be significantly reduced under inflammatory conditions[117] and accelerate the hydrazone bond cleavage. Other biochemical factors, such as the elevated presence of reactive oxygen species (ROS), which is often associated with inflammatory pathologies,[118] may also be considered as a trigger for prodrug activation at inflammation.[119]

Due to the use of hydrazone as an activation trigger, ZSJ-0228 can have multiple isomers. Since the activation product from these isomers is the same (i.e. dexamethasone), and their ratio from different batches remains consistent, the presence of these isomers in ZSJ-0228 are not a concern during the preclinical Chemistry, Manufacturing, and Controls (CMC) development. Though not used in our synthesis, we are aware of the development of single molecular weight discrete PEG (dPEG), which has become commercially available. Different from traditional macromolecular prodrug design, the use of dPEG in the synthesis of ZSJ-0228 will produce a single molecular weight polymeric prodrug, which will further reduce potential regulatory hurdles during the product development.

2.5 Conclusions

A PEG-based dexamethasone prodrug was successfully synthesized. The amphiphilic molecule self-assembles into micelles. The chemical structure of

PEG-Dex and self-assembled micelles were fully characterized. The results demonstrated that PEG-Dex prodrug was successfully developed. Additionally, critical micellar concentration (CMC), DLS, and TEM results confirmed the micellar structure. Dexamethasone can be released in the acidic environment (pH4.5~5), which provided the fundamental preconditions for the lysosome-based controlled release in inflammatory kidney.

CHAPTER III

DEXAMETHASONE PRODRUG MICELLES ATTENUATES NEPHRITIS IN LUPUS-PRONE MICE WITHOUT APPARENT GLUCOCORTICOID SIDE EFFECTS

3.1 Introduction

Systemic lupus erythematosus (SLE) or lupus is a chronic complex autoimmune disease for which there is no cure. It is characterized by B and T cell hyperactivation, overproduction of autoantibodies, and the deposition of immune complexes in various tissues/organs. The symptoms of lupus among patients are highly heterogeneous, which may include skin rash, arthritis, pericarditis, neuropsychiatric disorders, and nephritis. The Lupus Foundation of America estimates that 1.5 million Americans, and at least five million people worldwide, have a form of lupus.[1] Lupus affects mostly women of childbearing age and has a significantly higher prevalence among African Americans.[120] According to a report by the U.S. Centers for Disease Control and Prevention in 2002, the death rates attributed to lupus have increased by approximately 70% over a 20-year period among African American women aged 45-64 years.[121]

Nephritis is one of the most damaging complications of lupus. It is the leading cause of morbidity and mortality among lupus patients. Around 35% adult lupus patients in the US have clinical evidence of nephritis at the time of diagnosis. An additional 15-25% patients will develop nephritis within ten years of their initial diagnosis.[2] Lupus nephritis (LN) is initiated by abnormal immune complex deposition on the basement membrane of renal glomeruli and the subsequent activation of the immune effector cells (e.g. macrophages and neutrophils), leading to damages of the renal tissues.[122] If not effectively managed, LN can progress rapidly to impair renal function, and eventually results in kidney failure.[123]

Among the limited treatment options,[124] glucocorticoid (GC) is one of the most potent and widely used classes of medication for lupus. According to the American College of Rheumatology (ACR)'s recent guidelines,[2, 61] a pulse GC treatment followed by low/high-dose daily GC plus an immunosuppressive are recommended as a standard treatment regimen for clinical management of LN.[125] Due to their potent anti-inflammatory efficacy and the lack of alternatives,[126, 127] GC continue to be the mainstay for clinical management of lupus symptoms.[2, 61] Some lupus pathologies, such as arthritis and skin rash can be effectively managed with short-term GC. Serious lupus complications, including progressive nephritis, however, necessitate long-term GC therapy, which is often associated with severe adverse events involving the musculoskeletal, endocrinal, hematopoietic, and cardiovascular systems.[128]

The diverse biological effects of GCs are thought to be mediated via transrepression, which elicits GC's anti-inflammatory effects; and transactivation, which is responsible for the GC-associated side effects.[129] Selective glucocorticoid receptor modulators (SEGRMs) that can preferentially activate the transrepression relative to the transactivation pathway have been developed.[130, 131] These compounds, however, do not exhibit strict pathway selectivity and still produce GC-related side effects.[129, 132]

Recognizing the therapeutic potential of GC in the clinical management of LN, their accompanying severe toxicities and the limited progress made in developing SEGRMs, we proposed to address this challenge through the development of a GC prodrug nanomedicine. Conceptually, this approach is based upon an inflammation targeting mechanism, which we discovered and termed as the "ELVIS".[133] It involves the Extravasation of the nanomedicine through Leaky Vasculature at inflammation, and its subsequent Inflammatory cell-mediated Sequestration, which would alter the pharmacokinetics/biodistribution (PK/BD) profile of the parent drug, enabling its inflammatory tissues/organs specificity. When tested in a spontaneous LN mouse model (female NZB/W F1 mice), the GC prodrug (ZSJ-0228) nanomedicine we developed demonstrated superior therapeutic efficacy than dose equivalent dexamethasone 21-phosphate disodium (Dex) in ameliorating nephritis and improving kidney functions, with no apparent GC toxicities.

3.2 Materials & Methods

3.2.1 Materials & Instruments

The MTT cell proliferation assay was purchased from ATCC (Manassas, VA, USA). Penicillin/streptomycin, Trypsin-EDTA, Dulbecco's PBS, and RPMI 1640 were from Gibco (Grand Island, NY, USA). Fetal bovine serum was purchased from BenchMark (Gemini Bio-Products, West Sacramento, CA). All solvents and other reagents if not specified were purchased from Fisher Scientific or ACROS and used without further purification.

In vivo near-infrared fluorescence (NIRF)-based optical imaging was accomplished on an LI-COR PearlTM Impulse Small Animal Imaging System (Lincoln, NE, USA). Bone qualities were analyzed using a high-resolution Skyscan 1172 micro-CT system (Bruker microCT, Kontich, Belgium). Digital images were acquired using a KeenView high-resolution camera and analyzed using Soft Imaging Solutions AnalySIS ITEM digital software. The quantification of fluorescence signal intensities of IRDye 800 CW, Alexa Fluor 488, Alexa Fluor 647 and pyrene were measured using Spectramax M2 spectrofluorometer (Molecular Devices, Sunnyvale, CA, USA). The flow cytometry experiments were performed on a BD LSRII Green flow cytometer (San Jose, CA, USA) and analyzed using FlowJo software (Treestar, Inc., San Carlos, CA, USA). Confocal

microscope images were acquired under an LSM 800 Zeiss Airyscan microscope (Carl Zeiss, Oberkochen, Germany) and analyzed using ZEN Lite software.

3.2.2 Experimental Animals and Drug Treatment

Beginning at twenty weeks of age, NZB/W F1 female mice (Jackson Laboratories, Bar Harbor, ME) were randomized into three groups (saline control, Dex and ZSJ-0228). The urine protein level was monitored weekly using Albustix Reagent Strips (Siemens Healthineers, Erlangen, Germany). Only mice with established nephritis, as evidenced by sustained albuminuria ($\geqslant$100 mg/dL) over two weeks, were enrolled in the study. ZSJ-0228 treatment (106 mg/kg, containing 28 mg/kg of dexamethasone, n = 10) and saline (n = 12) were administered as a monthly i.v. injection. A total of 2 injections of ZSJ-0228 were given during the two months treatment period. The Dex treatment (dexamethasone 21-phosphate disodium, 1.32 mg/kg, containing 1.00 mg/kg of dexamethasone, n = 11) was given as daily i.v. injection. All treatments continued for eight weeks. The body weight and proteinuria level of the animals were monitored weekly. Every four weeks, peripheral blood was sampled from the saphenous vein for serum analyses. Mice that developed severe proteinuria ($\geqslant$ 2000 mg/dL) or showed signs of distress (e.g. reduced mobility, weight loss > 20 %, edema, unkempt appearance) were sacrificed immediately. At two months post-treatment initiation, all surviving mice were euthanized by CO_2 asphyxiation,

with major tissues and organs isolated, weighted and processed at necropsy. The animal procedures were approved by the Institutional Animal Care and Use Committee (IACUC) of University of Nebraska Medical Center (UNMC).

3.2.3 Periodic Acid–Schiff (PAS) Staining and Pathological Scores

Paraffin sections from mouse kidneys were deparaffinized, rehydrated, washed with water, and stained with Periodic acid–Schiff (PAS) for evidence of glomerulonephritis by light microscopy. Glomerulonephritis was assessed by a pathologist (KWF) using a semi-quantitative 0-4 scale as described previously.[134] Briefly, a score of 0 represents healthy condition; a score of 1 represents mild focal disease; a score of 2 represents moderate focal disease; scores of 3 and 4 represent diffuse disease (namely severe glomerulonephritis). The scores of 0, 1, 2, 3 and 4 indicate that 0, 1-19, 20-50, 51-75, >75% of the glomeruli were affected. Fifty glomeruli per mouse were evaluated.

3.2.4 Immunohistochemistry Study

Immune complexes and macrophage infiltration were observed via immunohistochemistry. Rabbit anti-mouse IgG (Abcam) and rabbit anti-mouse F4/80 IgG (Abcam) were used as the primary antibodies. After deparaffinization

and rehydration, a rabbit specific HRP/DAB (ABC) detection IHC kit (Abcam) was applied. Briefly, the slides were first incubated in pH 6.0 citrate buffer (0.1 M), washed, and then incubated in H_2O_2. The slides were blocked and incubated with the primary antibodies. Antibody binding was visualized using the DAB chromogen. The staining intensity (represented as arbitrary gray units) of 50 glomeruli per mouse was quantified using Zeiss AxioVision software (version 4.6.3.0). Another set of slides stained for immune complexes and macrophages were counterstained with hematoxylin; these slides were used for illustration purposes only.

3.2.5 Immunofluorescence Study

For confocal microscopy, kidneys were dissected, fixed, dehydrated, and frozen in 2-methyl-butane in a dry ice bath. Sections (20 µm) were cut on a Bright's cryostat (Bright Instrument Co., Huntingdon, UK), thaw mounted onto slides, and stored at -80°C until stained. The sections were stained with anti-mouse CD11b (Santa Cruz), CD 133 and CD146 (Abcam), and then incubated with Alexa Fluor 488 labeled secondary antibody (Thermo Fisher Scientific, Bremen). Cells were visualized via immunofluorescence under a Zeiss LSM 800confocal microscope. The images were processed using Carl Zeiss Zen 2.3 software.

3.2.6 Analysis of Bone Quality

Femoral bone quality was analyzed using a Skyscan 1172 micro-CT system. The scanning parameters were set as the following: voltage 48 kV, current 187 μA, exposure time 620 msec, resolution 6.07 μm, and aluminum filter 0.5 mm. Three-dimensional reconstructions were achieved using NRecon and DataViewer software (Bruker micro-CT). A consistent polygonal region of interest (ROI) of trabecular bone at the distal femur, from 20 slices (0.25 mm) to 100 slices proximal (1.25 mm) to the growth plate, was selected for bone quality analysis. The mean bone mineral density (BMD), bone volume/tissue volume (BV/TV), trabecular number and thickness were quantified using Bruker CTAn software.

3.2.7 Analysis of Serum Immunoglobulin and Autoantibody Levels

Serum levels of immunoglobulin were assessed via enzyme-linked immunosorbent assay (ELISA). Total serum IgG levels were measured using a commercial ELISA kit (Innovation Research). Serum anti-dsDNA IgG levels were determined by ELISA (Alpha Diagnostic) as described previously.[106]

3.2.8 Near-infrared Optical Imaging

After the proteinuria was established, NZB/W F1 mice and NZW mice were given ZSJ-0228-IRDye (IRDye 800 CW dose at 148 nmol/kg, dexamethasone equivalent dose of 28 mg/kg) via tail vein injection. At selected time points (1 and 4-day post-injection), the mice were euthanized and perfused with saline. All major organs (i.e. heart, lung, liver, spleen, kidney and adrenal gland) were isolated and imaged using an LI-COR PearlTM Impulse imager. The two imaging time points (1 and 4-day post-injection) were selected to avoid the early dynamic distribution phase when the prodrug concentrations in different organs and tissues change dramatically in a short period of time. All images were collected under the channel of 800 nm with the same resolution (170 μm) settings.

3.2.9 Flow Cytometry Analysis

After the proteinuria was established, NZB/W F1 mice (n = 3 for each time point) and NZW mice (n = 5 for each time point) were given ZSJ-0228-AF647 (Alexa Fluor 647 dose at 300 nmol/kg, dexamethasone equivalent dose of 28 mg/kg) via tail vein injection. The animals were euthanized and perfused at 1 and 4-day post-administration. Blood, bone marrow, heart, lung, kidney, liver and spleen were harvested and processed to obtain single-cell suspensions. These cells were marked by the following antibodies: BV711-labeled anti-mouse CD11b, BV786-labeled anti-mouse CD3e, BUV395-labeled anti-mouse NK1.1, PerCP-Cy5.5 labeled-CD146, PE-Cy7-labeled CD19, BV510-labeled anti-mouse CD11c, APC-eFluor 780-labeled anti-mouse Ly-6G (BD Biosciences), APC-labeled anti-

mouse F4/80 and PE-labeled anti-mouse CD326 (eBioscience Inc.). The cells were analyzed using a BD LSR II Green flow cytometer with FlowJo software.

3.2.10 Cell Culture Study

The cell viability was quantified using the 3-[4, 5-dimethylthiazol-2-yl]-2, 5 diphenyltetrazolium bromide (MTT) cell proliferation assay from ATCC (Manassas, VA, USA). Briefly, human proximal tubule epithelial (HK-2) cells28 were seeded in 96-well plates (1×10^4 cells/well) overnight and treated with different concentrations of ZSJ-0228 (0.01 - 2000 μM dexamethasone equivalent), Dex (0.01 μM – 2000 μM dexamethasone equivalent) and mPEG (0.005 – 1000 μM ZSJ-0228 equivalent). PBS was used as a control. The cells were incubated for 24, 48 and 72 hours. At each time point, 10 μL MTT was added to each well and incubates at 37 ºC for 4 hours. MTT detergent reagent (100 μL/well) was added to dissolve the insoluble formazan, then incubated for 2 hours in dark at room temperature. A microplate reader (Fisherbrand™ accuSkan™ FC Filter-Based Microplate Photometer) was then used to measure the UV absorbance at 570nm and 660nm (reference wavelength). The cell viability results are presented as the percentage of PBS control (100 %).

3.2.11 *In Vitro* Internalization Kinetics Study

To investigate the internalization of Alexa Fluor 488-labeled ZSJ-0228 (ZSJ-0228-AF488), HK-2 cells were seeded on the 24-well plastic plate and incubated overnight with lipopolysaccharide (LPS, 10 μg/mL) to mimic the lupus nephritis condition. ZSJ-0228-AF488 (final concentration of 200 μg/mL) was added to LPS-stimulated HK-2 cells. The HK-2 cells without LPS treatment were used as control. At 1, 4, 24, 48 and 72-hours' time intervals, the cells were rinsed, fixed and analyzed by flow cytometry.

3.2.12 Immunocytochemistry Study

For the subcellular localization studies, HK-2 cells were cultured overnight with LPS and then incubated with ZSJ-0228-AF488 (200 μg/mL) for 24 hours on the cover clips in the 24-well plates. Cells were rinsed and incubated with LysoTracker DND-99 (Invitrogen, 75 nM) for 3 hours. Then the cells were rinsed, stained with DAPI, fixed, mounted, and observed under confocal microscope.

3.2.13 Statistical Analysis

IBM SPSS 17.0 (IBM Corp., Armonk, NY, USA) or SAS 9.4 (SAS Institute, Cary, NC, USA) were used for statistical analyses in this study. Continuous

outcomes were compared among ⩾3 groups using the Analysis of Variance (ANOVA) or Kruskal-Wallis tests. Tukey’s post hoc t-test or Mann-Whitney U test with Bonferroni method for multiple comparisons were used for the pairwise comparisons. The outcome of surviving rate was compared among three groups using Log-rank Mantel-Cox test. Multiple comparisons was corrected with Bonferroni’s method. The binary outcome of having proteinuria reading values of 2 and above at the 8-week time point was compared among three groups using the Fisher’s exact test. Bonferroni’s pairwise comparison was used to control for multiple testing. The generalized estimating equation (GEE) method was used to model the repeated measurements of a continuous outcome to account for the correlation within the subject. The GEE method is robust to the misspecification of the distribution of the outcome. Tukey’s pairwise comparison between groups was performed to control for multiple testing in the GEE model.

3.3 Results

3.3.1 ZSJ-0228 Effectively Ameliorated Proteinuria and Improved the Survival of NZB/W F1 Mice with Established Nephritis

The therapeutic effects of ZSJ-0228 were evaluated in NZB/W F1 female mice (~ 28 weeks old) with fully developed nephritis (proteinuria ⩾ 100 mg/dL for two

weeks). The mice were given two monthly intravenous injections of ZSJ-0228 (28 mg/kg, dexamethasone equivalent). Dose equivalent daily Dex (1 mg/kg, dexamethasone equivalent, i.v.) 18 and monthly saline administration (i.v.) were used as controls. At the end of two months, all animals were euthanized. As shown in Figure 3A, the mice in saline group maintained a 100% incident rate of proteinuria. Eight out of twelve mice (75 %) demonstrated increased proteinuria level over the course of the experiment, with albustix reading increased from 2 to 4. For the Dex treatment group, the level of proteinuria increased in 36% of the mice (albustix reading increased from 2 to 4) and was normalized in 18% of the mice (albustix reading decreased from 2 to 1), suggesting that the Dex treatment can partially impede LN progression. In the ZSJ-0228 treatment group, only one mouse showed an increased level of proteinuria, with albustix reading increased from 2 to 4. Three mice maintained the same level of proteinuria (albustix reading at 2). The levels of urine proteins for the rest of the mice (60%) was normalized, with albustix reading decreased to 0 or 1. This result is significantly better than the saline control ($P < 0.01$), suggesting that the prodrug treatment is very effective in the amelioration of LN.

ZSJ-0228 treated NZB/W F1 mice also showed a significantly better survival rate than the saline control mice ($P < 0.05$). Before the end of the treatment (mice at 36 weeks of age), a total of 42% of mice in the saline group died due to severe nephritis (Figure 3B). This is in general agreement with the literature reports of the median survival of saline-treated NZB/W F1 female mice (~ 35 weeks).[104,

134-136] In comparison, two out of eleven mice treated with Dex died, and all ZSJ-0228 treated mice survived. The apparent trend of ZSJ-0228 group's better survival rate than the Dex group did not reach statistical significance (P = 0.17). All deceased animals exhibited the highest level of proteinuria (albustix reading at 4) before death.

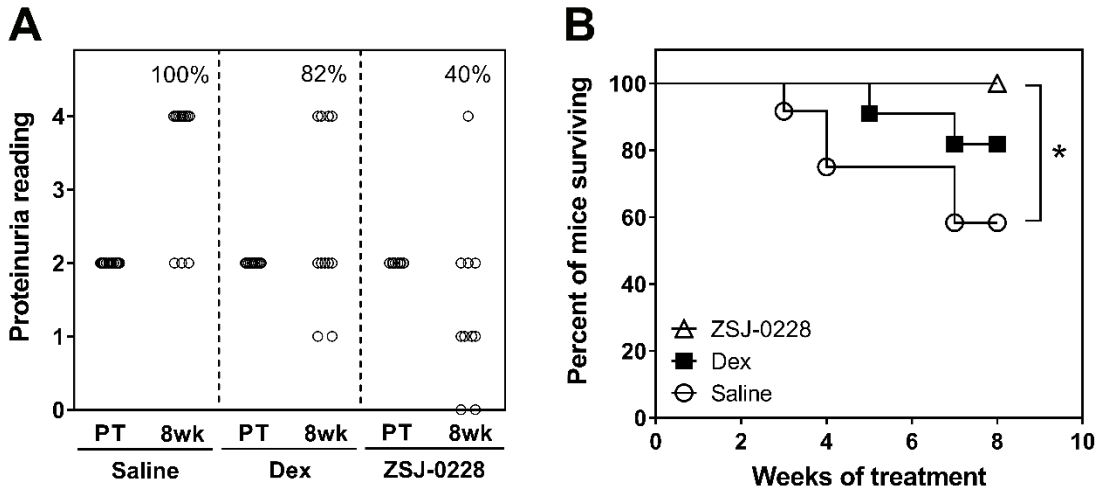

Figure 3. Monthly ZSJ-0228 treatment demonstrates superior therapeutic efficacy when compared to dose equivalent daily Dex treatment. A. Monthly ZSJ-0228 treatment normalized albuminuria among 60% of NZB/W F1 mice (with established nephritis), while dose equivalent daily Dex treatment only normalized 18 % at the end of 2-months treatment. PT = pretreatment. The percentages shown accounted for those animals with proteinuria reading value of 2 and above at the 8-week time point. Each data point represents an individual mouse. P = 0.003, Fisher's exact test. B. Kaplan-Meier survival curves for ZSJ-0228, Dex and saline treatment groups are shown. Only ZSJ-0228 treatment results in 100%

survival after two months treatment, which is significantly better than Saline control (*, $P < 0.05$). No significant difference between ZSJ-0228 and Dex groups was found ($P = 0.17$). Log-rank Mantel-Cox test with Bonferroni correction.

To further validate the superior therapeutic efficacy of ZSJ-0228, kidneys isolated at necropsy were sectioned, stained with Periodic acid–Schiff (PAS) and evaluated by a pathologist (KWF, who was blinded to the grouping arrangement). The tissue sections were graded using a histopathologic scoring system with a 4-point scale.[134] Compared to the ZSJ-0228-treated mice, more than 40% of saline and Dex-treated mice had a higher percentage of damaged glomeruli (scoring 3 and 4 points). Evidence of acute glomerular injury included endocapillary hypercellularity as well as the presence of wire-loop lesions,/hyaline thrombi (indicating immune complex deposition), cellular crescents, *etc*. (Figure 4). In contrast, only ~11% of the mice in ZSJ-0228 treated group was graded with severe glomerulonephritis (with the rest in the mild and moderate categories), which was much lower than that of the saline (~43%) and Dex (~44%) groups. In addition, when individual glomeruli were evaluated histologically, abnormities were observed in 26% glomeruli from ZSJ-0228 treated mice, which is close to the frequency (21.6%) found in the NZW mice (healthy control, which do develop anti-dsDNA antibodies, high serum levels of retroviral gp70 antigen, and nephritis later in life [137]). Compared to this observation, 40% and 52% glomeruli in Dex and saline groups were found to be abnormal, respectively. Though these

differences are not statistically significant (P = 0.19), the apparent trend further supports the superior efficacy of ZSJ-0228 in treating LN (Figure 4F).

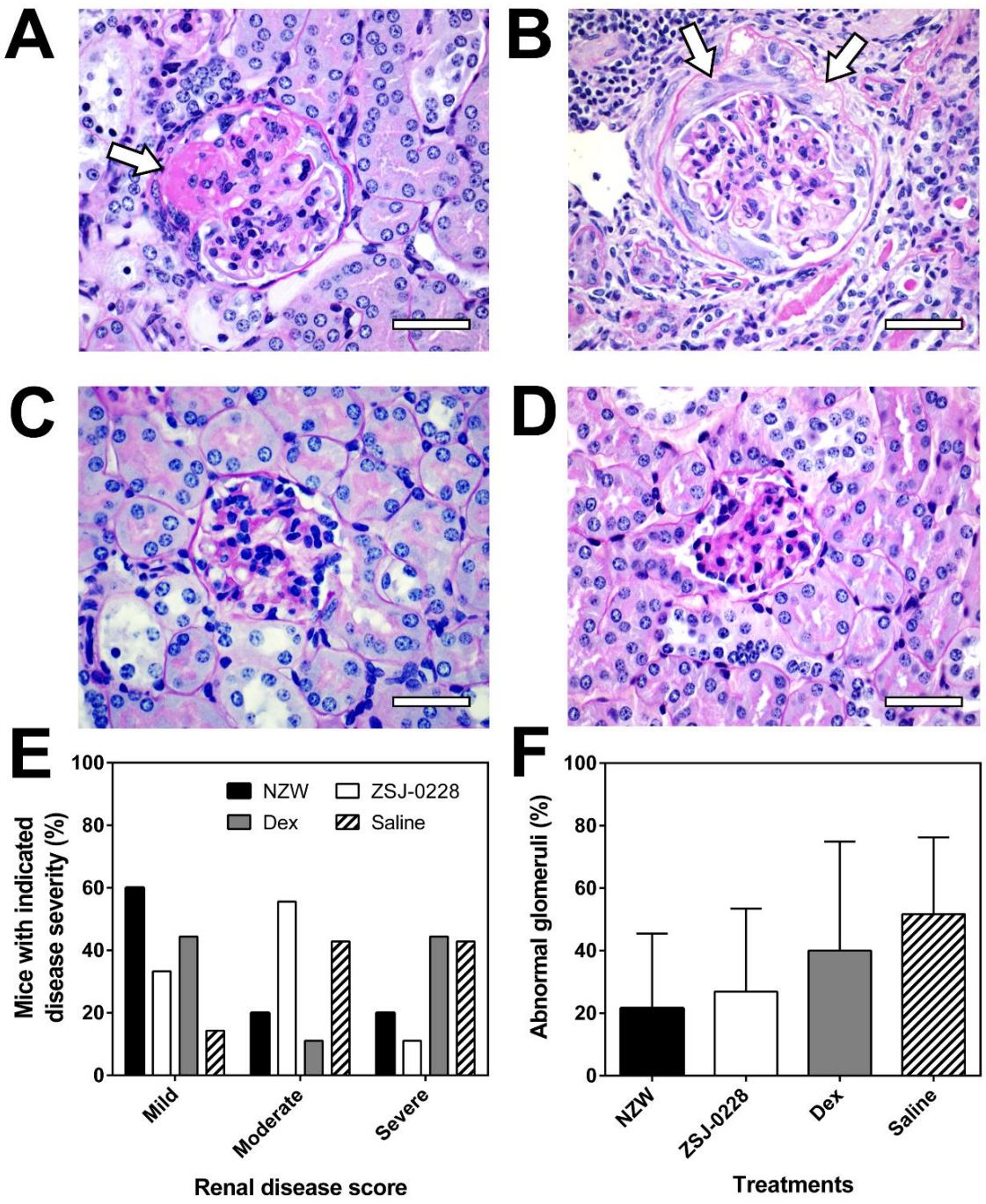

Figure 4. Histological evaluation of kidneys from different treatment groups. The tissues were formalin-fixed, sectioned (3 μm) and stained with Periodic acid–Schiff (PAS) for visual examination and grading by a pathologist (KWF), who was blinded to the group design. A. PAS-stained kidney section from the saline group showing wire-loop lesions (arrow). B. PAS-stained kidney section from the Dex-treated group showing a cellular crescent (arrow). C. PAS-stained kidney section from ZSJ-0228 treated group, showing less severe glomerular injury with a healthier appearance similar to the NZW control. D. PAS-stained kidney section from NZW control group. All scale bar = 50 μm. E. The fractions of mice in each group with mild, moderate and severe renal disease. Results are expressed as percentage of mice with indicated disease severity. F. The average percentage of abnormal glomeruli found in each group. Results are expressed as mean ± SD. No statistically significant difference was found among the groups. P = 0.19, one-way analysis of variance or ANOVA with Bonferroni Tukey's correction.

3.3.2 ZSJ-0228 Treatment Showed No Apparent GC Toxicities

The viability of HK-2 cells (an immortalized renal proximal tubule epithelial cell line from the normal adult human kidney) was evaluated after 72 hours incubation with ZSJ-0228, Dex and mPEG. As can be seen in Figure 5, ZSJ-0228 and Dex showed minimal cytotoxicity to HK-2 cells within the tested range of

dexamethasone equivalent concentrations (0.01 – 2,000 μM). mPEG was also found to be non-toxic.

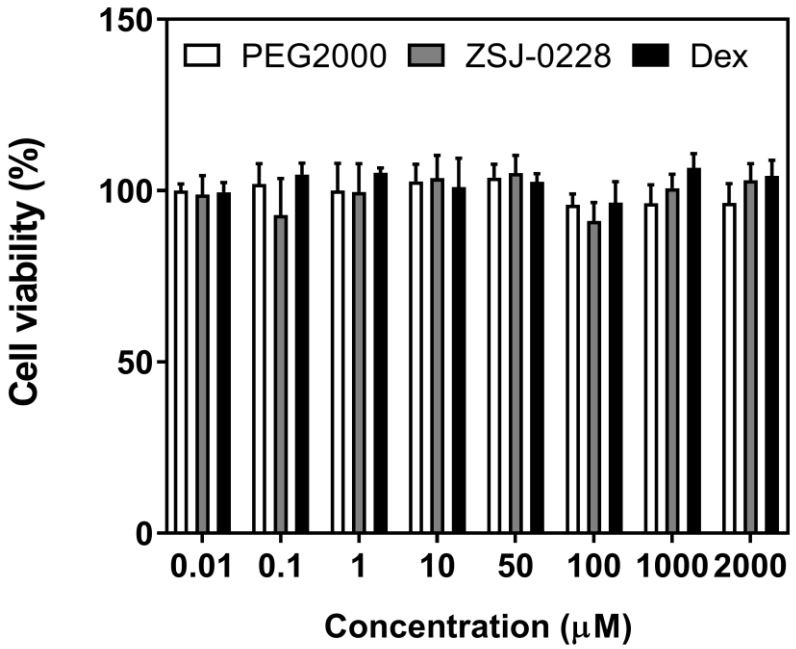

Figure 5. Impact of mPEG, ZSJ-0228, and Dex on HK-2 cell viability after 72 h of incubation, as assessed by the MTT assay. For ZSJ-0228 and Dex, they were tested at dexamethasone equivalent concentrations (0.01−2000 μM). mPEG was tested at ZSJ-0228 equivalent concentrations (0.005−1000 μM). Each ZSJ-0228 has one mPEG and two dexamethasone molecules.

During the two months treatment study, no significant difference in body weight was observed among ZSJ-0228, Dex and saline groups (Figure 6). On average, all tested groups maintained within 90% of original body weight at the

end of the two months treatments. Different from saline and ZSJ-0228 groups, an early trend of body weight decrease was observed in the Dex group, suggesting potential adverse effects of the treatment (Figure 6). It is important to note that several mice from the saline and Dex groups have died earlier (Figure 3B) due to severe nephritis and significant loss of body weight (> 20%). Their body weight values at the time of death were recorded. Should they be living at the end of the two months treatment, significant difference among the three tested groups may be observed.

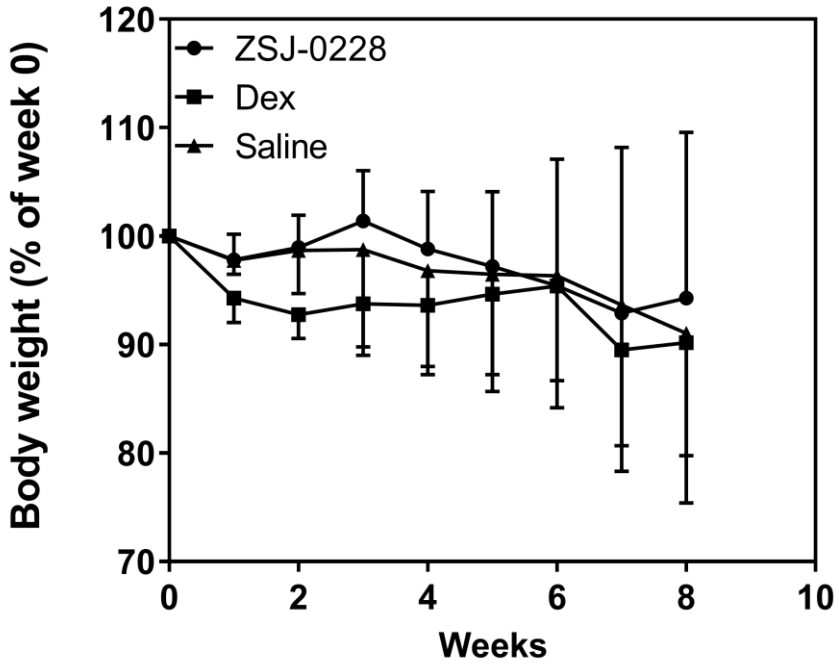

Figure 6. Body weight (% of week 0) of NZB/W F1 mice during the two-month treatments with ZSJ-0228 and Dex (dexamethasone dose equivalent). Saline was used as a control. ZSJ-0228 treatment did not affect the mice body weight. An

early trend of decreased body weight was observed in the Dex group, suggesting a potential adverse effect of the treatment.

One of the major adverse effects associated with GC use is osteopenia. To understand the impact of ZSJ-0228 treatment on the skeleton, we evaluated the femoral bone quality using a high-resolution micro-CT (Skyscan 1172). The bone mineral density (BMD) and trabecular thickness in the femoral trabecular bone of ZSJ-0228 treated mice were significantly higher than those from the saline and Dex-treated groups (Figure 7A and 7C; $P < 0.05$). A trend toward higher trabecular bone volume/tissue volume (BV/TV) value was also observed (Figure 7B, $P = 0.69$).

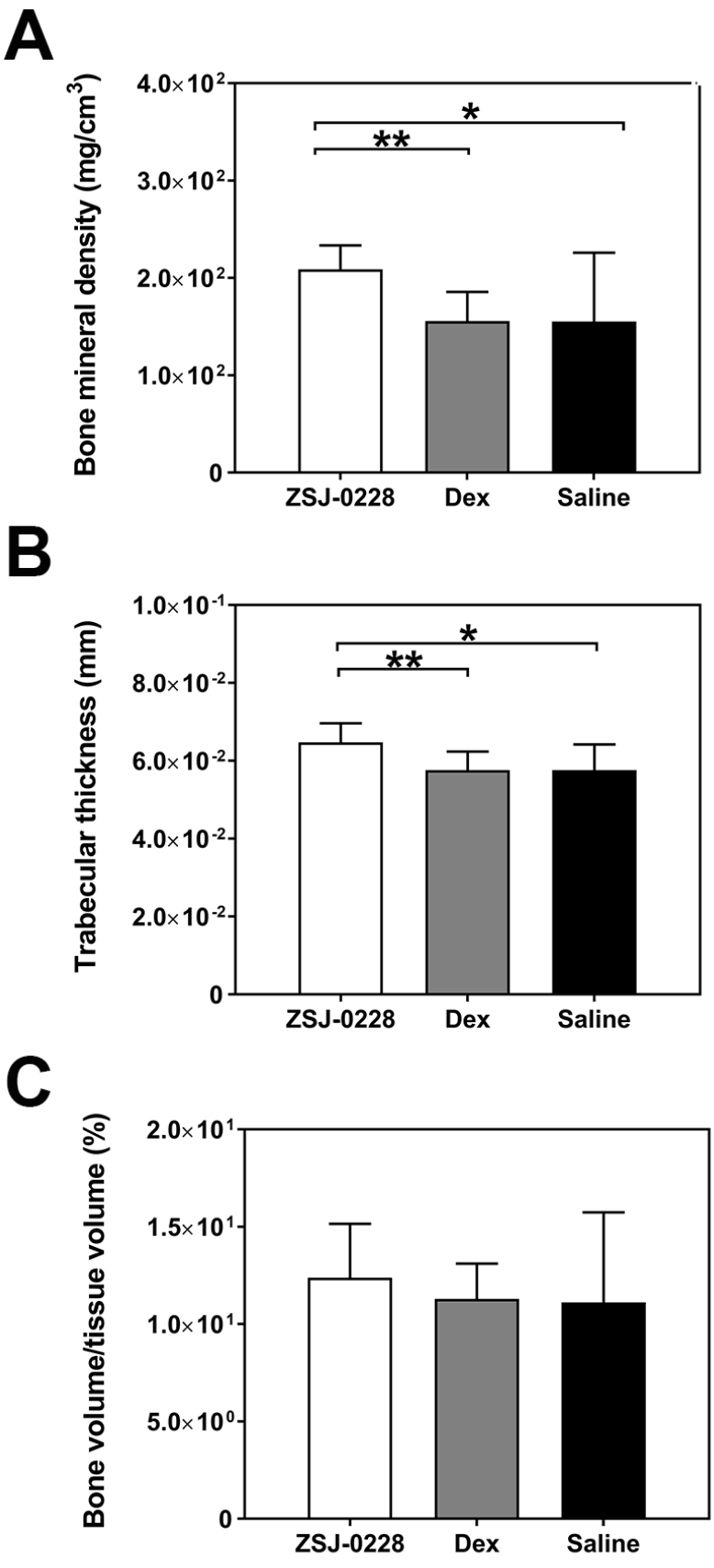
A
Bone mineral density (mg/cm3)
4.0×10²
3.0×10²
2.0×10²
1.0×10²
0
*
**
ZSJ-0228
Dex
Saline
B
Trabecular thickness (mm)
1.0×10⁻¹
8.0×10⁻²
6.0×10⁻²
4.0×10⁻²
2.0×10⁻²
0
*
**
ZSJ-0228
Dex
Saline
C
Bone volume/tissue volume (%)
2.0×10¹
1.5×10¹
1.0×10¹
5.0×10⁰
0
ZSJ-0228
Dex
Saline

Figure 7. ZSJ-0228 treatment does not affect the bone quality of lupus prone mice. (A) ZSJ-0228 treatment is significantly better at preserving bone mineral density than Dex treatment and the saline controls. (B) ZSJ-0228-treated mice trended toward a higher bone volume/tissue volume than Dex treatment and saline controls (P = 0.69). (C) ZSJ-0228-treated mice have a significantly higher trabecular thickness value than Dex treatment and saline controls. For bone quality (A, B, and C), samples were available for analysis only from the subset of mice surviving at the final time point (8-week): 10 mice for the ZSJ-0228 group, 9 mice for the Dex group, 7 mice for the saline group. Results are expressed as mean ± SD. Statistical analysis of data in panels A and C was performed using the Kruskal−Wallis test with Bonferroni's pairwise comparison. For panels B, the statistical analysis was performed using one-way ANOVA with Tukey's pairwise comparison. *, $P < 0.05$, **, $P < 0.01$.

Chronic exposure to GC therapy is known to be associated with systemic immunosuppression. To understand if ZSJ-0228 as a GC prodrug would be similarly immunosuppressive, we evaluated the total serum IgG level and the peripheral white blood cell (WBC) counts at designated time points. As shown in Figure 8A, ZSJ-0228 treated mice exhibited similar WBC counts as the saline group, but the value is significantly higher than that of the Dex-treated mice ($P < 0.05$). As shown in Figure 8B, total serum IgG levels were not altered in the ZSJ-0228 treated mice during the treatment. In contrast, the animals treated with daily Dex had a significant drop of serum IgG value after only one month of treatment

(P < 0.001) and continued to the end of the experiment (P < 0.0001). These data collectively suggest the immune system is not being further suppressed in animals treated with ZSJ-0228.

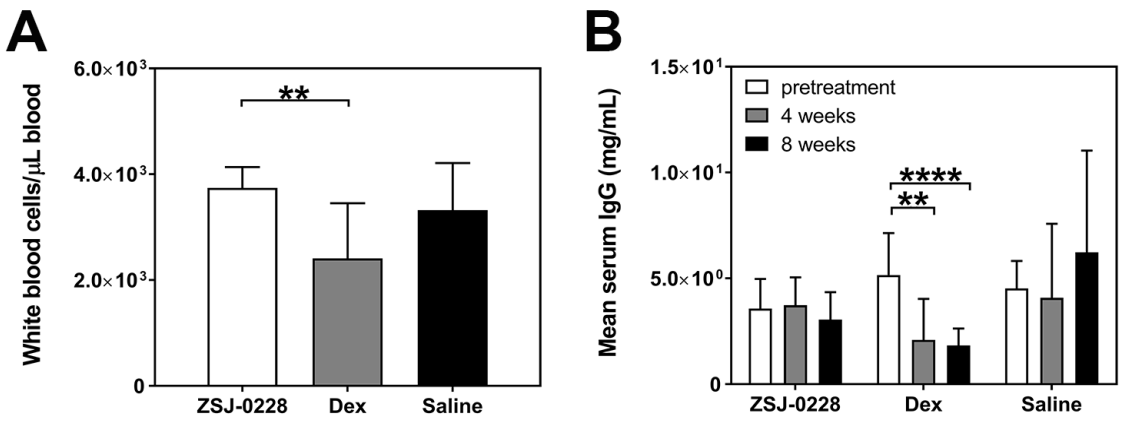

Figure 8. ZSJ-0228 does not elicit apparent immunosuppression in the circulating blood system. (A) The average white blood cell (WBC) count of the ZSJ-0228-treated mice was similar to that of the saline group, but was significantly higher than the Dex group. (B) Total serum IgG levels for mice in ZSJ-0228 (n = 10), Dex (n = 11), and saline (n = 12) groups were determined by ELISA at pretreatment, 4-week, and 8-week time points. The ZSJ-0228 treatment did not significantly reduce total serum IgG levels, whereas Dex treatment did, suggesting potential immune suppression. Fore WBC counts (A), samples were available for analysis only from the subset of mice surviving at the final time point (8-week): 10 mice for the ZSJ-0228 group, 9 mice for the Dex group, 7 mice for the saline group. For total serum IgG levels (B), the ZSJ-0228 group has 10 mice at 4-week and 8-week time points; the Dex group has 11 and 9 mice at the 4-week and 8-week

time points, respectively; and the saline group has 11 and 7 mice at the 4-week and 8-week time points, respectively. Results are expressed as mean ± SD. For panels A, the statistical analysis was performed using one-way ANOVA with Tukey's pairwise comparison. For panel B, the statistical analysis was performed using the generalized estimating equation (GEE) method with Tukey's pairwise comparison. **, $P < 0.01$, ****, $P < 0.0001$.

GC exposure, even in the short-term, is known to suppress hypothalamic-pituitary-adrenal (HPA) axis, leading to clinical atrophy of the adrenal gland.[138] To understand if ZSJ-0228 treatment would cause adrenal gland atrophy in NZB/W F1 mice, the adrenal glands from all treatment groups were isolated and weighed at necropsy. The mean value of adrenal gland mass in the Dex group was significantly lower than that from the ZSJ-0228 group (Figure 9; $P < 0.05$). No significant difference in adrenal gland mass was found between the ZSJ-0228 and saline groups (Figure 9; $P = 0.22$). These data suggest the treatment with ZSJ-0228 does not lead to adrenal gland atrophy.

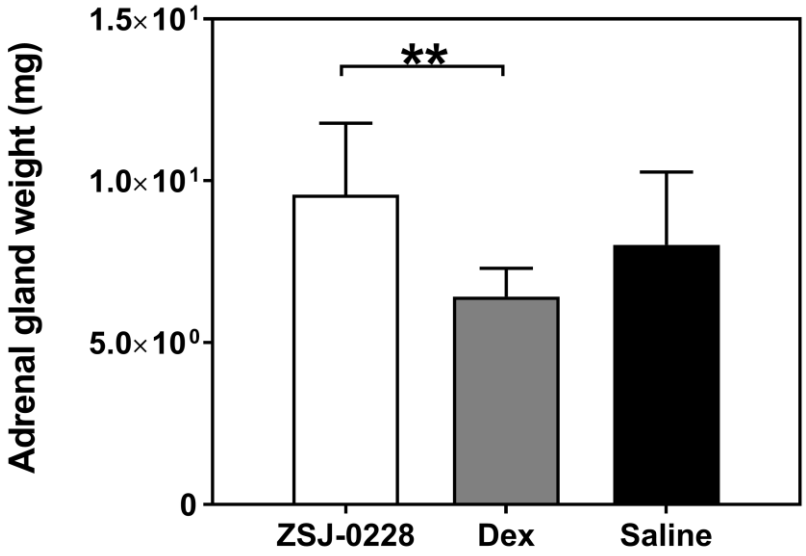

Figure 9. Different from Dex treatment, ZSJ-0228 treatment did not induce adrenal gland atrophy. Samples were available for analysis only from the subset of mice surviving at the final time point (8-week): 10 mice for the ZSJ- 0228 group, 9 mice for the Dex group, 7 mice for the saline group. Results are expressed as mean ± SD. Statistical analysis of data in this panels wa performed using the Kruskal−Wallis test with Bonferroni's pairwise comparison. **, $P < 0.01$.

3.3.3 ZSJ-0228 Treatment Ameliorates Renal Immune Complexes but does not Alter Serum Anti-dsDNA Level

GCs have been shown to exert some of its therapeutic effects on lupus partially through the down-regulation of anti-dsDNA antibody levels.[139] Therefore, it was important to evaluate whether ZSJ-0228 attained its therapeutic effect through this mechanism. As shown in Figure 10, ZSJ-0228 treatment

showed no impact on serum anti-dsDNA IgG during the treatment. But, it was found to significantly reduce renal immune complex deposition when compared to the saline control. Daily Dex treatment, on the other hand, was found to significantly reduce serum anti-dsDNA IgG level at 4- and 8-weeks post-treatment initiation ($P<0.05$); but had no impact on renal immune complex deposition. These results suggest that the immunosuppressive effect of ZSJ-0228 is not systemic but restricted to the inflamed kidneys.

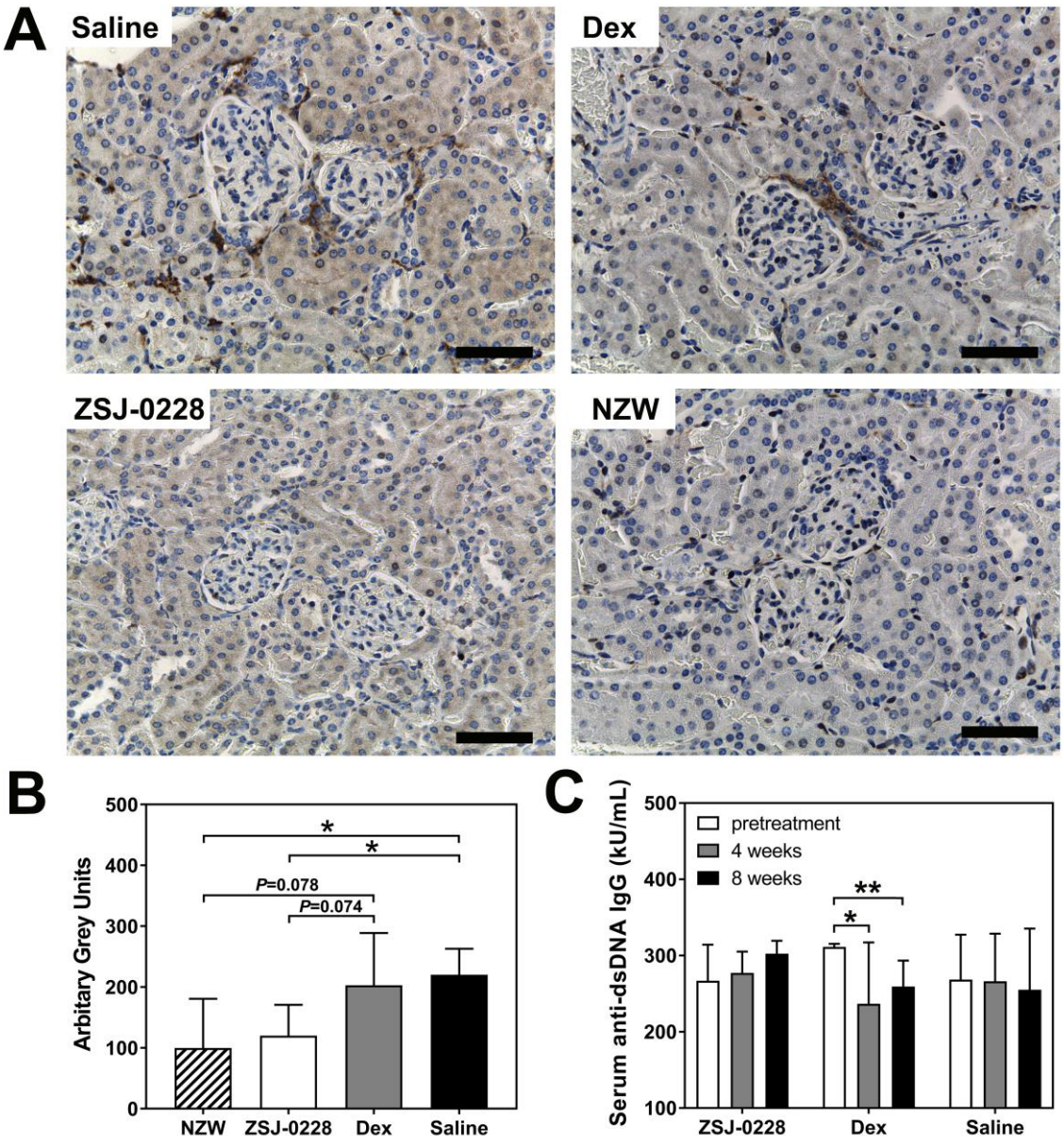

Figure 10. The effect of different treatments on the renal immune complexes deposition and serum anti-dsDNA IgG levels. ZSJ-0228 treatment was found to significantly reduce renal immune complexes deposition. While Dex daily treatment significantly reduced the serum anti-dsDNA IgG level, it had no impact on renal immune complexes deposition. A. Representative kidney sections from each treatment group, immunohistochemically stained for renal deposition of anti-

mouse IgG. Scale bar = 50 μm. B. Quantification of kidney immune complex staining. Results are expressed as mean ± SD. *, $P < 0.05$, one-way ANOVA test with Tukey's correction; C. Serum anti-dsDNA IgG levels at the pretreatment, 4-week, and 8-week time points, as determined by enzyme-linked immunosorbent assay. Results are expressed as mean ± SD. Statistical analysis of the data in panel C was done using GEE method with Tukey's pairwise comparison.

3.3.4 ZSJ-0228 Reduced Renal Macrophages Infiltration

To further understand ZSJ-0228's working mechanism, we examined the infiltration of macrophages into the kidney, an indicator of chronic renal inflammation. The macrophage marker F4/80 was used in kidney tissue sections from all the treatment groups (Figure 11A). Quantification of F4/80 staining suggested that Dex treatment did not significantly reduce macrophage infiltration when compared to the saline control. In contrast, ZSJ-0228 treatment significantly lowered the renal macrophage level when compared with Dex treatment and saline control (Figure 11B). These results suggested that the ZSJ-0228 treatment may partially exert its therapeutic effects through ameliorating macrophage infiltration to the kidneys.

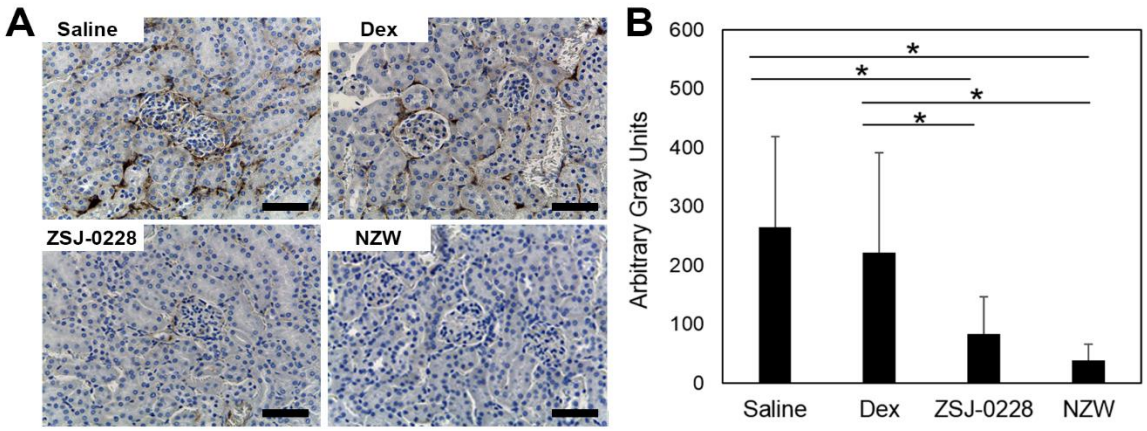

Figure 11. Impact of different treatments on renal macrophage infiltration. A. Representative kidney sections from each treatment group, immunohistochemically stained for renal deposition of anti-mouse F4/80. Scale bars = 50 μm. B. Quantification of immune complex staining. Results are expressed as mean ± SD, *, $P < 0.05$, Kruskal-Wallis test with Mann-Whitney correction.

3.3.5 ZSJ-0228 Targeted the Nephritic Kidneys in NZB/W F1 Mice

To understand the therapeutic efficacy and reduced GC-associated toxicities of ZSJ-0228, the *in vivo* biodistribution of ZSJ-0228 was qualitatively analyzed using near-infrared optical imaging. Both NZB/W F1 and NZW mice (healthy control) received i.v. injections of IRDye 800 CW-labeled ZSJ-0228 (ZSJ-0228-IRDye). As shown in Figure 12A, in NZB/W F1 mice, ZSJ-0228-IRDye primarily accumulated in the kidneys and could be detected for at least four days. ZSJ-0228-IRDye was also found to accumulate in NZW mice's kidneys, but the

intensity of the signal was at a much lower level, especially at 4-day post-administration. These observations seem to suggest that the severe nephritis of NZB/W F1 mice may have contributed to the targeting and retention of ZSJ-0228 in the kidneys.

To better appreciate the kidney retention mechanism of ZSJ-0228 on the cellular level, Alexa Fluor 647-labeled ZSJ-0228 (ZSJ-0228-AF647) was i.v. administered to NZB/W F1 and NZW mice. All major organs, including kidneys, were processed for flow cytometry analysis at 1 and 4-day post-injection. As shown in Figure 12B, ~56% of kidney cells from NZB/W F1 mice were positive for ZSJ-0228-AF647, while only ~38% of kidney cells from NZW mice were ZSJ-0228-AF647 positive. The presence of ZSJ-0228-AF647 positive cells in other organs were all less than 10%. For NZW mice, the percentage of ZSJ-0228-AF647 positive cells at 4-day post-injection decreased significantly (to ~23%, $P < 0.0001$) when compared to the value at 1-day post-injection. No significant ZSJ-0228-AF647 positive cell reduction was observed in kidneys of NZB/W F1 mice from 1 to 4-day post-injection. These flow cytometry data confirm ZSJ-0228-AF647's targeting to the inflamed kidneys of NZB/W F1 mice found in the optical imaging study and attributes the prodrug's retention in the kidney to cell-mediated sequestration.

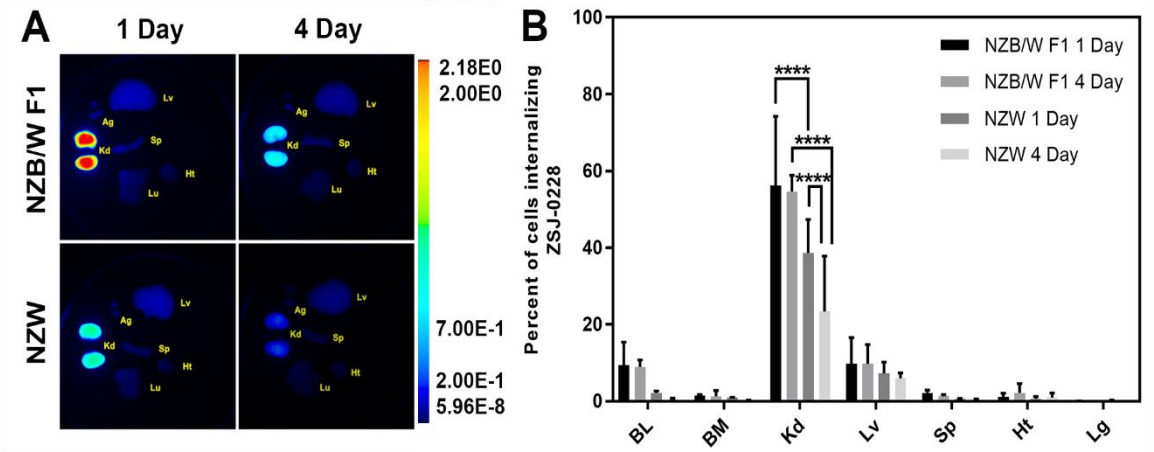

Figure 12. The targeting and retention of ZSJ-0228 in the kidneys of NZB/W F1 mice. A. Representative optical images of organs isolated from NZB/W F1 mice and NZW mice (healthy control). Images were obtained at 1 and 4-day post i.v. injections of IRDye 800 CW-labeled ZSJ-0228 (ZSJ-0228-IRDye). Pseudo color-coded signal intensity reflects the level of ZSJ-0228-IRDye within the organ examined. All the images were acquired with the same condition and share the same color bar. Ht, heart; Lv, liver; Kd, kidney; Sp, spleen; Lu, lung; BL, blood; BM, bone marrow. B. Flow cytometry analysis of cells isolated from organs of NZB/W F1 and NZW mice at 1 and 4-day post i.v. injections of Alexa Fluor 647-labeled ZSJ-0228 (ZSJ-0228-AF647). Results are expressed as mean ± SD. ****, $P < 0.0001$, one-way ANOVA with Bonferroni Tukey's correction.

3.3.6 Profiling of Kidney Cells that Internalized ZSJ-0228

Additional flow cytometry analysis was performed to further profile the ZSJ-0228-AF647 positive cells in the kidneys after systemic administration of the prodrug. In the nephrotic kidney, ~70% CD11b+ (myeloid) cells internalized ZSJ-0228-AF647 at 1-day post-injection; these cells include CD11c+ (dendritic cell), NK1.1+ (natural killer cell), Ly6G+ (neutrophil) and F4/80+ (macrophage) subphenotypes [140] (Figure 13A). At 4-day post-injection, ~50% of these cells still remain positive for the prodrug. In comparison, ~30% of the myeloid cells in NZW mice group internalized the prodrug at 1-day post-injection, and only one-third of the cells remained positive for the prodrug at 4-day post injection. Moreover, ~60% of the CD326+ (proximal tubular epithelium) and CD146+ (endothelium) cells in nephrotic kidneys retained ZSJ-0228-AF647 at 4-day post-injection, which is 50% higher than the control kidneys. These results suggest that both inflammatory cells and resident renal cells (including CD326+ and CD146+ cells) in the nephrotic kidneys have sequestered ZSJ-0228 and retained it as compared to the control. To account for ZSJ-0228-AF647's cellular distribution pattern, ~20-40% of the prodrug was found in the CD11b+ cells of the nephrotic kidney, with less than 10% in the control kidneys (Figure 13B). Around 30-40% of ZSJ-0228-AF647 was internalized by the CD326+ cells of both NZB/W F1 and NZW mice, suggesting that the prodrugs primarily distribute to the renal myeloid cells and proximal tubular epithelium. The rest of the ZSJ-0228-AF647 positive cells remain unidentified due to the lack of specific marker.

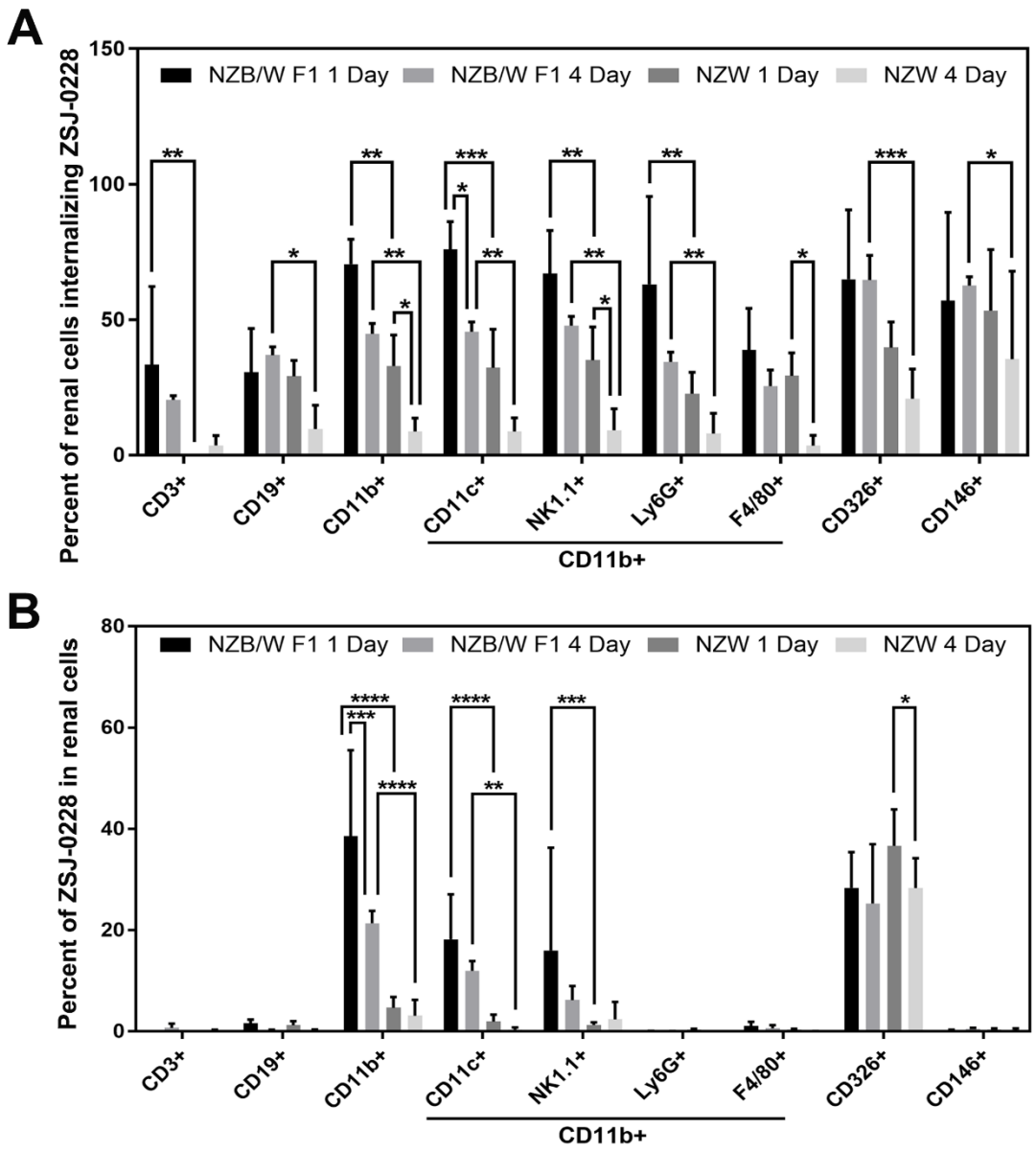

Figure 13. Profiling the cellular internalization and retention of ZSJ-0228 by kidney cells. Flow cytometry was used to analyze cells isolated from kidneys of NZB/W F1 and NZW mice at 1 and 4-day post-injection of ZSJ-0228-AF647. A. The percentage of renal cells internalized ZSJ-0228-AF647. B. The percentage of ZSJ-0228-AF647 internalized by different cells in the kidney. Results are

expressed as mean ± SD. *, $P < 0.05$; **, $P < 0.01$; ***, $P < 0.001$; ****, $P < 0.0001$, one-way ANOVA with Bonferroni Tukey's correction.

To validate renal cells' sequestration of ZSJ-0228-AF647 (red) observed by flow cytometry, nephrotic kidneys were harvested, sectioned, and immunohistochemically stained at 1-day post i.v. administration of the prodrug for confocal microscope analysis. As can be seen in Figure 13, fluorescent signal co-localization of CD133 (injured/activated proximal tubular epithelial cell[141]), CD146 (endothelium), or CD11b (myeloid cells) with ZSJ-0228-AF647 was observed at both low and high magnification images. This confirms the sequestration of ZSJ-0228-AF647 by these cells in the nephrotic kidney, which further support the findings in Figure 13.

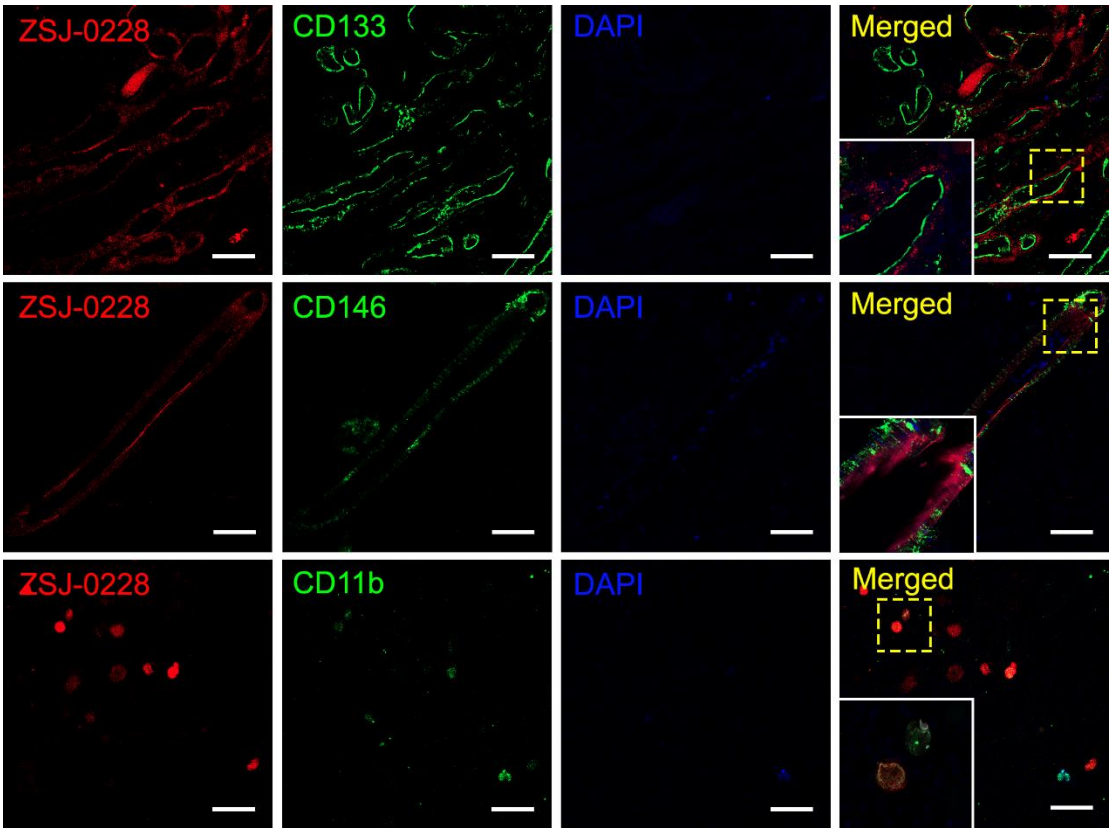

Figure 14. Immunohistochemical analysis of kidney cells' sequestration of ZSJ-0228-AF647. NZB/W F1 mice were i.v. administered ZSJ-0228-AF647 (red) and euthanized at 1-day post-injection. Kidneys were sectioned and stained with anti-mouse CD133, CD146, and CD11b (green). Nuclei were stained with DAPI (blue). Merged images were shown at the right panels. The higher magnification (63×) images were shown within the lower magnification (10×) images at the lower left corner. Scale bar = 100 μm.

3.3.7 Internalization Kinetics and Subcellular Location of ZSJ-0228

As an immortalized renal proximal tubule epithelial cell (RPTEC) line from normal adult human kidney, HK-2 cells can reproduce experimental results obtained with freshly isolated RPTECs on the basis of its histochemical, immunocytochemical, and functional characteristics.[142] As RPTEC represents one of the main cellular populations identified to sequester ZSJ-0228, HK-2 cell culture was used to recapitulate the internalization kinetics of prodrug and its subcellular location. Alexa Fluor 488-labeled ZSJ-0228 (ZSJ-0228-AF488) was used in this particular experiment. As shown in Figure 15A, HK-2 cells rapidly internalized ZSJ-0228-AF488 and the fluorescent signal intensity increased over time. Inflammatory conditions are known to be associated with accelerated endocytosis.[143, 144] The introduction of lipopolysaccharide (LPS), however, did not accelerate the internalization process as anticipated, suggesting it may not be sufficient to recapitulate the *in vivo* inflammatory environment.

To define the subcellular location of ZSJ-0228 in HK-2 cells, the cells were incubated with ZSJ-0228-AF488 and LysoTracker (lysosome marker, DND-99, red) and then examined under the confocal microscope. The partial co-localization of internalized ZSJ-0228-AF488 (green) with DND-99 (red) indicates that ZSJ-0228 was endocytosed and processed in the acidic lysosomal compartment, which is ideal for the hydrazone-based acid cleavable ZSJ-0228 prodrug design (Figure 15B).

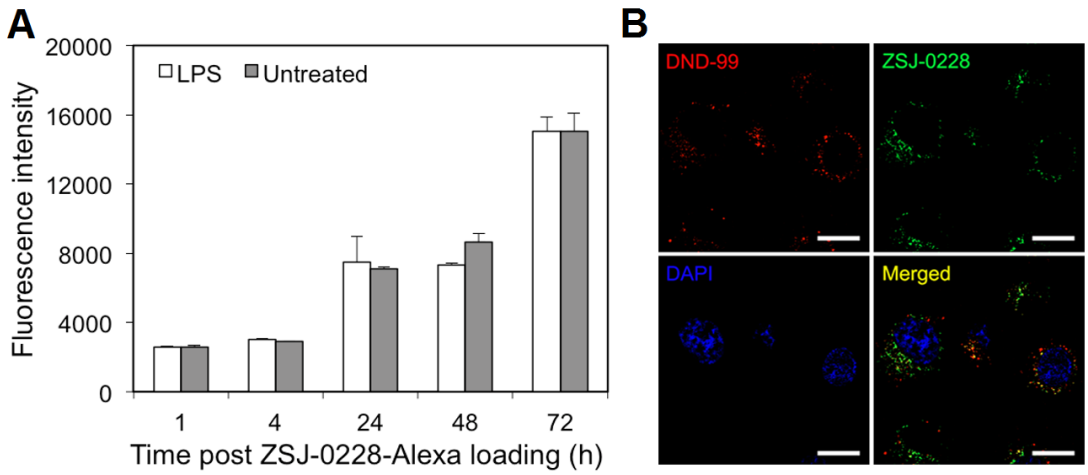

Figure 15. *In vitro* internalization kinetics and subcellular location of Alexa Fluor 488 labeled ZSJ-0228 in human proximal tubule epithelial (HK-2) cells. A. The cellular internalization kinetics of ZSJ-0228-Alexa 488 by HK-2 cells with or without lipopolysaccharide (LPS, 10 μg/mL) activation over a 72-hour time course. Results are expressed as mean ± SD. B. Representative confocal images exhibiting internalization and subcellular trafficking of ZSJ-0228-AF488 in LPS-activated (10 μg/mL) HK-2 cells. LysoTracker DND-99 signal (red), ZSJ-0228-AF488 signal (green), DAPI signal (blue). Scale bar = 20 μm.

3.4 Discussions

Previously, daily dexamethasone treatment (1 mg/kg) was found to attenuate the nephritis and improve survival of NZB/W F1 mice.[145] In the present study, it was used as a benchmark to compare with ZSJ-0228 prodrug treatment. Dose equivalent monthly Dex treatment (28 mg/kg dexamethasone equivalent) was not

used as a control due to severe adverse events observed immediate after administration. As anticipated, when tested in NZB/W F1 mice with established nephritis, ZSJ-0228 monthly treatment effectively attenuated albuminuria and maintained 100% animal survival for the entire experimental duration. Dose equivalent daily Dex treatment (1 mg/kg), on the other hand, only presented with moderate efficacy and 80% survival (Figure 3). These observations were further supported by the glomerular histologic findings in which ZSJ-0228 treatment was found to more effectively prevent glomerular injury with disease severity rated mostly mild to moderate (Figure 4).

ZSJ-0228 seems to also possess an improved safety profile. As shown in Figure 5 A, ZSJ-0228 showed minimal cytotoxicity in HK-2 cells culture. During the two-month treatment study, the prodrug treatment did not significantly alter the mice's body weight (Figure 6). Compared to dose equivalent daily Dex treatment, the monthly ZSJ-0228 treatment did not induce osteopenia (Figure 7A-C); neither did it cause immunosuppression as evidenced by WBC and total serum IgG levels comparable to the saline group (Figure 8A&B). Furthermore, mice treated monthly with ZSJ-0228 were found to have significantly higher adrenal gland mass than the dose equivalent daily Dex-treated mice, suggesting the absence of adrenal gland atrophy (Figure 9). It is very important to recognize that the WBC reduction induced by GC treatment is being interpreted as immunosuppression in NZB/W F1 mice.[146] It is well-recognized that the opposite effect (i.e. leukocytosis) is commonly observed in human patients when

GC is being used[147] Therefore, ZSJ-0228's impact on WBC in the NZB/W F1 mice should not be directly extrapolated to human. Collectively, these data provide clear evidence of ZSJ-0228's superior therapeutic efficacy than Dex and significantly improved safety when compared to Dex and P-Dex[104, 106] in the treatment of NZB/W F1 mice.

In probing the working mechanism of ZSJ-0228, near-infrared imaging-based *in vivo* biodistribution data (Figure 12A) suggests that the prodrug's main distribution organ in NZB/W F1 mice was the inflamed kidney. The distribution to other organs was limited, which is in stark contrast to the observation in human treated with dexamethasone (with fast extrarenal elimination and high liver deposition)[148] and in mice with P-Dex (with higher liver and spleen deposition).[104, 106] Different from P-Dex treatment, ZSJ-0228 treatment has no impact on splenomegaly (data not shown), which supports the optical imaging findings. The significantly lower ZSJ-0228 positive cells in other organs counted by the flow cytometry further validated the nephrotropic distribution pattern of ZSJ-0228 (Figure 12B).

Several promising nanoformulations have been developed for dexamethasone delivery.[149-151] Comparing to ZSJ-0228, they have the advantage of significantly reduced cost of manufacture and lower barrier for regulatory approval. Similar to P-Dex, their biodistribution patterns favor the MPS

system. We speculate that their relatively higher liver/spleen distribution may be associated with their high molecular weight or large size.[152] ZSJ-0228, on the other hand, is considerably smaller (~ 3 kDa). The water-soluble prodrug consists of a mPEG 1900 and two dexamethasone molecules (Scheme 1). Considering the hydrodynamic radius of PEG 3000 is around 15 Å,[153] the structurally more compact ZSJ-0228 should be even smaller than that. Our ongoing pharmacokinetic study estimates the $t1/2_{(\beta)}$ of ZSJ-0228 to be around 12 hr, which is significantly shorter than that of P-Dex.[113, 114] We believe the relatively smaller size and shorter serum half-life may be the main contributing factor for ZSJ-0228's nephrotropicity and low MPS distribution.

Two additional factors may also be considered in understanding ZSJ-0228's high distribution to kidney: (1) It has been reported that there is an inverse size dependency in the renal clearance of sub-nanometer gold nanoclusters (AuNCs), which is distinctly different from the general understanding that smaller nanoparticles always clear more rapidly through the kidney than the larger ones.[154] We postulate that the proposed mechanism of physical retention of AuNCs by the glycocalyx of the glomeruli may have also helped to slow down the clearance of ZSJ-0228 from kidney and thus contributed to its high kidney distribution. (2) According to ELVIS mechanism, inflammatory cells' accelerated sequestration is one of the major contributors to the nanomedicine's high retention by inflammatory tissues. As shown in Figure 12B, the kidney cells of NZB/W F1

mice certainly have demonstrated substantially higher sequestration of ZSJ-0228 than the control NZW mice.

It is interesting to note that ZSJ-0228 was also somewhat retained by kidney/kidney cells of NZW mice (Figures 8 & 9). This is probably due to the advanced age (> 28 weeks) of the animals being used in this study. NZB/W F1 mice are the offspring of an NZB female (Stock # 000684, Jackson Laboratory) and an NZW male (Stock # 001058, Jackson Laboratory). Both inbred parental strains may occasionally develop autoimmune abnormalities that are observed in the F1, but not necessarily with the same onset or severity. While the NZW mice have a normal life span, some do develop anti-DNA antibodies, high serum levels of retroviral gp70 antigen, and nephritis at an advanced age.[137]

Further flow cytometry profiling of kidney cells that internalizes ZSJ-0228 revealed that myeloid cells and proximal tubular epithelial cells were the major players in sequestration and retention of ZSJ-0228 in the inflamed kidneys of NZB/W F1 mice (Figure 13). These findings are not surprising as infiltrate myeloid cells in LN are known to be phagocytic.[155] It has been reported that inflammatory insults could reprogram the myeloid cells' endocytic machinery from receptor-mediated endocytosis to macropinocytosis,[156] which would accelerate the rate of cell internalization in a receptor-independent fashion. Proximal tubular epithelial cells, on the other hand, recycle the albumin via a receptor-mediated

endocytosis mechanism when exposed to the proteins.[157] One may suggest the observed endocytosis of ZSJ-0228 (Figures 9-11) by tubular epithelial cells is a “bystander” effect associated with the cells’ internalization/recycle of albumin. Due to the potential binding of ZSJ-0228 to albumin,[158, 159] it is also possible that the prodrug may piggyback albumin and be internalized through the receptor-mediated endocytic process intended for albumin.

We noticed that while the majority (50%) of renal CD146+ cells (endothelial cells) internalized ZSJ-0228 (Figure 13B) and IHC analysis suggests a high CD146+ cellular uptake of the prodrug (Figure 14), the flow cytometry data shows low prodrug distribution (<1%) to this cell population (Figure 13B). This discrepancy may be attributed to the difficulty in isolating endothelial cells from the kidneys. Typically, a collagenase-based tissue dissociation reagent, Liberase Blendzyme, can be used to efficiently isolate endothelial cells from tissues. Its application, however, often results in the damages to other cells.[160-162] Thus, a gentler cell isolation protocol was used in the present study. We speculate that this limitation of the current flow cytometry tissue isolation protocol may have inadvertently lowered the number of endothelial cell population isolated from kidney and underestimated their contribution to the kidney sequestration of ZSJ-0228.

While ZSJ-0228 demonstrated strong nephrotropicity on the lupus-prone NZB/W F1 mice, it did not stay in the kidney permanently. The presence of ZSJ-0228 in kidney decreased over time (Figures 8 and 9). This is especially true for the CD11b+ myeloid cells isolated from the kidneys of NZB/W F1 mice. The percentage of CD326+ cells (proximal tubular epithelium) that internalized ZSJ-0228 did not change from day 1 to day 4 post-administration (Figure 13). It has been reported that GC treatment can induced myeloid cell apoptosis.[163] Renal epithelial cells, on the other hand, are insensitive to GC treatment.[164] Therefore, it is possible that the ZSJ-0228 sequestered by myeloid cells may have induced their apoptosis, leading to the prodrug's gradual clearance from the kidney. Since FcR-bearing myeloid cells are responsible for triggering LN,[165] ZSJ-0228's specific sequestration by the myeloid cells in kidney may also be a plausible explanation for ZSJ-0228's superior efficacy than Dex. Such notion conforms to the finding shown in Figure 11, where the number of macrophage was significantly reduced after two months treatment with ZSJ-0228. Clearly, further investigations are needed to better understand ZSJ-0228's working mechanism on the cellular and molecular levels.

The present study does have its limitations. ZSJ-0228 was designed for the improved efficacy and safety of GC treatment for lupus nephritis, but not for other lupus complications such as arthritis. Since its main distribution organ is kidney, ZSJ-0228 may not be effective in managing inflammation at other anatomical sites of the body. P-Dex17 and other GC nanoformulations,[149-151] which have

longer serum half-lives may be better suited for these conditions. We speculate that the development of a GC prodrug that would be effective and safe for most of the lupus symptoms may necessitate a macromolecular prodrug system that is conditionally degradable.[166] Regarding administration route, ZSJ-0228 was given as a monthly i.v. injection in this study. Though the treatment schedule is favorable, the i.v. route would require healthcare professionals for administration in clinical setting. Previous work[167] indicates that s.c. and i.p. administrated polymeric prodrug may enter the circulation through the lymphatic system. Therefore, we speculate it is possible that ZSJ-0228 may also be given via these routes and be effective. This approach would enable self-administration of the medication and further improve the patients' compliance to the treatment.

3.5 Conclusions

A micelle-forming PEG-based dexamethasone prodrug (ZSJ-0228) was developed with superior and sustained therapeutic efficacy against nephritis on lupus-prone female NZB/W F1 mice. No apparent glucocorticoids (GC) side effects was observed. While as a prodrug of dexamethasone, ZSJ-0228 does not change the parent drug's anti-inflammatory and immunosuppressive mechanism on the molecular level, it indeed alters the pharmacology physiologically by restricting its distribution to the inflamed kidneys, providing sustained and localized immunosuppressive and anti-inflammatory effect. We believe ZSJ-0228

can be further developed into a viable new drug candidate for the better clinical management of lupus nephritis. We further suggest that this GC prodrug may also be explored for the clinical management of other renal pathologies, such as kidney transplant, IgA nephropathy, focal segmental glomerulosclerosis, minimal change disease and Goodpasture syndrome, in which GCs are frequently used as first-line therapy.

CHAPTER IV

PHARMACOKINETIC AND BIODISTRIBUTION STUDY OF PEG-BASED DEXAMETHASONE PRODRUG

4.1 Introduction

In the previous chapters, we have fully evaluated the therapeutic efficacy, adverse effects and potential mechanisms of PEG-based dexamethasone prodrugs in lupus prone mice. These studies demonstrated that PEG-Dex not only retains the efficacy but also overcomes the cumulative toxicities of P-Dex as HPMA is non-biodegradable [104]. Near infrared *in vivo* imaging showed that PEG-Dex was highly accumulated in the kidney at 1-day and was retained in the kidney for at least 4 days, while significantly lower fluorescence-labeled PEG-Dex signal was detected in the other critical organs including liver. This result was further validated by a flow cytometry study which showed that approximately 60% of renal cells internalized PEG-Dex while less than 10% of cells in the other organs took up the drug. Furthermore, the majority of PEG-Dex was sequestered by activated myeloid cells and epithelial cells in the kidney. This *in vivo* biodistribution study lasted for only 4 days. However, the therapeutic effects of PEG-Dex in lupus prone mice appears to last for 1 month as the mice were treated with PEG-Dex at single dose per month.

In preliminary studies, both P-Dex and PEG-Dex showed superior efficacy, compared to dose equivalent free Dex, in the prevention and treatment of lupus nephritis. While both can overcome the GC-induced skeletal complications, PEG-Dex micelle was the only one found to be able to avoid WBC count reduction and adrenal gland atrophy. Our preliminary imaging data suggesting that the two prodrug nanomedicine's passive targeting to the kidney may explain their superior therapeutic efficacy and we postulate that their differential distribution patterns to the rest of the body and especially the distribution pattern of the Dex released from the nanomedicine may help explain their different safety profiles. A head-to-head comparative PK/BD study is therefore planned to provide insight to PEG-Dex micelle's working mechanism.

4.2 Materials and Methods

4.2.1 Materials

The $Na^{125}I$ and Dexameshason-d4 were purchased from PerkinElmer (Waltham, MA). PD-10 column was purchased from GE HealthCare (Piscataway, NJ). The urine protein level was monitored weekly using Albustix Reagent Strips (Siemens Healthineers, Erlangen, Germany). All the organic solvents were

purchased from Fisher Scientific (Pittsburgh, PA). All compounds used in this experiment were reagent grade or higher and used without further purification.

4.2.2 Instruments

HPLC analyses were performed on an Agilent 1100 HPLC system (Agilent Technologies, Inc., Santa Clara, CA) with a reverse phase C_{18} column (Agilent, 4.6 × 250 mm, 5 µm). A Packard Cobra II Gamma Counter (PerkinElmer, Waltham, MA) was used for tissue radioactivity counting in the gamma counter-based PK/BD study. The dexamethasone concentration was measured by LC-MS/MS (Agilent Technologies, Inc., Santa Clara, CA).

4.2.3 Synthesis of ^{125}I-Labeled PEG-Dex

The PEG-Dex-Tyr was labeled with ^{125}I using a standard chloramine-T assay. $Na^{125}I$ solution (basic solution to prevent the evaporation of I_2) and chloramine-T were dissolved in 0.1N NaOH solution. This solution was stirred at room temperature for 10 min followed by the addition of the PEG-Dex-Tyr for another 30 min stirring. The reaction was quenched by $Na_2S_2O_3$, purified over a PD-10 column twice, and the resulting eluate demonstrated strong radioactivity (~1.2 mCi). The entire labeling process was done according to a protocol approved by

the University of Nebraska Medical Center Radiation Safety Office in a fume hood with a face velocity of 100 FPM and with lead shield protection. Post-labeling cleaning and contamination surveys were performed to ensure the absence of any radiation contamination in the working area.

4.2.3 Animal Experiment

The NZB/W F1 mouse, which is F1 hybrid between the New Zealand Black (NZB) and New Zealand White (NZW) strains, is a lupus prone strain that was utilized in this study. Mice were housed under controlled humidity, temperature and lighting conditions in facilities accredited by the American Association for Accreditation of Laboratory Animal Care, operating in accordance with standards set by the Guide for the Care and Use of Laboratory Animals (The National Academies Press, 1996). All procedures involving live animals were performed in accordance with protocols evaluated and approved by the Institutional Animal Care and Use Committee (IACUC) of the University of Nebraska Medical Center.

Beginning at 20 weeks of age, NZB/W F1 female mice were monitored weekly for albuminuria using Albustix. Readings between 1 and 2 (30-99 mg/dL) are considered 'normal', whereas readings of $\geqslant$2+ ($\geqslant$100 mg/dL) indicate the presence of albuminuria. Only the mice in each group with established nephritis,

evidenced by sustained albuminuria (⩾100 mg/dL) for 2 weeks, were officially included in the study.

A total of 54 mice were used in this experiment. The ^{125}I-labeled and unlabeled PEG-Dex were mixed and administered to mice (polymer dosage = 5.4 mg/mouse, ~50 g body weight) via tail vein injection. These mice were randomly assigned into 9 groups containing 6 mice in each group. These groups were sacrificed at 9 different time points (0.5, 2, 4, 6, 24, 72, 168 and 336 h) after injection. Blood and other major organs were collected at selective time point without perfusion.

4.2.4 Pharmacokinetic and Biodistribution Analysis

Each tissue sample was weighed and counted on the gamma counter to determine the amount of drug (via radioactivity) in each tissue. After counting, each tissue sample was homogenized in 3-volumes of $H_2O$and 100 µL was added to 1 mL of ethyl acetate to extract free dexamethasone and to remove polymer. After extraction, the supernatant (900 µL) was withdrawn and transferred to a new tube with the addition of Internal Standard (IS) solution (10 µL Dexamethasone-d4, 1000 ng/mL). The samples were then evaporated, and the residue was dissolved for LC-MS/MS analysis to determine the free dexamethasone concentration.

Spiking solutions in 50% MeOH at different analyte concentrations (1, 2, 5, 10, 20, 50, 100, 200, 500, 1000, 2000, 5000, 10000 ng/mL), a blank and a (zero analyte + IS) spiking solution were prepared beforehand. Spiking solution (10 µL each) was added to blank tissue/organ homogenate (100 µL). Then these standard samples were extracted with 1 mL of Ethyl Acetate. Tthe samples were evaporated under a vacuum and reconstituted in 100 µL of 50% methanol. Samples were analyzed using LC-MS/MS to obtain the dexamethasone levels.

The PK/BD analysis includes two parts. One is the PK/BD profile of PEG-Dex analyzed using gamma counter-based data; and the other is the analysis of free dexamethasone (Dex) released from PEG-Dex, of which the Dex concentration was analyzed using LC-MS/MS. The pharmacokinetic parameter, such as biological half-life ($t_{1/2}$), the maximum concentration (C_{max}) and mean residence time (MRT) were determined using the bolus intravenous input noncompartmental analysis WinNonlin (version 6.3, Pharsight, Mountain View, CA). The area under the curve (AUC) was calculated using the trapezoidal rule.

4.3 Results

4.3.1 Pharmacokinetic profiles of PEG-Dex by Gamma Counter

The established noncompartmental analytical method was successfully applied to determine the concentrations of ^{125}I-labeled PEG-Dex in the major organs of established lupus nephritis mice. The concentration-time profile of PEG-Dex after a single i.v. dose of 5.4 mg per mouse is shown in Figure 16. The reduction of PEG-Dex concentration as a function of time in all the tested organs was determined. The concentration of ^{125}I-labeled PEG-Dex in the kidney dropped from ~9%/g at 0.5 hour to ~4% ID/g at 2 hour post-injection, and plateaued. Up to 24 hours after i.v. injection, ~3%ID/g of PEG-Dex still retained in kidney, which was significantly higher than the concentrations (<1%ID/g) in the other organs at the same time course. Similarly, the concentration of PEG-Dex in the organs at different time points were compared (Figure 17) and the levels in the kidney were dramatically higher than other organs, suggesting that the majority of PEG-Dex is accumulated in the nephritic kidney in the first 5 time points (0.5, 2, 4, 6, 24 hour). From 3 day to 28 day, the concentration of PEG-Dex in all the organs decreased below 0.5 %ID/g, even though the liver showed a higher level of drug accumulation than other organs during these times.

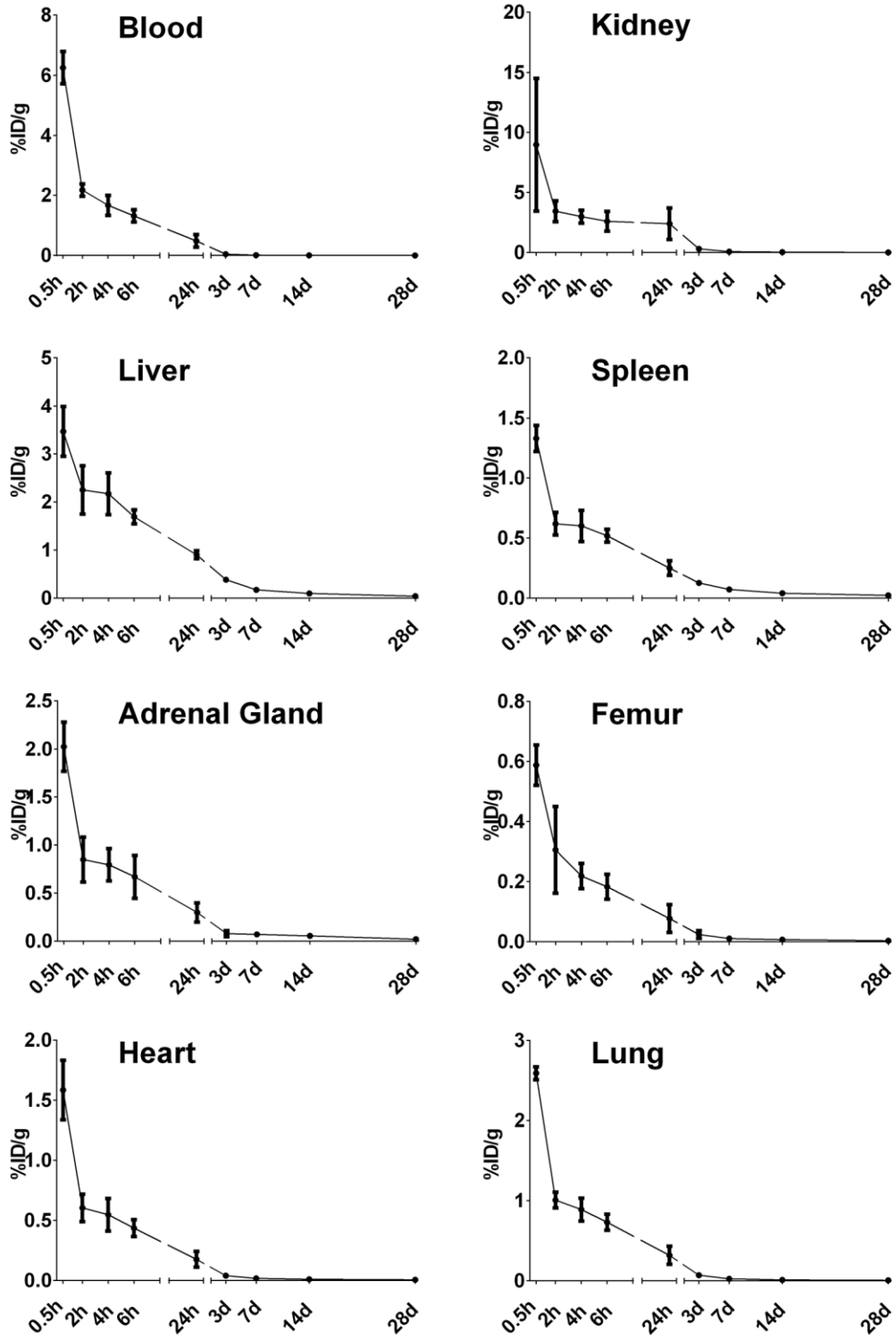
Blood
%ID/g
0
2
4
6
8
0.5h
2h
4h
6h
24h
3d
7d
14d
28d
Kidney
%ID/g
0
5
10
15
20
Liver
%ID/g
0
1
2
3
4
5
Spleen
%ID/g
0.0
0.5
1.0
1.5
2.0
Adrenal Gland
%ID/g
0.0
0.5
1.0
1.5
2.0
2.5
Femur
%ID/g
0.0
0.2
0.4
0.6
0.8
Heart
%ID/g
0.0
0.5
1.0
1.5
2.0
Lung
%ID/g
0
1
2
3

Figure 16. The concentration-time profiles of PEG-Dex in blood and major organs/tissues after a single dose (5.4mg PEG-Dex per mouse) of intravenous administration (n=5~6, mean ± SD).

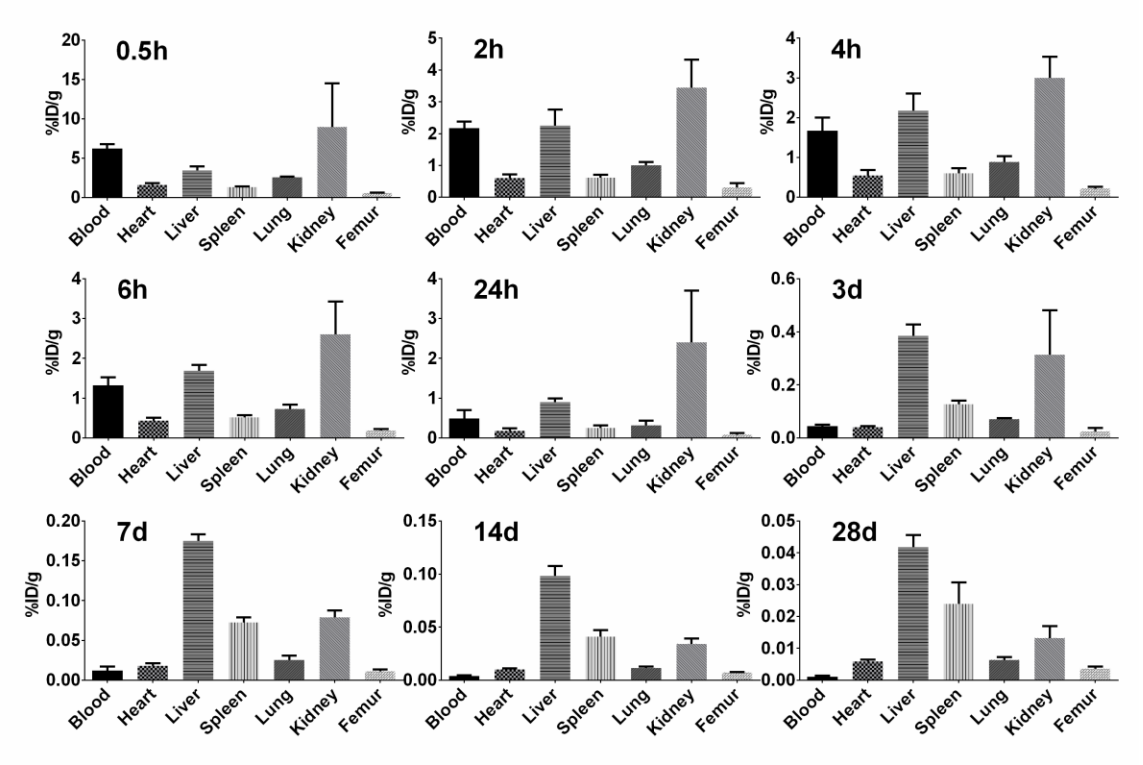

Figure 17. Pharmacokinetic profiles of PEG-Dex in blood and major organs/tissues at selective time points after a single dose (5.4mg PEG-Dex per mouse) of intravenous administration (n=5-6, mean ± SD).

Pharmacokinetic parameters of the major organs estimated by WinNonlin were summarized in Table 1, in which AUC is the area under the concentration-time curve, $t_{1/2}$ is the biological half-life including alpha phase $t_{1/2}(\alpha)$ associated

with distribution and beta phase $t_{1/2}(\beta)$ associated with elimination, C_{max} is the maximum concentration, and MRT is mean residence time. The AUC of kidney is significantly higher than other organs suggesting the highest drug exposure is found in the kidney. The kidney showed very fast distribution rate ($t_{1/2}(\alpha)$=0.48 h) and slowest clearance rate ($t_{1/2}(\beta)$=31.9 h) amongst other major organs, indicating the inflamed kidney can be rapidly perfused by PEG-Dex and retain the drug in the kidney for a longer time after reaching distribution equilibrium. The highest maximum concentration (C_{max}) and mean residence time (MRT) were also observed in the kidney, which are the additional evidences for the hypothesis that PEG-Dex can be sequestered mainly by renal tissues and reside in the inflamed kidney for a longer time compared to the other critical organs.

Table 1. Pharmacokinetic (PK) parameters of PEG-Dex after a single dose of intravenous administration.

Parameters (unit)	**Blood**	**Kidney**
AUC (h·DPM/g)	720622.66 ± 17664.65	2803827.58 ± 500811.86
$t_{1/2}(\alpha)$ (h)	0.52 ± 0.01	0.48 ± 0.12
$t_{1/2}(\beta)$ (h)	11.87 ± 0.49	31.9 ± 7.33
C_{max} (DPM/g)	196058.55 ± 2694.12	277785.86 ± 37419.8
MRT (h)	14.38 ± 0.63	43.56 ± 10.3
Parameters (unit)	**Liver**	**Spleen**
AUC (h·DPM/g)	1351035.5 ± 213537.15	391741.9 ± 73666.42

$t_{1/2}(\alpha)$ (h)	0.99 ± 0.38	0.44 ± 0.19
$t_{1/2}(\beta)$ (h)	24.7 ± 5.55	22.73 ± 5.63
C_{max} (DPM/g)	76256.39 ± 6294.3	41105.8 ± 9558.24
MRT (h)	33.88 ± 7.57	31.24 ± 7.89

4.3.2 Pharmacokinetic profiles of released dexamethasone by LC/MS.

The weight ratio-time profiles of dexamethasone released from PEG-Dex prodrugs in major organs (including blood, kidney, heart, liver, spleen and lung) were shown in Figure 18. In liver, the content of dexamethasone decreases as a function of time. The C_{max} is observed at 2 hours post-injection in liver and is higher than the other organs suggesting the liver is the major metabolic organ for PEG-Dex cleaving dexamethasone from PEG-Dex prodrugs. However, the elimination phase in kidney is different from liver. In kidney, the content of dexamethasone reduces slowly in the first 6 hours after injection, and then reaches a peak with ~120 ng/g dexamethasone at the 24 hour time point, suggesting a high content of released dexamethasone accumulated in the inflamed kidney after it was cleaved from PEG-Dex in liver. The similar elimination phase was observed in the other tested organs but at dramatically lower levels of the dexamethasone content. Similarly, when analyzing the dexamethasone content in major organs at selective time points, a relatively higher accumulation

of released dexamethasone was observed in the kidney for up to 7 days after injection, suggesting the controlled release phase of PEG-Dex occurs in the nephritic kidney.

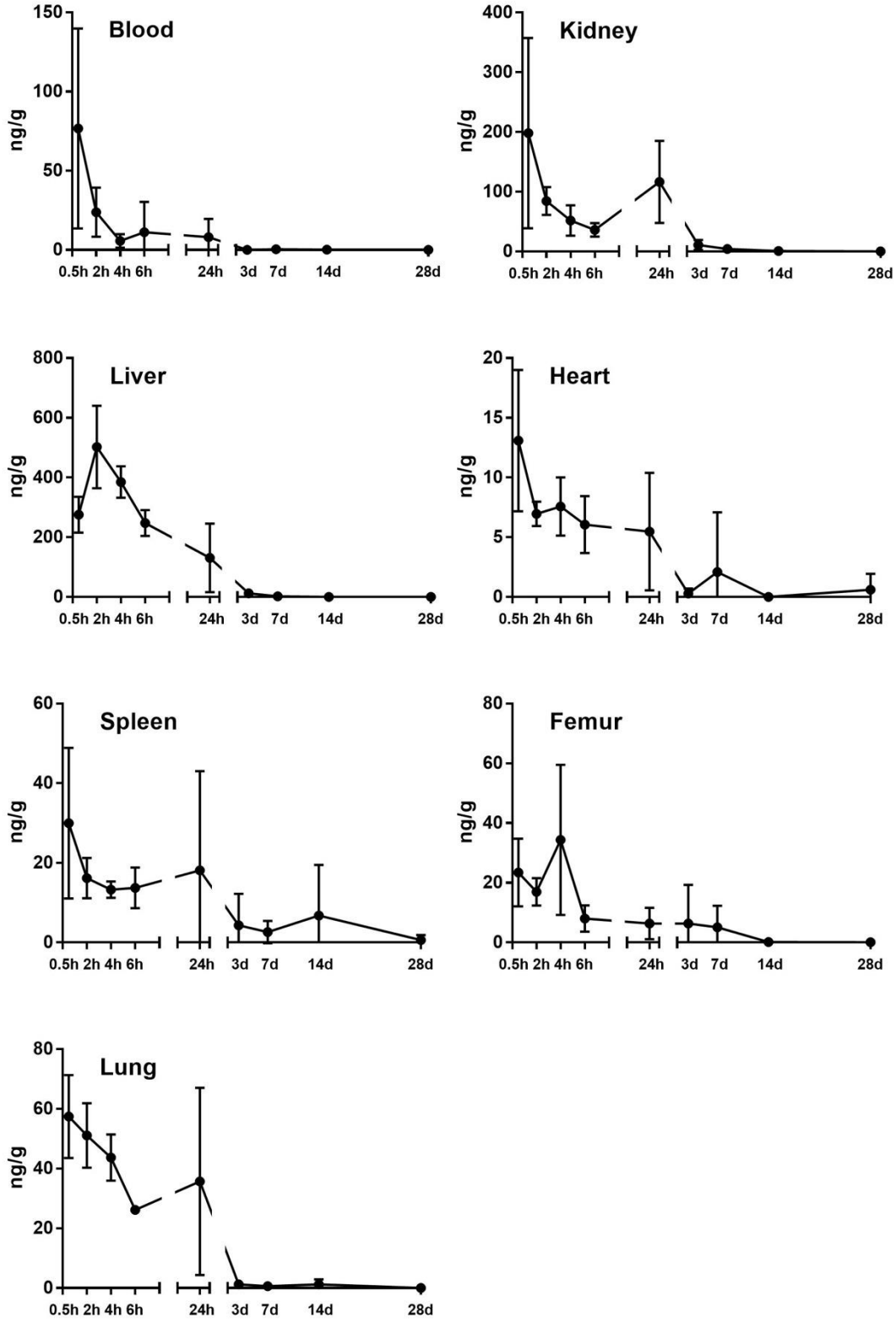
Blood
ng/g
150
100
50
0
0.5h 2h 4h 6h 24h 3d 7d 14d 28d
Kidney
ng/g
400
300
200
100
0
0.5h 2h 4h 6h 24h 3d 7d 14d 28d
Liver
ng/g
800
600
400
200
0
0.5h 2h 4h 6h 24h 3d 7d 14d 28d
Heart
ng/g
20
15
10
5
0
0.5h 2h 4h 6h 24h 3d 7d 14d 28d
Spleen
ng/g
60
40
20
0
0.5h 2h 4h 6h 24h 3d 7d 14d 28d
Femur
ng/g
80
60
40
20
0
0.5h 2h 4h 6h 24h 3d 7d 14d 28d
Lung
ng/g
80
60
40
20
0
0.5h 2h 4h 6h 24h 3d 7d 14d 28d

Figure 18. The dexamethasone content-time profiles of free dexamethasone released from the PEG-Dex blood and major organs/tissues after a single dose (5.4mg PEG-Dex per mouse) of intravenous administration (n=5~6, mean ± SD).

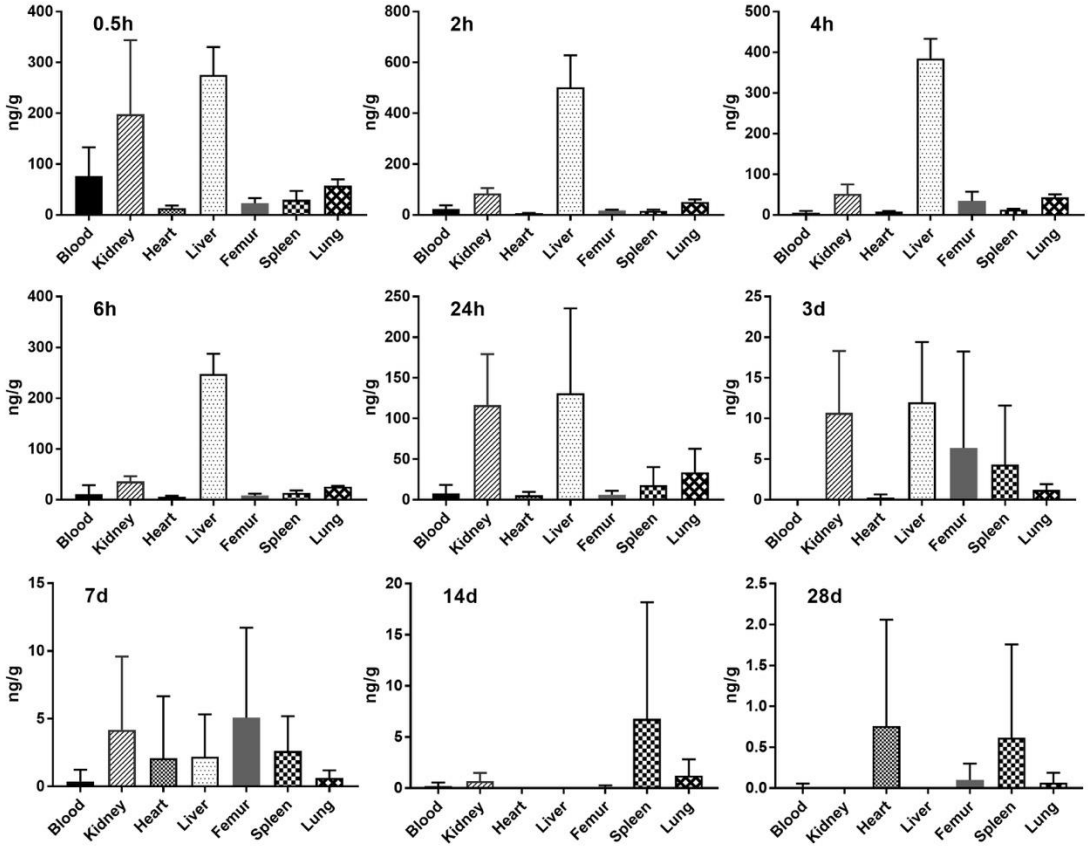

Figure 19. Pharmacokinetics profiles of Dex released from PEG-Dex in blood and major organs/tissues at each time point post i.v. administration. n=5~6.

4.4 Discussion

The PEG-Dex was designed to reduce GCs-associated side effects in the treatment of lupus nephritis through a novel GC prodrug nanomedicine development. Conceptually, this passive inflammation targeting was based on the mechanism “ELVIS” which stands for Extravasation through Leaky Vasculature and Inflammatory cell-mediated Sequestration, in which the nanomedicine would extravasate through the leaky vasculature at the inflammatory lesion,[13] and its subsequent inflammatory cell-mediated sequestration would alter the PK/BD profile of the parent drug, enabling inflammatory tissues/organs specificity.

In this study, we evaluated the pharmacokinetic and biodistribution (PK/BD) profiles of PEG-Dex in a lupus nephritis mouse model using ^{125}I-labeling/gamma counter techniques and LC-MS/MS. The focus of this study was to validate the preferential distribution of PEG-Dex polymer to inflammatory kidney and its superior and long-lasting therapeutic effect. As the main activation sites of the prodrug are probably the organs of its major distribution, the therapeutic effect and safety profile of the prodrug would be directly related to their PK/BD profiles.[15]

The pharmacokinetic profiles showed that the concentration of PEG-Dex in blood decreased rapidly after injection and the beta half-life is only 11.87 hours. As evident in Figure 16 and Figure 17, a fast distribution and longer retention of PEG-Dex polymer in kidney comparing to other organs, and the alpha half-life and

beta half-life are 0.48 hours and 31.9 hours, respectively. Those results proved that the polymers quickly distributed to kidneys from the blood system after the systemic injection. The kidney also showed the highest Cmax (277785.86 DPM/g) and MRT (43.56 hours), which means the kidney was the main organ of drug distribution. As shown in Figure 17, the majority of PEG-Dex was found in the liver after 3 days. We speculate this may be due to the liver being the major metabolic organ of PEG-Dex.

The PK/BD profiles of Dex released from PEG-Dex was presented in Figure 18 and 19. It showed there is a trend toward the slow release trend of PEG-Dex in the kidney as there were two peaks in the Dex-content vs time curve in kidney and blood (Figure 18). Also, the kidney showed a greater accumulation of Dex compared to other organs except the liver, which may explain the superior therapeutic efficacy of PEG-Dex for treating Lupus nephritis. Due to the Dex concentration in the liver, which increased at first, peaked at 2 h post injection and then decreased continuously, we speculate that Dex is mainly metabolized in the liver.

4.5 Conclusion

In this study, the *in vivo* pharmacokinetic and biodistribution (PK/BD) profiles of PEG-Dex were investigated in a lupus nephritis mouse model using ^{125}I-

labeling/gamma counter and LC MS/MS. The study found that the PEG-Dex was preferentially distributed to the kidney and showed a long-lasting therapeutic effect by constantly releasing Dex. After injection, the PEG-Dex prodrug distributed to the kidney and reached a steady state within 2 hours, which was the main organ of the drug distribution. The free dexamethasone was released from PEG-Dex in the inflamed kidney and its concentration peaked at 24 h, after a decrease from 0.5 h to 6 h post administration. The findings in this study will assist in the further design and optimization of PEG-Dex and the understanding of its nephrotropism.

CHAPTER V. SUMMARY AND FUTURE PERSPECTIVES

5.1 SUMMARY

As one of the most severe complications of SLE, lupus nephritis is highly correlated with lupus patients' survival and life quality. The pathogenesis of lupus nephritis involves a complex of pathogenic mechanisms. Although the trigger that initiates SLE in a genetically susceptible person is still unknown, the etiology of the widely recognized renal autoantibody can be summarized in two parts, the extrarenal and intrarenal. The extrarenal etiology involves immune complexes from circulating blood depositing on the glomerular basement membrane that triggers a cascade of immune events [23], while intrarenal etiology refers to the subsequent immune response stimulated by the apoptosis of renal cells injured by the infiltrated leukocytes migrating from circulating blood [55, 56].

Although the prognosis of proliferative nephritis has been relatively improved by glucocorticoids plus immunosuppressives [62], long-term use of glucocorticoids needs to be cautiously applied due to the various adverse effects involving multiple systems (i.e. musculoskeletal, endocrine, cardiovascular, hematopoietic and gastrointestinal systems) [168]. These adverse side effects dramatically increase the morbidity of lupus patients. According to the most

recent ACR (American College of Rheumatology) guidance for clinical management of lupus nephritis [61], the major change is that new immunosuppressants (e.g. mycophenolate mofetil) have been added as alternatives to cyclophosphamide. No alternatives have been recommended for GC.

The actions of GC are mediated through two distinct pathways: transactivation and transrepression, which are postulated to be related to GC-associated side effects and anti-inflammatory effects, respectively [169]. GC receptor agonists can activate the transrepression responses while with low sensitivity and still elicit GC-associated side effects through triggering the transactivation pathway [132].

Nanomedicine-based drug delivery system seems to be a potential approach to retain the GC efficacy as well as diminish GC-associated side effects by means of modifying GC's PK/BD profiles. In our previous study, we conjugated dexamethasone to a water-soluble N-(2-hydroxypropyl)-methacrylamide (HPMA) copolymer via an acid-labile hydrazone linker to obtain a macromolecular prodrug of Dex (P-Dex). The enhancement of the therapeutic efficacy of P-Dex and avoidance of osteoporosis were observed, however, a relatively high accumulation of P-Dex in the liver and other GC-related side effects such as adrenal gland atrophy and WBC reduction still existed. Herein, to address the

residual toxicities, we designed a new Dex prodrug using polyethylene glycol (PEG) as a carrier.

In **chapter 2**, we conjugated a dexamethasone dimer to PEG chain terminus via glutamic acid/glycine/hydrazone linker system. The amphiphilic molecule self-assembles into micelles. The chemical structure of PEG-Dex and self-assembled micelles were fully characterized. The results demonstrated that PEG-Dex prodrug was successfully developed. Additionally, critical micellar concentration (CMC), DLS, and TEM results confirmed the micellar structure.

To evaluate the therapeutic effects of PEG-Dex, pre-clinical treatment studies were performed on the established lupus nephritis mouse model (**chapter 3**). Additionally, the safety profile and the potential mechanism of cellular interaction with the prodrug were further explored in this part. When tested in NZB/W F1 mice with established nephritis, the micelle demonstrated similar potent efficacy as P-Dex, but showed no apparent GC side effects. The potential reason might be attributed to the modified biodistribution of PEG-Dex in major organs, for PEG-Dex was passively targeted to the nephritic kidney evidenced by the *in vivo* imaging, SPECT-CT and flow cytometry data. Furthermore, we also found that proximal tubular epithelial is one of the major drug uptaking cells in the kidney, and *in vitro* study of human epithelial cell line suggested that the intracellular lysosome is the primary reservoir for PEG-Dex prodrugs.

To further address the working mechanism of long-term efficacy of PEG-Dex in the treatment of lupus nephritis, the pharmacokinetic studies were performed on mice with established lupus nephritis (**chapter 4**). In brief, PEG-Dex was labelled with ^{125}I and a single dose of PEG-Dex was intravenously administrated through the tail vein. At selected time points, the major organs were harvested and their radioactivity representative of the PEG-Dex concentration was examined by gamma counter. In addition, the released free dexamethasone from PEG-Dex was extracted from organs and the dexamethasone content was measured by LC/MS. The pharmacokinetic profiles demonstrated that nephritic kidney has the highest accumulation of PEG-Dex in the first 24 hours after injection. The liver may be the major metabolic organ for PEG-Dex as it has the highest maximum dexamethasone content (C_{max}) at 2 hours after injection, while C_{max} was reached much more rapidly. It worth noting that kidney has a cumulative peak concentration of dexamethasone at the 24 hour time point and maintain a relatively higher dexamethasone content for up to 7 days. These results further confirm our hypothesis that PEG-Dex prodrug can passively target to the inflamed kidney in the condition of lupus nephritis and release the dexamethasone locally in a controlled release manner.

5.2 Future Perspectives

At the end of the project, we anticipate being able to identify the final optimized PEG-Dex micelle formulation that can be further developed for clinical translation. To achieve this goal, there are a few concepts that should be further investigated.

1) Optimization of the PEG-based prodrug micelle system. In the current PEG-based prodrug micelle system, there are a few issues need to be noted. The hydrazone structure formed at each reaction site has a pair of cis-trans isomers due to the double bond. As we conjugate a dexamethasone dimer (containing two dexamethasone molecules, one at each side) to the PEG backbone, even though we induced TBS to sterically hinder hydrazine bonds forming at one carbonyl group (C-3), we may still have 4 possible isomers in the final product, which will make purification complicated and difficult for bulk production. A possible solution is to selectively introduce a symmetrical structural linker plus TBS to theoretically avoid all the isomers. Moreover, the length/MW of PEG polymers should be further investigated as the cellular interaction with the prodrug and *in vivo* PK/BD profiles will be dramatically changed accordingly. Finally, simpler synthetic routes and repetitive yields need to be further controllable and stabilized, which is the precondition for the bulky production by the industry.

2) To better guide the structural design for PEG-Dex, the cell-prodrug interaction mechanism at the molecular level needs to be further explored.

Whether PEG-Dex enters cells through a receptor-mediated pathway or a non-specific internalization is still unknown. Some transfected receptor library may be applied for the receptor screening, which can help determine if there are specific receptors that will bind with the PEG-Dex moieties. Some other mechanism might work together to improve the renal internalization of PEG-Dex. It is well known that PEGylated nanomedicine has a longer half-life in the circulating blood due to the crown-like structures formed by PEG which can prevent the recognition and internalization by immune cells. However, very interestingly, a large proportion of renal cells internalized PEG-Dex in the inflamed kidney, which seems to contradictto common knowledge about PEG's property. Recent research has shown that a possible reason for the avoidance of immune cell internalization ofPEGlyated nanoparticles is that there are some specific proteins in the microenvironment which can stop PEG carriers from being internalized by the cells, i.e., clusterin. Also, researchers reported that the serum level of clusterin in lupus patients is lower than the healthy people, while a high level of albumin is detected in the renal inflammation and albumin can increase the drug internalization. Taken together, an interesting hypothesis is that the lower level of clusterin and high accumulation of albumin working synergistically to speed up the renal cells internalization of PEG-Dex prodrugs. However, more research will be needed to support this hypothesis.

3) Human lupus is a highly heterogeneous disease characterized by aberrations in multiple immunological processes. Disease heterogeneity is also

observed in spontaneous murine models of lupus suggesting that preclinical studies should encompass a number of different lupus models to more accurately reflect the complexity of human lupus. Therefore, the original PEG-Dex micelle will be tested in NZM2410 and MRL/lpr mice to further validate its efficacy and safety. Additionally, it will also be tested in collagen-induced arthritis (CIA) mice to validate its potential to ameliorate the arthritis comorbidity of lupus. Based on the outcome of these experiments and our understanding of the working mechanism of PEG-Dex micelles, the structure of PEG-Dex will be fine-tuned and validated in NZB/W F1 mice for its long term (1 year) efficacy and safety in preparation for clinical application.

Reference

1. *Lupus Foundation of America.*; Available from: https://resources.lupus.org/entry/facts-and-statistics.
2. Hahn, B.H., et al., *American College of Rheumatology guidelines for screening, treatment, and management of lupus nephritis.* Arthritis Care Res (Hoboken), 2012. **64**(6): p. 797-808.
3. Ortega, L.M., et al., *Review: Lupus nephritis: pathologic features, epidemiology and a guide to therapeutic decisions.* Lupus, 2010. **19**(5): p. 557-74.
4. Cervera, R., M.A. Khamashta, and G.R. Hughes, *The Euro-lupus project: epidemiology of systemic lupus erythematosus in Europe.* Lupus, 2009. **18**(10): p. 869-74.
5. Pickering, M. and H.T. Cook, *Complement and glomerular disease: new insights.* Curr Opin Nephrol Hypertens, 2011. **20**(3): p. 271-7.
6. Clynes, R., C. Dumitru, and J.V. Ravetch, *Uncoupling of immune complex formation and kidney damage in autoimmune glomerulonephritis.* Science, 1998. **279**(5353): p. 1052-4.
7. Cameron, J.S., *Lupus nephritis.* J Am Soc Nephrol, 1999. **10**(2): p. 413-24.
8. Jakes, R.W., et al., *Systematic review of the epidemiology of systemic lupus erythematosus in the Asia-Pacific region: prevalence, incidence, clinical features, and mortality.* Arthritis Care Res (Hoboken), 2012. **64**(2): p. 159-68.

9. Dooley, M.A., et al., *Cyclophosphamide therapy for lupus nephritis: poor renal survival in black Americans. Glomerular Disease Collaborative Network.* Kidney Int, 1997. **51**(4): p. 1188-95.

10. Hiraki, L.T., et al., *End-stage renal disease due to lupus nephritis among children in the US, 1995-2006.* Arthritis Rheum, 2011. **63**(7): p. 1988-97.

11. Eisenberg, R., *Mechanisms of autoimmunity.* Immunol Res, 2003. **27**(2-3): p. 203-18.

12. Kong, P.L., et al., *Intrinsic T cell defects in systemic autoimmunity.* Ann N Y Acad Sci, 2003. **987**: p. 60-7.

13. Wiltshire, S., et al., *'I came back here and started smoking again': perceptions and experiences of quitting among disadvantaged smokers.* Health Educ Res, 2003. **18**(3): p. 292-303.

14. Tsokos, G.C., *Systemic lupus erythematosus.* N Engl J Med, 2011. **365**(22): p. 2110-21.

15. Kalaaji, M., et al., *Nephritogenic lupus antibodies recognize glomerular basement membrane-associated chromatin fragments released from apoptotic intraglomerular cells.* Am J Pathol, 2006. **168**(6): p. 1779-92.

16. Kalaaji, M., et al., *Critical comparative analyses of anti-alpha-actinin and glomerulus-bound antibodies in human and murine lupus nephritis.* Arthritis Rheum, 2006. **54**(3): p. 914-26.

17. Mostoslavsky, G., et al., *Lupus anti-DNA autoantibodies cross-react with a glomerular structural protein: a case for tissue injury by molecular mimicry.* Eur J Immunol, 2001. **31**(4): p. 1221-7.

18. Kalaaji, M., et al., *Glomerular apoptotic nucleosomes are central target structures for nephritogenic antibodies in human SLE nephritis.* Kidney Int, 2007. **71**(7): p. 664-72.

19. Manson, J.J., et al., *Relationship between anti-dsDNA, anti-nucleosome and anti-alpha-actinin antibodies and markers of renal disease in patients with lupus nephritis: a prospective longitudinal study.* Arthritis Res Ther, 2009. **11**(5): p. R154.

20. Marchini, M., et al., *HLA class II antigens associated with lupus nephritis in Italian SLE patients.* Hum Immunol, 2003. **64**(4): p. 462-8.

21. Taylor, K.E., et al., *Risk alleles for systemic lupus erythematosus in a large case-control collection and associations with clinical subphenotypes.* PLoS Genet, 2011. **7**(2): p. e1001311.

22. Turnberg, D. and H.T. Cook, *Complement and glomerulonephritis: new insights.* Curr Opin Nephrol Hypertens, 2005. **14**(3): p. 223-8.

23. Davidson, A. and C. Aranow, *Lupus nephritis: lessons from murine models.* Nat Rev Rheumatol, 2010. **6**(1): p. 13-20.

24. Watanabe, H., et al., *Modulation of renal disease in MRL/lpr mice genetically deficient in the alternative complement pathway factor B.* J Immunol, 2000. **164**(2): p. 786-94.

25. Elliott, M.K., et al., *Effects of complement factor D deficiency on the renal disease of MRL/lpr mice.* Kidney Int, 2004. **65**(1): p. 129-38.

26. Bao, L., M. Haas, and R.J. Quigg, *Complement factor H deficiency accelerates development of lupus nephritis.* J Am Soc Nephrol, 2011. **22**(2): p. 285-95.

27. Wenderfer, S.E., et al., *C5a receptor deficiency attenuates T cell function and renal disease in MRLlpr mice.* J Am Soc Nephrol, 2005. **16**(12): p. 3572-82.

28. Sekine, H., et al., *The dual role of complement in the progression of renal disease in NZB/W F(1) mice and alternative pathway inhibition.* Mol Immunol, 2011. **49**(1-2): p. 317-23.

29. Wang, Y., et al., *Amelioration of lupus-like autoimmune disease in NZB/WF1 mice after treatment with a blocking monoclonal antibody specific for complement component C5.* Proc Natl Acad Sci U S A, 1996. **93**(16): p. 8563-8.

30. Korb, L.C. and J.M. Ahearn, *C1q binds directly and specifically to surface blebs of apoptotic human keratinocytes: complement deficiency and systemic lupus erythematosus revisited.* J Immunol, 1997. **158**(10): p. 4525-8.

31. Sekine, H., et al., *The benefit of targeted and selective inhibition of the alternative complement pathway for modulating autoimmunity and renal disease in MRL/lpr mice.* Arthritis Rheum, 2011. **63**(4): p. 1076-85.

32. Ytterberg, S.R. and T.J. Schnitzer, *Serum interferon levels in patients with systemic lupus erythematosus.* Arthritis Rheum, 1982. **25**(4): p. 401-6.

33. Kaser, A., et al., *Interleukin-18 attracts plasmacytoid dendritic cells (DC2s) and promotes Th1 induction by DC2s through IL-18 receptor expression.* Blood, 2004. **103**(2): p. 648-55.

34. Tucci, M., et al., *Glomerular accumulation of plasmacytoid dendritic cells in active lupus nephritis: role of interleukin-18.* Arthritis Rheum, 2008. **58**(1): p. 251-62.

35. Bengtsson, A.A., et al., *Activation of type I interferon system in systemic lupus erythematosus correlates with disease activity but not with antiretroviral antibodies.* Lupus, 2000. **9**(9): p. 664-71.

36. Gao, Y., et al., *Dynamic accumulation of plasmacytoid dendritic cells in lymph nodes is regulated by interferon-beta.* Blood, 2009. **114**(13): p. 2623-31.

37. Jego, G., et al., *Plasmacytoid dendritic cells induce plasma cell differentiation through type I interferon and interleukin 6.* Immunity, 2003. **19**(2): p. 225-34.

38. Gallagher, K.M., et al., *Type I interferon (IFN alpha) acts directly on human memory CD4+ T cells altering their response to antigen.* J Immunol, 2009. **183**(5): p. 2915-20.

39. Ramos, H.J., et al., *Reciprocal responsiveness to interleukin-12 and interferon-alpha specifies human CD8+ effector versus central memory T-cell fates.* Blood, 2009. **113**(22): p. 5516-25.

40. Hsu, H.C., et al., *Interleukin 17-producing T helper cells and interleukin 17 orchestrate autoreactive germinal center development in autoimmune BXD2 mice.* Nat Immunol, 2008. **9**(2): p. 166-75.

41. Odegard, J.M., et al., *ICOS-dependent extrafollicular helper T cells elicit IgG production via IL-21 in systemic autoimmunity.* J Exp Med, 2008. **205**(12): p. 2873-86.

42. Pisitkun, P., et al., *Interleukin-17 cytokines are critical in development of fatal lupus glomerulonephritis.* Immunity, 2012. **37**(6): p. 1104-15.

43. Vinuesa, C.G., et al., *A RING-type ubiquitin ligase family member required to repress follicular helper T cells and autoimmunity.* Nature, 2005. **435**(7041): p. 452-8.

44. Crispin, J.C., et al., *T cells as therapeutic targets in SLE.* Nat Rev Rheumatol, 2010. **6**(6): p. 317-25.

45. Pernis, A.B., *Th17 cells in rheumatoid arthritis and systemic lupus erythematosus.* J Intern Med, 2009. **265**(6): p. 644-52.

46. Theofilopoulos, A.N., et al., *The role of IFN-gamma in systemic lupus erythematosus: a challenge to the Th1/Th2 paradigm in autoimmunity.* Arthritis Res, 2001. **3**(3): p. 136-41.

47. Crow, M.K., *Type I interferon in organ-targeted autoimmune and inflammatory diseases.* Arthritis Res Ther, 2010. **12 Suppl 1**: p. S5.

48. Davidson, A., *Targeting BAFF in autoimmunity.* Curr Opin Immunol, 2010. **22**(6): p. 732-9.

49. Elkon, K.B. and A. Wiedeman, *Type I IFN system in the development and manifestations of SLE.* Curr Opin Rheumatol, 2012. **24**(5): p. 499-505.

50. Theofilopoulos, A.N., *TLRs and IFNs: critical pieces of the autoimmunity puzzle.* J Clin Invest, 2012. **122**(10): p. 3464-6.

51. Yu, Y. and K. Su, *Neutrophil Extracellular Traps and Systemic Lupus Erythematosus.* J Clin Cell Immunol, 2013. **4**.

52. Weidenbusch, M., et al., *Beyond the LUNAR trial. Efficacy of rituximab in refractory lupus nephritis.* Nephrol Dial Transplant, 2013. **28**(1): p. 106-11.

53. Sanz, I. and F.E. Lee, *B cells as therapeutic targets in SLE.* Nat Rev Rheumatol, 2010. **6**(6): p. 326-37.

54. Townsend, M.J., J.G. Monroe, and A.C. Chan, *B-cell targeted therapies in human autoimmune diseases: an updated perspective.* Immunol Rev, 2010. **237**(1): p. 264-83.

55. Segerer, S. and D. Schlondorff, *B cells and tertiary lymphoid organs in renal inflammation.* Kidney Int, 2008. **73**(5): p. 533-7.

56. Jeruc, J., et al., *Tubulo-interstitial involvement in lupus nephritis with emphasis on pathogenesis.* Wien Klin Wochenschr, 2000. **112**(15-16): p. 702-6.

57. Steinmetz, O.M., et al., *Analysis and classification of B-cell infiltrates in lupus and ANCA-associated nephritis.* Kidney Int, 2008. **74**(4): p. 448-57.

58. Chang, A., et al., *In situ B cell-mediated immune responses and tubulointerstitial inflammation in human lupus nephritis.* J Immunol, 2011. **186**(3): p. 1849-60.

59. Chan, O.T., et al., *A novel mouse with B cells but lacking serum antibody reveals an antibody-independent role for B cells in murine lupus.* J Exp Med, 1999. **189**(10): p. 1639-48.

60. Schwartz, M.M., *The pathology of lupus nephritis.* Semin Nephrol, 2007. **27**(1): p. 22-34.

61. *Guidelines for referral and management of systemic lupus erythematosus in adults. American College of Rheumatology Ad Hoc Committee on Systemic Lupus Erythematosus Guidelines.* Arthritis Rheum, 1999. **42**(9): p. 1785-96.

62. Chan, T.M., *Treatment of severe lupus nephritis: the new horizon.* Nat Rev Nephrol, 2015. **11**(1): p. 46-61.

63. Mishra, M.K., et al., *Kinetics of proinflammatory monocytes in a model of multiple sclerosis and its perturbation by laquinimod.* Am J Pathol, 2012. **181**(2): p. 642-51.

64. Schulze-Topphoff, U., et al., *Laquinimod, a quinoline-3-carboxamide, induces type II myeloid cells that modulate central nervous system autoimmunity.* PLoS One, 2012. **7**(3): p. e33797.

65. Comi, G., et al., *Placebo-controlled trial of oral laquinimod for multiple sclerosis.* N Engl J Med, 2012. **366**(11): p. 1000-9.

66. Finck, B.K., B. Chan, and D. Wofsy, *Interleukin 6 promotes murine lupus in NZB/NZW F1 mice.* J Clin Invest, 1994. **94**(2): p. 585-91.

67. Kitani, A., et al., *Autostimulatory effects of IL-6 on excessive B cell differentiation in patients with systemic lupus erythematosus: analysis of*

IL-6 production and IL-6R expression. Clin Exp Immunol, 1992. **88**(1): p. 75-83.

68. Kitani, A., et al., *Heterogeneity of B cell responsiveness to interleukin 4, interleukin 6 and low molecular weight B cell growth factor in discrete stages of B cell activation in patients with systemic lupus erythematosus.* Clin Exp Immunol, 1989. **77**(1): p. 31-6.
69. Ryffel, B., et al., *Interleukin-6 exacerbates glomerulonephritis in (NZB x NZW)F1 mice.* Am J Pathol, 1994. **144**(5): p. 927-37.
70. Mihara, M., et al., *IL-6 receptor blockage inhibits the onset of autoimmune kidney disease in NZB/W F1 mice.* Clin Exp Immunol, 1998. **112**(3): p. 397-402.
71. Linker-Israeli, M., et al., *Elevated levels of endogenous IL-6 in systemic lupus erythematosus. A putative role in pathogenesis.* J Immunol, 1991. **147**(1): p. 117-23.
72. Peterson, E., A.D. Robertson, and W. Emlen, *Serum and urinary interleukin-6 in systemic lupus erythematosus.* Lupus, 1996. **5**(6): p. 571-5.
73. Hillmen, P., et al., *The complement inhibitor eculizumab in paroxysmal nocturnal hemoglobinuria.* N Engl J Med, 2006. **355**(12): p. 1233-43.
74. Barilla-Labarca, M.L., K. Toder, and R. Furie, *Targeting the complement system in systemic lupus erythematosus and other diseases.* Clin Immunol, 2013. **148**(3): p. 313-21.

75. Morimoto, A.M., et al., *Association of endogenous anti-interferon-alpha autoantibodies with decreased interferon-pathway and disease activity in patients with systemic lupus erythematosus.* Arthritis Rheum, 2011. **63**(8): p. 2407-15.

76. McBride, J.M., et al., *Safety and pharmacodynamics of rontalizumab in patients with systemic lupus erythematosus: results of a phase I, placebo-controlled, double-blind, dose-escalation study.* Arthritis Rheum, 2012. **64**(11): p. 3666-76.

77. Merrill, J.T., et al., *Safety profile and clinical activity of sifalimumab, a fully human anti-interferon alpha monoclonal antibody, in systemic lupus erythematosus: a phase I, multicentre, double-blind randomised study.* Ann Rheum Dis, 2011. **70**(11): p. 1905-13.

78. Petri, M., et al., *Sifalimumab, a human anti-interferon-alpha monoclonal antibody, in systemic lupus erythematosus: a phase I randomized, controlled, dose-escalation study.* Arthritis Rheum, 2013. **65**(4): p. 1011-21.

79. Aran, A.A. and C. Putterman, *Treatment of lupus nephritis: facing the era of immunotherapy.* Panminerva Med, 2008. **50**(3): p. 235-45.

80. Cancro, M.P., *The BLyS/BAFF family of ligands and receptors: key targets in the therapy and understanding of autoimmunity.* Ann Rheum Dis, 2006. **65 Suppl 3**: p. iii34-6.

81. Zhang, J., et al., *Cutting edge: a role for B lymphocyte stimulator in systemic lupus erythematosus.* J Immunol, 2001. **166**(1): p. 6-10.

82. Gross, J.A., et al., *TACI and BCMA are receptors for a TNF homologue implicated in B-cell autoimmune disease.* Nature, 2000. **404**(6781): p. 995-9.

83. Navarra, S.e.a., *Belimumab, a BLyS-specific inhibitor, reduced disease activity, flares and prednisone use in patients with active SLe: efficacy and safety results from the Phase 3 BLISS-52 Study*, in *American College of Rheumatology Annual Meeting*. 2009 October: Philadelphia, PA.

84. Appel, G.B., et al., *Mycophenolate mofetil versus cyclophosphamide for induction treatment of lupus nephritis.* J Am Soc Nephrol, 2009. **20**(5): p. 1103-12.

85. Austin, H.A., 3rd, et al., *Therapy of lupus nephritis. Controlled trial of prednisone and cytotoxic drugs.* N Engl J Med, 1986. **314**(10): p. 614-9.

86. Illei, G.G., et al., *Combination therapy with pulse cyclophosphamide plus pulse methylprednisolone improves long-term renal outcome without adding toxicity in patients with lupus nephritis.* Ann Intern Med, 2001. **135**(4): p. 248-57.

87. Gourley, M.F., et al., *Methylprednisolone and cyclophosphamide, alone or in combination, in patients with lupus nephritis. A randomized, controlled trial.* Ann Intern Med, 1996. **125**(7): p. 549-57.

88. Boumpas, D.T., et al., *Controlled trial of pulse methylprednisolone versus two regimens of pulse cyclophosphamide in severe lupus nephritis.* Lancet, 1992. **340**(8822): p. 741-5.

89. Chan, T.M., et al., *Long-term study of mycophenolate mofetil as continuous induction and maintenance treatment for diffuse proliferative lupus nephritis.* J Am Soc Nephrol, 2005. **16**(4): p. 1076-84.

90. Tse, K.C., et al., *Quality of life comparison between corticosteroid- and-mycofenolate mofetil and corticosteroid- and-oral cyclophosphamide in the treatment of severe lupus nephritis.* Lupus, 2006. **15**(6): p. 371-9.

91. Bertsias, G., et al., *EULAR recommendations for the management of systemic lupus erythematosus. Report of a Task Force of the EULAR Standing Committee for International Clinical Studies Including Therapeutics.* Ann Rheum Dis, 2008. **67**(2): p. 195-205.

92. Rovin, B.H., et al., *Efficacy and safety of rituximab in patients with active proliferative lupus nephritis: the Lupus Nephritis Assessment with Rituximab study.* Arthritis Rheum, 2012. **64**(4): p. 1215-26.

93. Merrill, J.T., et al., *Efficacy and safety of rituximab in moderately-to-severely active systemic lupus erythematosus: the randomized, double-blind, phase II/III systemic lupus erythematosus evaluation of rituximab trial.* Arthritis Rheum, 2010. **62**(1): p. 222-33.

94. Pollard, R.P., et al., *Serum levels of BAFF, but not APRIL, are increased after rituximab treatment in patients with primary Sjogren's syndrome: data from a placebo-controlled clinical trial.* Ann Rheum Dis, 2013. **72**(1): p. 146-8.

95. Vallerskog, T., et al., *Differential effects on BAFF and APRIL levels in rituximab-treated patients with systemic lupus erythematosus and rheumatoid arthritis.* Arthritis Res Ther, 2006. **8**(6): p. R167.

96. Daikh, D.I. and D. Wofsy, *Cutting edge: reversal of murine lupus nephritis with CTLA4Ig and cyclophosphamide.* J Immunol, 2001. **166**(5): p. 2913-6.

97. Schiffer, L., et al., *Short term administration of costimulatory blockade and cyclophosphamide induces remission of systemic lupus erythematosus nephritis in NZB/W F1 mice by a mechanism downstream of renal immune complex deposition.* J Immunol, 2003. **171**(1): p. 489-97.

98. Wofsy, D., J.L. Hillson, and B. Diamond, *Abatacept for lupus nephritis: alternative definitions of complete response support conflicting conclusions.* Arthritis Rheum, 2012. **64**(11): p. 3660-5.

99. Hench, P.S., E.C. Kendall, and et al., *The effect of a hormone of the adrenal cortex (17-hydroxy-11-dehydrocorticosterone; compound E) and of pituitary adrenocorticotropic hormone on rheumatoid arthritis.* Proceedings of the staff meetings. Mayo Clinic, 1949. **24**(8): p. 181-97.

100. Hao, H.X., J.K. Wang, and Y.L. Wang, *Solubility of dexamethasone sodium phosphate in different solvents.* Journal of Chemical and Engineering Data, 2004. **49**(6): p. 1697-1698.

101. van Vollenhoven, R.F., et al., *Treat-to-target in systemic lupus erythematosus: recommendations from an international task force.* Ann Rheum Dis, 2014. **73**(6): p. 958-67.

102. Shi, L., et al., *Preparation, characterization, and in vitro drug release behavior of glutathione-sensitive long-circulation micelles based on polyethylene glycol prodrug.* J Biomater Sci Polym Ed, 2016. **27**(6): p. 472-89.

103. Pepic, I., et al., *A nonionic surfactant/chitosan micelle system in an innovative eye drop formulation.* J Pharm Sci, 2010. **99**(10): p. 4317-25.

104. Yuan, F., et al., *A dexamethasone prodrug reduces the renal macrophage response and provides enhanced resolution of established murine lupus nephritis.* PLoS One, 2013. **8**(11): p. e81483.

105. Ren, K., et al., *Macromolecular prodrug of dexamethasone prevents particle-induced peri-implant osteolysis with reduced systemic side effects.* J Control Release, 2014. **175**: p. 1-9.

106. Yuan, F., et al., *Dexamethasone prodrug treatment prevents nephritis in lupus-prone (NZB x NZW)F1 mice without causing systemic side effects.* Arthritis Rheum, 2012. **64**(12): p. 4029-39.

107. Quan, L., et al., *Nanomedicines for inflammatory arthritis: head-to-head comparison of glucocorticoid-containing polymers, micelles, and liposomes.* ACS Nano, 2014. **8**(1): p. 458-466.

108. Ren, K., et al., *Macromolecular glucocorticoid prodrug improves the treatment of dextran sulfate sodium-induced mice ulcerative colitis.* Clin Immunol, 2015. **160**(1): p. 71-81.

109. Dolman, M.E., et al., *Drug targeting to the kidney: Advances in the active targeting of therapeutics to proximal tubular cells.* Adv Drug Deliv Rev, 2010. **62**(14): p. 1344-57.

110. Zhou, P., X. Sun, and Z. Zhang, *Kidney-targeted drug delivery systems.* Acta Pharm Sin B, 2014. **4**(1): p. 37-42.

111. Lesniewska, B., K.W. Nowak, and L.K. Malendowicz, *Dexamethasone-induced adrenal cortex atrophy and recovery of the gland from partial, steroid-induced atrophy.* Exp Clin Endocrinol, 1992. **100**(3): p. 133-9.

112. Wang, D., et al., *Inhibition of cathepsin K with lysosomotropic macromolecular inhibitors.* Biochemistry, 2002. **41**(28): p. 8849-59.

113. Quan, L.D., et al., *Pharmacokinetic and biodistribution studies of N-(2-hydroxypropyl)methacrylamide copolymer-dexamethasone conjugates in adjuvant-induced arthritis rat model.* Mol Pharm, 2010. **7**(4): p. 1041-9.

114. Wei, X., et al., *Pharmacokinetic and Biodistribution Studies of HPMA Copolymer Conjugates in an Aseptic Implant Loosening Mouse Model.* Mol Pharm, 2017. **14**(5): p. 1418-1428.

115. Dong, H., et al., *Long-circulating 15 nm micelles based on amphiphilic 3-helix peptide-PEG conjugates.* ACS Nano, 2012. **6**(6): p. 5320-9.

116. Etrych, T., et al., *New HPMA copolymers containing doxorubicin bound via pH-sensitive linkage: synthesis and preliminary in vitro and in vivo biological properties.* J Control Release, 2001. **73**(1): p. 89-102.

117. Yu, M., et al., *Lysosomal pH Decrease in Inflammatory Cells Used To Enable Activatable Imaging of Inflammation with a Sialic Acid Conjugated Profluorophore.* Anal Chem, 2015. **87**(13): p. 6688-95.

118. Mittal, M., et al., *Reactive oxygen species in inflammation and tissue injury.* Antioxid Redox Signal, 2014. **20**(7): p. 1126-67.

119. Wang, Y., et al., *pH and hydrogen peroxide dual responsive supramolecular prodrug system for controlled release of bioactive molecules.* Colloids Surf B Biointerfaces, 2014. **121**: p. 189-95.

120. Pons-Estel, G.J., et al., *Understanding the epidemiology and progression of systemic lupus erythematosus.* Semin Arthritis Rheum, 2010. **39**(4): p. 257-68.

121. *From the Centers for Disease Control and Prevention. Trends in deaths from systemic lupus erythematosus--United States, 1979-1998.* JAMA, 2002. **287**(20): p. 2649-50.

122. Mohan, C., et al., *Genetic dissection of systemic lupus erythematosus pathogenesis: Sle2 on murine chromosome 4 leads to B cell hyperactivity.* J Immunol, 1997. **159**(1): p. 454-65.

123. Lau, K.K. and R.J. Wyatt, *Glomerulonephritis.* Adolesc Med Clin, 2005. **16**(1): p. 67-85.

124. Gurevitz, S.L., et al., *Systemic lupus erythematosus: a review of the disease and treatment options.* Consult Pharm, 2013. **28**(2): p. 110-21.

125. Radhakrishnan, J., et al., *Mycophenolate mofetil and intravenous cyclophosphamide are similar as induction therapy for class V lupus nephritis.* Kidney Int, 2010. **77**(2): p. 152-60.

126. Jordan, N. and D.P. D'Cruz, *Belimumab for the treatment of systemic lupus erythematosus.* Expert Rev Clin Immunol, 2015. **11**(2): p. 195-204.

127. Ostensen, M. and P.M. Villiger, *Nonsteroidal anti-inflammatory drugs in systemic lupus erythematosus.* Lupus, 2001. **10**(3): p. 135-9.

128. Firestein, G.S.a.K., W. N., *Kelley's textbook of rheumatology.* 9th ed. 2013, Philadelphia, PA: Elsevier/Saunders. 863-881.

129. Newton, R. and N.S. Holden, *Separating transrepression and transactivation: a distressing divorce for the glucocorticoid receptor?* Mol Pharmacol, 2007. **72**(4): p. 799-809.

130. Buckbinder, L. and R.P. Robinson, *The glucocorticoid receptor: molecular mechanism and new therapeutic opportunities.* Curr Drug Targets Inflamm Allergy, 2002. **1**(2): p. 127-36.

131. Kym, P.R., et al., *Nonsteroidal selective glucocorticoid modulators: the effect of C-10 substitution on receptor selectivity and functional potency of 5-allyl-2,5-dihydro-2,2,4-trimethyl-1H-[1]benzopyrano[3,4-f]quinolines.* J Med Chem, 2003. **46**(6): p. 1016-30.

132. Ayroldi, E., A. Macchiarulo, and C. Riccardi, *Targeting glucocorticoid side effects: selective glucocorticoid receptor modulator or glucocorticoid-induced leucine zipper? A perspective.* FASEB J, 2014. **28**(12): p. 5055-70.

133. Yuan, F., et al., *Development of macromolecular prodrug for rheumatoid arthritis.* Adv Drug Deliv Rev, 2012. **64**(12): p. 1205-19.

134. Bynote, K.K., et al., *Estrogen receptor-alpha deficiency attenuates autoimmune disease in (NZB x NZW)F1 mice.* Genes Immun, 2008. **9**(2): p. 137-52.

135. Howie, J.B. and B.J. Helyer, *The immunology and pathology of NZB mice.* Adv Immunol, 1968. **9**: p. 215-66.

136. Andrews, B.S., et al., *Spontaneous murine lupus-like syndromes. Clinical and immunopathological manifestations in several strains.* J Exp Med, 1978. **148**(5): p. 1198-215.

137. Rigby, R.J., et al., *A novel locus regulates both retroviral glycoprotein 70 and anti-glycoprotein 70 antibody production in New Zealand mice when crossed with BALB/c.* J Immunol, 2004. **172**(8): p. 5078-85.

138. Drakulic, D., et al., *Low-dose dexamethasone treatment promotes the pro-survival signalling pathway in the adult rat prefrontal cortex.* J Neuroendocrinol, 2013. **25**(7): p. 605-16.

139. Mosca, M., et al., *Glucocorticoids in systemic lupus erythematosus.* Clin Exp Rheumatol, 2011. **29**(5 Suppl 68): p. S126-9.

140. Wu, J., et al., *Immune activation caused by vascular oxidation promotes fibrosis and hypertension.* J Clin Invest, 2016. **126**(4): p. 1607.

141. Kusaba, T., et al., *Differentiated kidney epithelial cells repair injured proximal tubule.* Proc Natl Acad Sci U S A, 2014. **111**(4): p. 1527-32.

142. Ryan, M.J., et al., *HK-2: an immortalized proximal tubule epithelial cell line from normal adult human kidney.* Kidney Int, 1994. **45**(1): p. 48-57.

143. Utech, M., R. Mennigen, and M. Bruewer, *Endocytosis and recycling of tight junction proteins in inflammation.* J Biomed Biotechnol, 2010. **2010**: p. 484987.

144. Ivanov, A.I., A. Nusrat, and C.A. Parkos, *The epithelium in inflammatory bowel disease: potential role of endocytosis of junctional proteins in barrier disruption.* Novartis Found Symp, 2004. **263**: p. 115-24; discussion 124-32, 211-8.

145. Macanovic, M., et al., *The treatment of systemic lupus erythematosus (SLE) in NZB/W F1 hybrid mice; studies with recombinant murine DNase and with dexamethasone.* Clin Exp Immunol, 1996. **106**(2): p. 243-52.

146. Casey, T.P., *Systemic lupus erythematosus in NZB x NZW hybrid mice treated with the corticosteroid drug betamethasone.* J Lab Clin Med, 1968. **71**(3): p. 390-9.

147. Floyd, M., T.J. Muckle, and D.N. Kerr, *Prednisone-induced leucocytosis in nephrotic syndrome.* Lancet, 1969. **1**(7607): p. 1192-3.

148. Tsuei, S.E., et al., *Disposition of synethetic glucocorticoids. I. Pharmacokinetics of dexamethasone in healthy adults.* J Pharmacokinet Biopharm, 1979. **7**(3): p. 249-64.

149. Wang, Q., et al., *Targeted delivery of low-dose dexamethasone using PCL-PEG micelles for effective treatment of rheumatoid arthritis.* J Control Release, 2016. **230**: p. 64-72.

150. Krishnan, V., et al., *Dexamethasone-loaded block copolymer nanoparticles induce leukemia cell death and enhance therapeutic efficacy: a novel application in pediatric nanomedicine.* Mol Pharm, 2013. **10**(6): p. 2199-210.

151. Bruni, R., et al., *Ultrasmall polymeric nanocarriers for drug delivery to podocytes in kidney glomerulus.* J Control Release, 2017. **255**: p. 94-107.

152. Chow, E.K. and D. Ho, *Cancer nanomedicine: from drug delivery to imaging.* Sci Transl Med, 2013. **5**(216): p. 216rv4.

153. Lee, H., et al., *Molecular dynamics studies of polyethylene oxide and polyethylene glycol: hydrodynamic radius and shape anisotropy.* Biophys J, 2008. **95**(4): p. 1590-9.

154. Du, B., et al., *Glomerular barrier behaves as an atomically precise bandpass filter in a sub-nanometre regime.* Nat Nanotechnol, 2017. **12**(11): p. 1096-1102.

155. Bethunaickan, R., et al., *A unique hybrid renal mononuclear phagocyte activation phenotype in murine systemic lupus erythematosus nephritis.* J Immunol, 2011. **186**(8): p. 4994-5003.

156. Bosedasgupta, S. and J. Pieters, *Inflammatory stimuli reprogram macrophage phagocytosis to macropinocytosis for the rapid elimination of pathogens.* PLoS Pathog, 2014. **10**(1): p. e1003879.

157. Caruso-Neves, C., S.H. Kwon, and W.B. Guggino, *Albumin endocytosis in proximal tubule cells is modulated by angiotensin II through an AT2*

receptor-mediated protein kinase B activation. Proc Natl Acad Sci U S A, 2005. **102**(48): p. 17513-8.

158. Peets, E.A., M. Staub, and S. Symchowicz, *Plasma binding of betamethasone-3H, dexamethasone-3H, and cortisol-14C--a comparative study.* Biochem Pharmacol, 1969. **18**(7): p. 1655-63.

159. Zhao, P., et al., *Study of multiple binding constants of dexamethasone with human serum albumin by capillary electrophoresis-frontal analysis and multivariate regression.* Anal Bioanal Chem, 2009. **393**(1): p. 257-61.

160. Muczynski, K.A., et al., *Normal human kidney HLA-DR-expressing renal microvascular endothelial cells: characterization, isolation, and regulation of MHC class II expression.* J Am Soc Nephrol, 2003. **14**(5): p. 1336-48.

161. Westover, A.J., D.A. Buffington, and H.D. Humes, *Enhanced propagation of adult human renal epithelial progenitor cells to improve cell sourcing for tissue-engineered therapeutic devices for renal diseases.* J Tissue Eng Regen Med, 2012. **6**(8): p. 589-97.

162. Joraku, A., et al., *In vitro generation of three-dimensional renal structures.* Methods, 2009. **47**(2): p. 129-33.

163. Amsterdam, A., K. Tajima, and R. Sasson, *Cell-specific regulation of apoptosis by glucocorticoids: implication to their anti-inflammatory action.* Biochem Pharmacol, 2002. **64**(5-6): p. 843-50.

164. de Haij, S., et al., *Production of inflammatory mediators by renal epithelial cells is insensitive to glucocorticoids.* Br J Pharmacol, 2002. **137**(2): p. 197-204.

165. Bergtold, A., et al., *FcR-bearing myeloid cells are responsible for triggering murine lupus nephritis.* J Immunol, 2006. **177**(10): p. 7287-95.

166. Luo, K., et al., *Biodegradable Multiblock Poly[N-(2-hydroxypropyl)methacrylamide] via Reversible Addition-Fragmentation Chain Transfer Polymerization and Click Chemistry.* Macromolecules, 2011. **44**(8): p. 2481-2488.

167. Seymour, L.W., et al., *Effect of molecular weight (Mw) of N-(2-hydroxypropyl)methacrylamide copolymers on body distribution and rate of excretion after subcutaneous, intraperitoneal, and intravenous administration to rats.* J Biomed Mater Res, 1987. **21**(11): p. 1341-58.

168. Moghadam-Kia, S. and V.P. Werth, *Prevention and treatment of systemic glucocorticoid side effects.* Int J Dermatol, 2010. **49**(3): p. 239-48.

169. Stahn, C., et al., *Molecular mechanisms of glucocorticoid action and selective glucocorticoid receptor agonists.* Mol Cell Endocrinol, 2007. **275**(1-2): p. 71-8.